

AD-A267 549 TION PAGE

Form Approved
OMB No. 0704-0188



Do not fill in this area unless you are reporting on the data shown in the instructions. Send comments regarding this burden estimate or any aspect of this collection of information, including suggestions for reducing the burden, to Washington Headquarters Services, Directorate for Information Operations and Reports, 1215 Jefferson Management and Budget, Paperwork Reduction Project (704-0188), Washington, DC 20503.

1. AGENCY USE ONLY (Leave blank)		2. REPORT DATE MAY 1993		3. REPORT TYPE AND DATES COVERED THESIS/DISSERTATION	
4. TITLE AND SUBTITLE A Modified Two-Fluid Model of Conductivity for Superconducting Surface Resistance Calculation				5. FUNDING NUMBERS	
6. AUTHOR(S) Derek S. Linden					
7. PERFORMING ORGANIZATION NAME(S) AND ADDRESS(ES) AFIT Student Attending: Massachusetts Institute of Technology				8. PERFORMING ORGANIZATION REPORT NUMBER AFIT/CI/CIA- 93-077	
9. SPONSORING/MONITORING AGENCY NAME(S) AND ADDRESS(ES) DEPARTMENT OF THE AIR FORCE AFIT/CI 2950 P STREET WRIGHT-PATTERSON AFB OH 45433-7765				10. SPONSORING/MONITORING AGENCY REPORT NUMBER	
11. SUPPLEMENTARY NOTES					
12a. DISTRIBUTION / AVAILABILITY STATEMENT Approved for Public Release IAW 190-1 Distribution Unlimited MICHAEL M. BRICKER, SMSgt, USAF Chief Administration				12b. DISTRIBUTION CODE	
13. ABSTRACT (Maximum 200 words)					
<div data-bbox="941 776 1321 1042" data-label="Text"><p>DTIC ELECTE AUG 6 1993 S C D</p></div>					
14. SUBJECT TERMS				15. NUMBER OF PAGES 130	
				16. PRICE CODE	
17. SECURITY CLASSIFICATION OF REPORT		18. SECURITY CLASSIFICATION OF THIS PAGE		19. SECURITY CLASSIFICATION OF ABSTRACT	
				20. LIMITATION OF ABSTRACT	

93 8 05 1 19

93-18071



Abstract

Title: A Modified Two-Fluid Model of Conductivity for Superconducting Surface Resistance Calculation

Author: Derek S. Linden

Rank and branch: 2d Lt, USAF

Date: 1993

Number of pages: 130

Degree awarded: Master of Science in Electrical Engineering and Computer Science

Institution: The Massachusetts Institute of Technology

The traditional two-fluid model of superconducting conductivity was modified to make it accurate, while remaining fast, for designing and simulating microwave devices. The modification reflects the BCS coherence effects in the conductivity of a superconductor, and is incorporated through the ratio of normal to superconducting electrons. This modified ratio is a simple analytical expression which depends on frequency, temperature and material parameters. This modified two-fluid model allows accurate and rapid calculation of the microwave surface impedance of a superconductor in the clean and dirty limits and in the weak- and strong-coupled regimes. The model compares well with surface resistance data for Nb and provides insight into Nb₃Sn and Y₁Ba₂Cu₃O_{7-δ}. Numerical calculations with the modified two-fluid model are an order of magnitude faster than the quasi-classical program by Zimmermann [1], and two to five orders of magnitude faster than Halbritter's BCS program [2] for surface resistance.

Bibliography

[1] Zimmermann, W., E.H. Brandt, M. Bauer, E. Seider and L. Genzel. "Optical conductivity of BCS superconductors with arbitrary purity." *Physica C*. Vol 183, pp. 99-104, 1991.

Accession For		
NTIS	CRA&I	<input checked="" type="checkbox"/>
IC	TAB	<input type="checkbox"/>
Announced		<input type="checkbox"/>

Availability Codes

Dist	Available for Special
A-1	

DTIC QUALITY INSPECTED 3

Abstract

Title: A Modified Two-Fluid Model of Conductivity for Superconducting Surface Resistance Calculation

Author: Derek S. Linden

Rank and branch: 2d Lt, USAF

Date: 1993

Number of pages: 130

Degree awarded: Master of Science in Electrical Engineering and Computer Science

Institution: The Massachusetts Institute of Technology

The traditional two-fluid model of superconducting conductivity was modified to make it accurate, while remaining fast, for designing and simulating microwave devices. The modification reflects the BCS coherence effects in the conductivity of a superconductor, and is incorporated through the ratio of normal to superconducting electrons. This modified ratio is a simple analytical expression which depends on frequency, temperature and material parameters. This modified two-fluid model allows accurate and rapid calculation of the microwave surface impedance of a superconductor in the clean and dirty limits and in the weak- and strong-coupled regimes. The model compares well with surface resistance data for Nb and provides insight into Nb₃Sn and Y₁Ba₂Cu₃O_{7- δ} . Numerical calculations with the modified two-fluid model are an order of magnitude faster than the quasi-classical program by Zimmermann [1], and two to five orders of magnitude faster than Halbritter's BCS program [2] for surface resistance.

Bibliography

[1] Zimmermann, W., E.H. Brandt, M. Bauer, E. Seider and L. Genzel. "Optical conductivity of BCS superconductors with arbitrary purity." *Physica C*. Vol 183, pp. 99-104, 1991.

- [2] Halbritter, J. Kernforschungszentrum Karlsruhe Externer Bericht 3/70-6 Karlsruhe: Institute fuer Experimentelle Kernphysik, Juni 1970.
- [3] J.G. Bednorz and K.A. Mueller. *Z. Phys. B*. Vol 64, p. 189, 1986.
- [4] Hammond, Robert B., Gregory L. Hey-Shipton and George L. Matthaei. "Designing with Superconductors." *IEEE Spectrum*. Vol 30, no 4, pp. 34-39, April, 1993. .
- [5] Withers, Richard S. "Wideband Analog Signal Processing" *Superconducting Devices*. Steven T. Ruggiero and David A. Rudman, ed. Boston: Acad. Press, Inc., 1990. pp. 228-272.
- [6] Griffiths, David J. *Introduction to Electrodynamics*. 2nd ed. New Jersey: Prentice Hall, 1989.
- [7] Orlando, Terry P. and Kevin A. Delin. *Foundations of Applied Superconductivity*. Reading, Mass.: Addison-Wesley Publishing Co., 1991.
- [8] Kittel, Charles. *Introduction to Solid State Physics*. 6th ed. New York: John Wiley and Sons, Inc., 1986.
- [9] Tinkham, Michael. *Introduction to Superconductivity*. Malibar, Florida: Robert E. Krieger Publishing Co., 1980.
- [10] Hinken, Johann H. *Superconductor Electronics: Fundamentals and Microwave Applications*. Berlin: Springer-Verlag, 1988.
- [11] Muehlschlegel, Bernhard. "The Thermodynamic Functions of the Superconductor." *Zeitschrift fuer Physik*. Vol 155, pp. 313-327, 1959.
- [12] Mattis, D.C. and J. Bardeen. *Phys. Rev.* Vol 111, p. 412, 1958.
- [13] Abrikosov, A.A., L.P. Gor'kov and I.M. Khalatnikov. *Eksp. Teor. Fiz.* Vol 35, p. 265, 1958. [*Sov. Phys.—JETP* Vol 8, 1959. 182.]
- [14] Turneaure, J.P., J. Halbritter and H.A. Schwettman. "The Surface Impedance of Superconductors and Normal Conductors: The Mattis-Bardeen Theory." *Journal of Superconductivity*. Vol 4, no 5, pp. 341-355, 1991.
- [15] Turneaure, J. PhD Dissertation. Stanford University, 1967.

- [16] Abrikosov, A.A., L.P. Gor'kov, and I. Yu. Dzyaloshinskii. *Quantum Theoretical Methods in Statistical Physics*. New York: Pergamon Press, 1965.
- [17] D.C. Carless, H.E. Hall and J.R. Hook. "Vibrating Wire Measurements in Liquid ^3He : II. The Superfluid B Phase." *Journal of Low Temperature Physics*. Vol 50, Nos 5/6, pp. 605-633, 1983.
- [18] Ashcroft, Neil W. and David N. Mermin. *Solid State Physics*. Philadelphia: W. B. Saunders Co., 1976.
- [19] Gorter, C.J. and H.G.B. Casimir. *Phys. Z.*, Vol 35, 1934. 963. [21] London, F. *Superfluids: Macroscopic Theory of Superconductivity*. Vol 1. Dover Publications, Inc., 1961.
- [20] Puempin, B., H. Keller, W. Kuendig, W. Odermatt, I.M. Savic, J.W. Schneider, H. Simmler, P. Zimmermann, E. Kaldis, S. Rusiecki, Y. Maeno and C. Rossel. "Muon-spin-rotation measurements of the London penetration depths in $\text{YBa}_2\text{Cu}_3\text{O}_{6.97}$." *Physical Review B*. Vol 42, no 13, pp. 8019-8029, 1 November 1990.
- [21] London, F. *Superfluids: Macroscopic Theory of Superconductivity*. Vol 1. Dover Publications, Inc., 1961.
- [22] Orlando, T.P., E.J. McNiff, S. Foner and M.R. Beasley. "Critical fields, Pauli paramagnetic limiting, and material parameters of Nb_3Sn and V_3Si ." *Phys. Rev. B*. Vol 19, no 9, pp. 4545-4561, 1 May 1979.
- [23] Bonn, D. A., P. Dosanjh, R. Liang and W.N. Hardy. "Evidence for Rapid Suppression of Quasiparticle Scattering below T_c in $\text{YBa}_2\text{Cu}_3\text{O}_{7-\delta}$." *Physical Review Letters*. Vol 68, no 15, pp. 2390-2393, 13 April 1992.
- [24] Berlinski, A. John, C. Kallin, G. Rose and A.-C. Shi, at the Institute for Materials Research and Department of Physics and Astronomy, McMaster University, Hamilton, Ontario. "Two-Fluid Interpretation of the Conductivity of Clean BCS Superconductors." Submitted to *Phys. Rev. B*. on 5 March, 1993.
- [25] Siebert, William McC. *Circuits, Signals and Systems*. Cambridge, MA: The MIT Press, 1986.
- [26] Andreone, Antonello and Vladimir Z. Kresin. "On Microwave Properties of High- T_c Oxides." Presented at the Applied Superconductivity Conference, Chicago, August 1992.
- [27] Piel, H. and G. Mueller. "The Microwave Surface Impedance of High- T_c Superconductors." *IEEE Trans. on Mag.* Vol 27, no 2, pp. 854-862, March 1991.

[28] Lyons, W. G. "Surface Resistance (After Piel, U. Wuppertal)" Internal Slide for MIT Lincoln Laboratory #2325B TCLGS/aml.

[29] Werthamer, N. R., in *Superconductivity*. R. E. Parks, ed. New York: Marcel Dekker, 1969. Vol 2, p. 321.

Addendum: The author hereby grants to the United States Air Force permission to reproduce and to distribute publicly copies of this thesis document in whole or in part.

**A Modified Two-Fluid Model of Conductivity for Superconducting Surface
Resistance Calculation**

by

Derek S. Linden

B.S., Applied Physics
United States Air Force Academy
1991

Submitted to the Department of
Electrical Engineering and Computer Science
in Partial Fulfillment of the Requirements
for the Degree of

Master of Science
at the

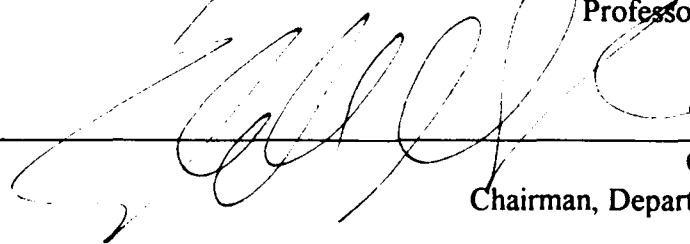
Massachusetts Institute of Technology
May, 1993

© Derek S. Linden 1993
All rights reserved

The author hereby grants to MIT permission to reproduce and to
distribute publicly copies of this thesis document in whole or in part.

Signature of Author 
Department of Electrical Engineering and Computer Science

Certified by 
Professor Terry P. Orlando
Thesis Supervisor

Accepted by 
Campbell L. Searle
Chairman, Departmental Committee

Abstract

A Modified Two-Fluid Model of Conductivity for Superconducting Surface Resistance Calculation

by

Derek S. Linden

Submitted to the Department of Electrical Engineering and Computer Science
on May 7, 1993 in partial fulfillment of the requirements
for the Degree of Master of Science in Electrical Engineering and Computer Science

The traditional two-fluid model of superconducting conductivity was modified to make it accurate, while remaining fast, for designing and simulating microwave devices. The modification reflects the BCS coherence effects in the conductivity of a superconductor, and is incorporated through the ratio of normal to superconducting electrons. This modified ratio is a simple analytical expression which depends on frequency, temperature and material parameters. This modified two-fluid model allows accurate and rapid calculation of the microwave surface impedance of a superconductor in the clean and dirty limits and in the weak- and strong-coupled regimes. The model compares well with surface resistance data for Nb and provides insight into Nb₃Sn and Y₁Ba₂Cu₃O_{7- δ} . Numerical calculations with the modified two-fluid model are an order of magnitude faster than the quasi-classical program by Zimmermann [1], and two to five orders of magnitude faster than Halbritter's BCS program [2] for surface resistance.

Thesis Supervisor: Terry P. Orlando
Title: Professor of Electrical Engineering

Contents

1 Introduction	17
1.1 Motivation.....	17
1.2 Surface Resistance	19
2 The BCS Model Programs	23
2.1 Introduction.....	23
2.2 BCS Conductivity and Surface Impedance Calculations.....	25
2.2.1 The Zimmermann Program.....	26
2.2.2 The Halbritter Program.....	31
3 The Two-Fluid Models	35
3.1 Introduction.....	35
3.2 Two-Fluid Models—Overview.....	35
3.3 The Traditional Model	40
3.4 The Modified Two-Fluid Model.....	42
3.4.1 Parameter Relationships.....	43
3.4.2 The Temperature Dependence of $\lambda^2(T)$	45
3.4.3 The Cutoff Frequency.....	46
3.4.4 The Normal-Total Electron Ratio $\eta(\omega, T)$	47
3.4.5 The Sum Rule and Kramers-Kronig Relationships.....	52
4 Surface resistance results	57
4.1 Introduction.....	57
4.2 Comparison to BCS Calculations	57
4.2.1 Surface Resistance Comparison of BCS and MTF Models.....	60
4.2.2 Surface Reactance Comparison of BCS and MTF Models	68
4.3 Comparison of BCS and MTF Models to Another Model.....	77
4.4 Comparison to Niobium.....	79
4.5 Comparison to Nb ₃ Sn.....	83
4.6 Comparison to Y ₁ Ba ₂ Cu ₃ O _{7-δ}	87
5 Summary	91
Bibliography.....	93
Appendix A: Comprehensive List of Equations for the MTF Model.....	97

Appendix B: Pascal Code Translation of Zimmermann Program [1].....	101
Appendix C: FORTRAN and C code for Halbritter's BCS Surface Impedance Program [2]	107
Appendix D: The Transport Scattering Time and Normal-Total Electron Ratio from The Sum Rule	127

List of Figures

1.1	Electromagnetic wave in linear media incident to superconductor. λ refers to the magnetic penetration depth of the superconductor.	19
2.1	Comparison of Pascal program to FORTRAN program output from [1]. Input parameters to both programs are identical, and listed above. Figures are from [1].	28
2.2	Anomalous output of Zimmermann program. Frequency dependence is on a logarithmic scale; temperature dependence is on a linear scale. Material parameters: $\Delta_0 = 7.6\text{meV}$, $\Delta_0/k_B T_C = 1.75$, $\sigma_0 = 8 \cdot 10^7 (\Omega\text{-m})^{-1}$, and $\xi_0/l = 1/35.16$	30
3.1	Lumped Circuit Representation of the Two-fluid Model. LPF = low pass filter (ideal), HPF = high pass filter (ideal).	39
3.2	$\eta_{\text{MTF}}(\omega, T)$, $\eta_{\text{BCS}}(\omega, T)$ from [1] and $\eta_{\text{TF}}(T)$ versus ω . $\omega_c = 6.4\text{THz}$, $T = 0.5T_C$, mean free path $l = 2\text{nm}$, coherence length $\xi_0 = 2\text{nm}$, penetration depth $\lambda(0) = 140\text{nm}$, $\Delta_0/k_B T_C = 1.75$	42
3.3	Various theoretical temperature dependencies of $\lambda^2(0)/\lambda^2(T)$ (after Figure 9 in [20]).	46
3.4	$\eta(\omega, T)$ of the MTF model vs. temperature and frequency	48
3.5	$\eta_{\text{MTF}}(\omega, T)$, $\eta_{\text{H}}(\omega, T)$ [10] and $\eta_{\text{TF}}(T)$ versus T . Frequency = 1GHz, mean free path $l = 2\text{nm}$, coherence length $\xi_0 = 2\text{nm}$, penetration depth $\lambda(0) = 140\text{nm}$, $\Delta_0/k_B T_C = 1.75$	50
3.6	$\eta_{\text{MTF}}(\omega, T)$, $\eta_{\text{H}}(\omega, T)$ [10] and $\eta_{\text{TF}}(T)$ versus ω . $\omega_c = 6.4\text{THz}$, $T = 0.5T_C$, mean free path $l = 2\text{nm}$, coherence length $\xi_0 = 2\text{nm}$, penetration depth $\lambda(0) = 140\text{nm}$, $\Delta_0/k_B T_C = 1.75$	50

4.1 "Parameter space" representation of the comparisons of the MTF model with the BCS calculations. Each point indicates a set of parameters where a comparison was made. Each point with a circle around it corresponds to a figure graphically comparing the BCS and MTF model calculations for that set of parameters.	59
4.2 Weak-clean comparison to BCS calculations (using [2]) from $0.022T_c$ to $0.94T_c$. Penetration depth temperature dependence is proportional to $(1-(T/T_c)^3-T/T_c)^{-1/2}$. $\Delta_0/k_B T_c = 1.75$, $\lambda(0) = 140\text{nm}$, $\xi_0 = 2\text{nm}$, $l = 200\text{nm}$, Frequency = 10GHz.	60
4.3 Weak-dirty comparison to BCS calculations (using [2]) from $0.022T_c$ to $0.94T_c$. Penetration depth temperature dependence is proportional to $(1-(T/T_c)^3-T/T_c)^{-1/2}$. $\Delta_0/k_B T_c = 1.75$, $\lambda(0) = 140\text{nm}$, $\xi_0 = 2\text{nm}$, $l = 0.02\text{nm}$, Frequency = 10GHz.	61
4.4 Strong-clean comparison to BCS calculations (using [2]) from $0.022T_c$ to $0.94T_c$. Penetration depth temperature dependence is proportional to $(1-(T/T_c)^3-T/T_c)^{-1/2}$. $\Delta_0/k_B T_c = 2.75$, $\lambda(0) = 140\text{nm}$, $\xi_0 = 2\text{nm}$, $l = 200\text{nm}$, Frequency = 10GHz.	61
4.5 Strong-dirty comparison to BCS calculations (using [2]) from $0.022T_c$ to $0.94T_c$. Penetration depth temperature dependence is proportional to $(1-(T/T_c)^3-T/T_c)^{-1/2}$. $\Delta_0/k_B T_c = 2.75$, $\lambda(0) = 140\text{nm}$, $\xi_0 = 2\text{nm}$, $l = 0.02\text{nm}$, Frequency = 10GHz.	62
4.6 Mid-range comparison to BCS calculations (using [2]) from $0.022T_c$ to $0.94T_c$. Penetration depth temperature dependence is proportional to $(1-(T/T_c)^3-T/T_c)^{-1/2}$. $\Delta_0/k_B T_c = 2.25$, $\lambda(0) = 140\text{nm}$, $\xi_0 = 2\text{nm}$, $l = 2\text{nm}$, Frequency = 10GHz.	62
4.7 MTF model surface resistance/BCS surface resistance mean comparison for clean to dirty and strong to weak parameters. The mean is taken across a temperature range from $0.022T_c$ to $0.94T_c$. Penetration depth temperature dependence is proportional to $(1-(T/T_c)^3-T/T_c)^{-1/2}$. $\lambda(0) = 140\text{nm}$, $\xi_0 = 2\text{nm}$, Frequency = 10GHz.	63
4.8 Weak-clean comparison to BCS calculations (using [2]) from $0.022T_c$ to $0.94T_c$. Penetration depth temperature dependence is proportional to $(1-(T/T_c)^4)^{-1/2}$. $\Delta_0/k_B T_c = 1.75$, $\lambda(0) = 140\text{nm}$, $\xi_0 = 2\text{nm}$, $l = 200\text{nm}$, Frequency = 10GHz.	64

4.9 Weak-dirty comparison to BCS calculations (using [2]) from $0.022T_c$ to $0.94T_c$. Penetration depth temperature dependence is proportional to $(1-(T/T_c)^4)^{-1/2}$. $\Delta_0/k_B T_c = 1.75$, $\lambda(0) = 140\text{nm}$, $\xi_0 = 2\text{nm}$, $l = 0.02\text{nm}$, Frequency = 10GHz.	65
4.10 Strong-clean comparison to BCS calculations (using [2]) from $0.022T_c$ to $0.94T_c$. Penetration depth temperature dependence is proportional to $(1-(T/T_c)^4)^{-1/2}$. $\Delta_0/k_B T_c = 2.75$, $\lambda(0) = 140\text{nm}$, $\xi_0 = 2\text{nm}$, $l = 200\text{nm}$, Frequency = 10GHz.	65
4.11 Strong-dirty comparison to BCS calculations (using [2]) from $0.022T_c$ to $0.94T_c$. Penetration depth temperature dependence is proportional to $(1-(T/T_c)^4)^{-1/2}$. $\Delta_0/k_B T_c = 2.75$, $\lambda(0) = 140\text{nm}$, $\xi_0 = 2\text{nm}$, $l = 0.02\text{nm}$, Frequency = 10GHz.	66
4.12 Mid-range comparison to BCS calculations (using [2]) from $0.022T_c$ to $0.94T_c$. Penetration depth temperature dependence is proportional to $(1-(T/T_c)^4)^{-1/2}$. $\Delta_0/k_B T_c = 2.25$, $\lambda(0) = 140\text{nm}$, $\xi_0 = 2\text{nm}$, $l = 2\text{nm}$, Frequency = 10GHz.	66
4.13 MTF model surface resistance/BCS surface resistance mean comparison for clean to dirty and strong to weak parameters. The mean is taken across a temperature range from $0.022T_c$ to $0.94T_c$. Penetration depth temperature dependence is proportional to $(1-(T/T_c)^4)^{-1/2}$. $\lambda(0) = 140\text{nm}$, $\xi_0 = 2\text{nm}$, Frequency = 10GHz.	67
4.14 Weak-clean comparison to BCS calculations (using [2]) from $0.022T_c$ to $0.94T_c$. Penetration depth temperature dependence is proportional to $(1-(T/T_c)^3 - T/T_c)^{-1/2}$. $\Delta_0/k_B T_c = 1.75$, $\lambda(0) = 140\text{nm}$, $\xi_0 = 2\text{nm}$, $l = 200\text{nm}$, Frequency = 10GHz.	69
4.15 Weak-dirty comparison to BCS calculations (using [2]) from $0.022T_c$ to $0.94T_c$. Penetration depth temperature dependence is proportional to $(1-(T/T_c)^3 - T/T_c)^{-1/2}$. $\Delta_0/k_B T_c = 1.75$, $\lambda(0) = 140\text{nm}$, $\xi_0 = 2\text{nm}$, $l = 0.02\text{nm}$, Frequency = 10GHz.	69
4.16 Strong-clean comparison to BCS calculations (using [2]) from $0.022T_c$ to $0.94T_c$. Penetration depth temperature dependence is proportional to $(1-(T/T_c)^3 - T/T_c)^{-1/2}$. $\Delta_0/k_B T_c = 2.75$, $\lambda(0) = 140\text{nm}$, $\xi_0 = 2\text{nm}$, $l = 200\text{nm}$, Frequency = 10GHz.	70
4.17 Strong-dirty comparison to BCS calculations (using [2]) from $0.022T_c$ to $0.94T_c$. Penetration depth temperature dependence is proportional to $(1-(T/T_c)^3 - T/T_c)^{-1/2}$. $\Delta_0/k_B T_c = 2.75$, $\lambda(0) = 140\text{nm}$, $\xi_0 = 2\text{nm}$, $l = 0.02\text{nm}$, Frequency = 10GHz.	70

4.18	Mid-range comparison to BCS calculations (using [2]) from $0.022T_c$ to $0.94T_c$. Penetration depth temperature dependence is proportional to $(1-(T/T_c)^3-T/T_c)^{-1/2}$. $\Delta_0/k_B T_c = 2.25$, $\lambda(0) = 140\text{nm}$, $\xi_0 = 2\text{nm}$, $l = 2\text{nm}$, Frequency = 10GHz.	71
4.19	Weak-clean comparison to BCS calculations (using [2]) from $0.022T_c$ to $0.94T_c$. Penetration depth temperature dependence is proportional to $(1-(T/T_c)^4)^{-1/2}$. $\Delta_0/k_B T_c = 1.75$, $\lambda(0) = 140\text{nm}$, $\xi_0 = 2\text{nm}$, $l = 200\text{nm}$, Frequency = 10GHz.	72
4.20	Weak-dirty comparison to BCS calculations (using [2]) from $0.022T_c$ to $0.94T_c$. Penetration depth temperature dependence is proportional to $(1-(T/T_c)^4)^{-1/2}$. $\Delta_0/k_B T_c = 1.75$, $\lambda(0) = 140\text{nm}$, $\xi_0 = 2\text{nm}$, $l = 0.02\text{nm}$, Frequency = 10GHz.	73
4.21	Strong-clean comparison to BCS calculations (using [2]) from $0.022T_c$ to $0.94T_c$. Penetration depth temperature dependence is proportional to $(1-(T/T_c)^4)^{-1/2}$. $\Delta_0/k_B T_c = 2.75$, $\lambda(0) = 140\text{nm}$, $\xi_0 = 2\text{nm}$, $l = 200\text{nm}$, Frequency = 10GHz.	73
4.22	Strong-dirty comparison to BCS calculations (using [2]) from $0.022T_c$ to $0.94T_c$. Penetration depth temperature dependence is proportional to $(1-(T/T_c)^4)^{-1/2}$. $\Delta_0/k_B T_c = 2.75$, $\lambda(0) = 140\text{nm}$, $\xi_0 = 2\text{nm}$, $l = 0.02\text{nm}$, Frequency = 10GHz.	74
4.23	Mid-range comparison to BCS calculations (using [2]) from $0.022T_c$ to $0.94T_c$. Penetration depth temperature dependence is proportional to $(1-(T/T_c)^4)^{-1/2}$. $\Delta_0/k_B T_c = 2.25$, $\lambda(0) = 140\text{nm}$, $\xi_0 = 2\text{nm}$, $l = 2\text{nm}$, Frequency = 10GHz.	74
4.24	Comparison of BCS calculations of [2] to MTF and model presented by Andreone and Kresin [26]. $l < \xi_0$ (i.e. dirty limit), Frequency = 10GHz and gap frequency = 7THz. $\Delta_0/k_B T_c = 1.76$	78
4.25	Comparison of Nb data to BCS model [2]. $\Delta_0/k_B T_c = 1.97$, $T_c = 9.2\text{K}$, $\lambda(0) = 28.3\text{nm}$, $\lambda_{L,0} = 21.7\text{nm}$, $\rho_0 = 0.32\mu\Omega\text{-cm}$, $l = 56.1\text{nm}$, $\xi_0 = 39\text{nm}$. Data from [27].....	80
4.26	Comparison of Nb data to BCS model, TTF model and MTF model. $\Delta_0/k_B T_c = 1.97$, $T_c = 9.2\text{K}$, $\lambda(0) = 28.3\text{nm}$, $\lambda_{L,0} = 21.7\text{nm}$, $\rho_0 = 0.32\mu\Omega\text{-cm}$, $l = 56.1\text{nm}$, $\xi_0 = 39\text{nm}$. Data from [27].	81

- 4.27 Fit of TTF model to Nb data from [27]. Given parameters into TTF model:
 $\Delta_0/k_B T_c = 1.97$, $T_c = 9.2\text{K}$, $\xi_0 = 39\text{nm}$. Adjusted to fit data: $\lambda(0) = 50\text{nm}$, $\sigma_0 = 40 \cdot 10^8 (\Omega\text{-m})^{-1}$ (or $\rho_0 = 0.025 \mu\Omega\text{-cm}$), $l = 361\text{nm}$ 82
- 4.28 Nb_3Sn compared with BCS theory, the TTF model, and MTF model.
 $\Delta_0/k_B T_c = 2.2$, $T_c = 18\text{K}$, $\lambda(0) = 75.9\text{nm}$, $\lambda_{L,0} = 29.3\text{nm}$, $\rho_0 = 10 \mu\Omega\text{-cm}$, $l = 1\text{nm}$,
 $\xi_0 = 5.7\text{nm}$. Data and parameters from [27], except for $\lambda(0)$, which was
derived from [1] and the other parameters. 84
- 4.29 Attempt to fit Nb_3Sn data from [27] with BCS theory, the TTF model, and
MTF model. Inputs are: $\Delta_0/k_B T_c = 1.88$, $T_c = 18\text{K}$, $\lambda(0) = 75.9\text{nm}$,
 $\lambda_{L,0} = 2.48\text{nm}$, $\rho_0 = 10 \mu\Omega\text{-cm}$, $l = 0.0061\text{nm}$, $\xi_0 = 5.7\text{nm}$ 85
- 4.30 Nb_3Sn compared with BCS theory, the TTF model, MTF model and
Adjusted MTF model using (4.1) for $\eta(\omega, T)$. $\Delta_0/k_B T_c = 2.2$, $T_c = 18\text{K}$,
 $\lambda(0) = 75.9\text{nm}$, $\lambda_{L,0} = 29.3\text{nm}$, $\rho_0 = 10 \mu\Omega\text{-cm}$, $l = 1\text{nm}$, $\xi_0 = 5.7\text{nm}$. Data and
parameters from [27], except for $\lambda(0)$, which was derived from [1] and the
other parameters..... 86
- 4.31 Comparison of MTF model to BCS model, TTF model, and data from
Lincoln Laboratory, et al. [28] Numbers used for calculations: $T_c = 91.8\text{K}$,
 $\Delta_0/k_B T_c = 1.75$, $\lambda(0) = 140\text{nm}$, $\rho = 71.4 \mu\Omega\text{-cm}$, $\xi_0 = 2.00\text{nm}$, $l = 2.55\text{nm}$.
After Piel and Mueller [27]..... 87
- 4.32 Transport scattering time vs. temperature from Bonn, et al. and MTF model
to give fit in Figure 4.33. 89
- 4.33 Surface resistance data from Bonn, et al. compared with TTF, MTF and
MTF with scattering time in previous figure. Parameters used for curves: T_c
 $= 91.5\text{K}$, $\Delta_0/k_B T_c = 1.76$, $\lambda_{L,0}(0) = 58\text{nm}$, $\rho(91.5\text{K}) = 49.5 \mu\Omega\text{-cm}$,
penetration depth temp. dependence proportional to $(1 - (T/T_c)^3 - T/T_c)^{-1/2}$ 89
- D.1 $\lambda(0) / \lambda_{L,0}$ versus ξ_0 / l , using four methods of finding this relationship:
Tinkham's equation (equation (3.25)), the Gor'kov relations [29], the sum
rule method, and Zimmermann's BCS program (from [1]). The ratio of ξ_0 / l
goes from clean to dirty going left to right. At larger ξ_0 / l , the Zimmermann
and Tinkham methods are nearly identical, as are the sum rule and Gor'kov
methods. 129
- D.2 Comparison of $\eta(\omega, T)$ from sum rule method and from TTF model. ξ_0/l for
the clean limit is 0.0124, while for the dirty limit it is 12.4..... 130

List of Tables

- 4.1 MTF model surface resistance/BCS surface resistance mean comparison for clean to dirty and strong to weak parameters. The mean is taken across a temperature range from $0.022T_c$ to $0.94T_c$. Penetration depth temperature dependence is proportional to $(1-(T/T_c)^3-T/T_c)^{-1/2}$. $\lambda(0) = 140\text{nm}$, $\xi_0 = 2\text{nm}$, Frequency = 10GHz.....71
- 4.2 MTF model surface resistance/BCS surface resistance mean comparison for dirty to clean (left to right) and strong to weak parameters. The mean is taken across a temperature range from $0.022T_c$ to $0.94T_c$. Penetration depth temperature dependence is proportional to $(1-(T/T_c)^4)^{-1/2}$. $\lambda(0) = 140\text{nm}$, $\xi_0 = 2\text{nm}$, Frequency = 10GHz.....75

Acknowledgments

I would like to thank Professor Terry P. Orlando for his consent to be my thesis advisor, his interest in me even before graduating from the Academy, and his constant support and patience. I thank him for sending me to the Applied Superconductivity Conference and the American Physical Society conference, and giving me a place to go for Thanksgiving. I am indebted to him for his able assistance and interest in this academic research and many other areas of my life. I would also like to thank Dr. W. Gregory Lyons of Lincoln Laboratory who was a great help in guiding my research and in writing it down, and gave me excellent advice and resources at the lab.

I thank the Fannie and John Hertz Foundation for providing the funding for my education at MIT, and their excellent staff who made sure the money came in on time. In addition, this work was conducted under the auspices of the Consortium for Superconducting Electronics with partial support by the Defense Advanced Research Projects Agency (Contract No. MDA972-90-C-0021).

I would like to thank the Air Force for allowing me the time to work on a Master's Degree while on active duty, and I acknowledge the excellent staff at AFIT/CISS, especially both of my program managers: Lt Col Waller and Maj Hogan.

I would like to thank the truly professional technicians at Lincoln Laboratory, particularly Rene R. Boisvert and Robert P. Konieczka. I thank Rene for his help in teaching me how to operate the lab equipment and computer programs, and for taking time out to help me when I got stuck. Thanks to Robert for helping with the lab equipment and fixing items that were not working.

Thanks to Dr. Kevin A. Delin who freely gave me advice on how to get along at MIT when I first arrived. Thanks, too, to Rebecca, my fiancée, who supported and encouraged me, and helped to edit this document. I thank my Mom and Dad who gave me

my start in life and the support and excellent advice which allowed me to end up here.

Finally, I acknowledge God who not only loaned me the talent and abilities necessary to complete this degree, but put me in the right circumstances so that I am where I am today. He is, at the root, responsible for all the acknowledgements above. In addition, He has provided for an eternity spent with Him through the death and resurrection of His Son, which is infinitely more than I deserve.

Chapter 1

Introduction

1.1 Motivation

Research and development performed on superconducting devices has accelerated since the discovery of high-temperature superconductors in 1986 [3]. One goal of this research is to develop devices which will have lower losses and better operating characteristics than normal metal devices. While the technology to fabricate such devices is new, expensive, and difficult to use with consistently good results, many devices are being designed, built and tested. As with other fabrication technologies, it is desirable to simulate these devices before they are actually built to save time and money [4].

One area in which simulation is particularly desirable is in microwave devices. Though resistive losses are much lower in superconducting microwave devices than in normal devices [5], they are not negligible. A value for the surface impedance, when coupled with the geometry of the device, tells the designer the expected resistive loss and reactive inductance and thus much about its expected performance. However, the surface impedance changes with the material parameters, the operating temperature, and the operating frequency.

Any model which will be used to determine the surface impedance must to be accurate over a wide range of material parameters, temperatures and frequencies in order

to be useful to Computer Aided Design (CAD). In addition to accuracy, speed is required so that the design can proceed at a reasonable rate. Thus, a means of calculating the surface impedance both accurately and quickly over a wide range of frequencies, temperatures, and material parameters is necessary.

Until now, no models existed that were both fast and accurate over a wide range of material parameters, temperatures and frequencies. The traditional two-fluid model, described in Chapter 3, is widely used as a first-order approximation for the surface resistance because it is fast, simple, intuitive and analytical. However, it ignores the energy gap, does not use the correct temperature dependence of the penetration depth, and does not take into account coherence effects. Hence, it is inaccurate, particularly at the lower end of the microwave regime (shown in Chapter 4).

On the other hand, a model which implements the Bardeen-Cooper-Schreiffer (BCS) theory of superconductivity is accurate for many conventional superconductors, but the equations of the BCS model are often not intuitive and require time-consuming numerical algorithms.

For applications such as CAD, then, a model is needed which incorporates the accuracy of the BCS theory with the speed and intuitive nature of the two-fluid model. In particular, microwave circuit design needs models for surface resistance which will allow rapid calculation and also give further insight into the operation of superconductors. In this thesis we present the results of our research: a Modified Two-Fluid (MTF) model for conductivity which has the desired characteristics for CAD applications and is optimized for frequencies at or below the microwave regime.

1.2 Surface Resistance

Surface resistance is the real component of the surface impedance. We will now derive the expression for the surface impedance, beginning with Maxwell's equations. Let us assume there is a transverse magnetic (TM) electromagnetic wave in a linear medium incident to a superconductor, as shown in Figure 1.1.

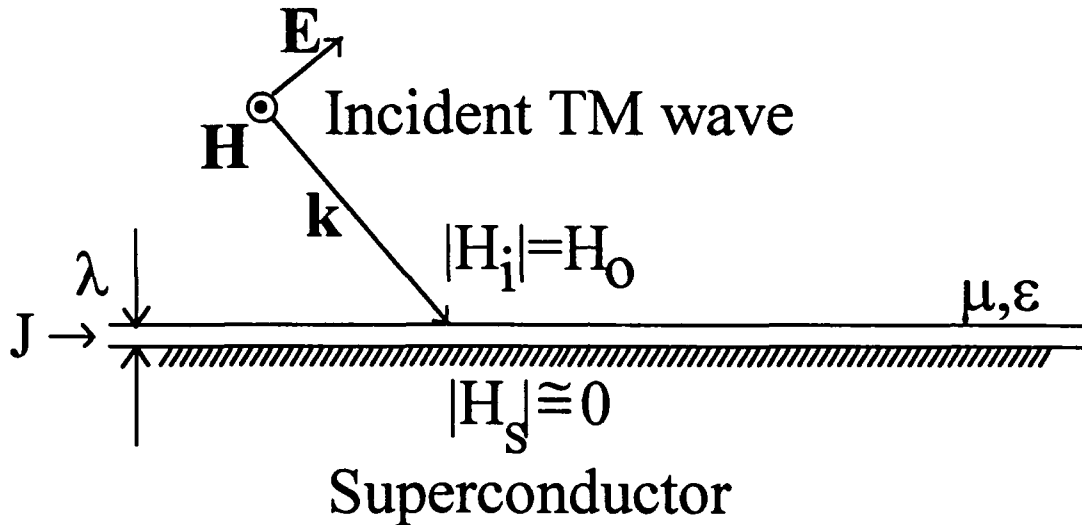


Figure 1.1. Electromagnetic wave in linear media incident to superconductor. λ refers to the magnetic penetration depth of the superconductor.

Ampere's Law for linear media is [6]:

$$\nabla \times \mathbf{H} = \mathbf{J} + \epsilon \frac{\partial \mathbf{E}}{\partial t} \quad (1.1)$$

Without loss of generality, we will assume that \mathbf{H} and \mathbf{E} are plane waves, that is, $|\mathbf{H}| = H_0 \exp[j(\omega t - \mathbf{k} \cdot \mathbf{r})]$ and $|\mathbf{E}| = E_0 \exp[j(\omega t - \mathbf{k} \cdot \mathbf{r})]$. (We lose no generality because the same arguments hold for any superposition of plane waves. Because every electromagnetic wave is a superposition of certain plane waves, we can apply the following argument in general.)

The above assumption implies that equation (1.1) can be written as

$$\nabla \times \mathbf{H} = \mathbf{J} + j\omega\epsilon\mathbf{E}$$

Recall that Ohm's Law is $\mathbf{J} = \sigma\mathbf{E}$, which implies

$$\nabla \times \mathbf{H} = \sigma \mathbf{E} + j\omega \epsilon \mathbf{E} = j\omega \underbrace{[\epsilon(1 - j\sigma/\omega\epsilon)]}_{\epsilon_{\text{eff}}} \mathbf{E} = j\omega \epsilon_{\text{eff}} \mathbf{E} \quad (1.2)$$

which is Ampere's law in a dielectric with a dielectric constant, ϵ_{eff} .

Since both of the resulting vectors on either side of equation (1.2) are in the same direction, and $|\nabla \times \mathbf{H}| = H_0 j k e^{j(\omega t - k \cdot r)}$, we can write

$$j\omega \epsilon_{\text{eff}} E_0 e^{j(\omega t - k \cdot r)} = H_0 j k e^{j(\omega t - k \cdot r)}$$

The ratio of $|\mathbf{E}|/|\mathbf{H}|$ is then

$$k / \omega \epsilon_{\text{eff}} = E_0 / H_0 \quad (1.3)$$

Next we use the following boundary conditions:

$$\begin{aligned} \mathbf{n} \cdot (\mathbf{H}_i - \mathbf{H}_s) &= 0 \\ \mathbf{n} \times (\mathbf{H}_i - \mathbf{H}_s) &= \mathbf{K}_s \end{aligned}$$

along with the knowledge that beyond the penetration depth, the magnetic field inside the superconductor (\mathbf{H}_s) is nearly zero [7] as shown in Figure 1.1. We can therefore treat the current in the superconductor that results from the incident wave as a surface current.

Since the wave is TM, the second boundary condition becomes

$$\mathbf{H}_i = \mathbf{K}_s$$

Substituting this relation into equation (1.3) gives

$$k / \omega \epsilon_{\text{eff}} = E_0 / K_s$$

But this relation is just an impedance for a surface current. Thus,

$$k / \omega \epsilon_{\text{eff}} = Z_s$$

where Z_s is the surface impedance. In addition, for linear media, we know $k^2 = \omega^2 \mu \epsilon$.

Therefore,

$$\begin{aligned}
 k / \omega \epsilon_{eff} &= \omega \sqrt{\mu \epsilon_{eff}} / \omega \epsilon_{eff} \\
 &= \sqrt{\mu / \epsilon_{eff}} \\
 &= \sqrt{\mu / \epsilon (1 - j \sigma / \omega \epsilon)}
 \end{aligned} \tag{1.4}$$

In a superconductor, we can assume $j\sigma/\omega\epsilon \gg 1$, and that μ is approximately μ_0 . Hence, we can simplify equation (1.4):

$$k / \omega \epsilon_{eff} = Z_s \approx \sqrt{j \omega \mu_0 / \sigma} \tag{1.5}$$

While we used an incident plane wave to arrive at this equation, it is just as valid if we have a surface current flowing in the superconductor that generates an electromagnetic (EM) wave. Because EM wave generation occurs if the frequency of the surface current is greater than zero and essentially no current flows below the penetration depth, we therefore can apply equation (1.5) to any non-DC current in a superconductor.

Since μ_0 is a known quantity, j is a constant, and the frequency is assumed to be given, the only parameter left to calculate in equation (1.5) is the conductivity. We used the BCS model and the two-fluid model to calculate the conductivity. Calculations with the two-fluid model give a conductivity directly, as shown in Chapter 3, while programs that implement the BCS model vary. Of the two programs we used, one calculated the conductivity directly, and the other simply calculated the surface resistance. They are described in the next chapter.

Chapter 2

The BCS Model Programs

2.1 Introduction

The Bardeen-Cooper-Schreiffer (BCS) theory of superconductivity was published in 1957 [8], and gives microscopic formulae for superconducting behavior in conventional superconductors. It is a complicated and detailed theory, but a basic premise is that the superconducting electrons are coupled by phonon interaction. Essentially, an electron interferes with the crystal lattice, giving up part of its energy in the form of a phonon, or packet of vibrational energy. The lattice transmits this phonon to another electron, which absorbs the energy. By this exchange, electrons are coupled and can travel without a net loss of energy. The BCS theory has accomplished much toward understanding superconducting behavior, including [8]:

1. Explaining why an attractive electron-electron interaction leads to a ground state that is separated from the excited normal states by an energy gap. This gap is important for most of the electromagnetic properties of the superconductor.
2. Giving a magnetic penetration depth and coherence length (described below) as natural consequences of the BCS theory. The London equation [7] is obtained for magnetic fields that change slowly in space, and thus the Meissner effect is explained theoretically.

3. Explaining that magnetic flux through a superconducting ring is quantized because the superconducting ground state involves pairs of electrons.

The distance spanned by the electron-electron interaction is called the coherence length, is a characteristic of the material, and is given by:

$$\xi_0 = \frac{\hbar v_f}{\pi \Delta_0} \quad (2.1)$$

where v_f is the fermi velocity of the electrons, and Δ_0 is the energy gap at zero temperature. Often related to the coherence length is the mean free path, which is given by [7]:

$$l = v_f \tau_{tr} \quad (2.2)$$

where τ_{tr} is the mean free time, or transport scattering time, of the material. When the mean free path is much shorter than the coherence length the material is said to be in the dirty limit, while if the opposite is true, the material is in the clean limit.

The magnetic penetration depth, denoted by λ , is characteristic of the material, temperature-dependent, and often directly measured. (The temperature dependence is discussed in Chapter 3.) It is related to a similar quantity called the London penetration depth λ_L , which is the theoretical value λ as the mean free path approaches infinite length, that is, the value of λ if the material were in the so-called clean limit [9]. Tinkham [9] found that the BCS relationship between these two quantities at zero temperature is best approximated by:

$$\lambda(0) = \lambda_{L,0} \left(1 + \frac{\xi_0}{l} \right)^{1/2}. \quad (2.3)$$

The energy gap, which in part determines ξ_0 , is characteristic of the material [8] and dependent on temperature. We can approximate the BCS temperature variation in the gap energy $\Delta(T)$ by [10]

$$\Delta(T) \approx \Delta_0 \left[\cos \left(\frac{\pi}{2} \left(\frac{T}{T_c} \right)^2 \right) \right]^{1/2} \quad (2.4)$$

which stays within 3% of the full BCS results listed in [11].

In the BCS theory, the critical temperature T_c is related to Δ_0 by the following constraint: $2\Delta_0/k_B T_c = 3.528$ [9], where k_B is Boltzmann's constant. This constraint is known as the weak-coupling limit [9] and it is characteristic of the BCS theory. Most superconductors do not follow this relationship exactly, but instead have a higher value for $2\Delta_0/k_B T_c$. If this ratio is large, the material is said to be strongly-coupled. However, if this ratio is not too large, the superconductor is still considered to be weakly-coupled, and the BCS theory is still accurate.

The BCS theory also predicts the presence of electrons which do not move losslessly and yet are not independent of one another. The presence of such electrons gives rise to a so-called coherence effect or coherence peak, which we discuss in Chapter 3.

2.2 BCS Conductivity and Surface Impedance Calculation

While the BCS theory is a microscopic theory of superconducting behavior, it requires some effort to apply this theory to calculations of surface impedance. Mattis and Bardeen [12] were the first, along with the independent group of Abrikosov, Gor'kov and Khalatnikov [13], to use the BCS theory to calculate exact expressions for the complex conductivity in 1958 [14]. The Mattis-Bardeen expressions allow one to calculate the complex surface impedance [14] and the complex conductivity normalized to the normal state DC conductivity [9]. They are not easy to use in complete form, as they require much integration. However, in certain limits, such as the low-frequency, dirty limit (where

$\xi_0 \ll 1$) or low-frequency, clean limit (where $\xi_0 \gg 1$), the expressions reduce to a manageable form [9, 14]. Though they have been around the longest, the Mattis-Bardeen equations are still the standard expressions for the BCS conductivity, and are explained in detail in [9] and [14]. Turneaure developed a numerical calculation for surface impedance from these equations in [15]. However, we used two different programs for our research, neither of which use the Mattis-Bardeen expressions.

In 1970, J. Halbritter implemented the BCS theory exactly (within numerical error) with his FORTRAN routine [2]. Unlike Mattis and Bardeen, his implementation does not calculate the conductivity, but directly calculates the surface impedance, and uses the Green's function formalism of Abrikosov, et al. [16, 14], though the Mattis-Bardeen expressions are nearly identical in form [14].

In 1991, W. Zimmermann et al. [1] published a C routine that calculates the complex conductivity, normalized to the normal state conductivity. The routine was primarily designed for optical frequency calculations. It uses a quasi-classical formalism of energy-integrated Green functions [1].

These two programs are described in detail in the following two subsections. Each subsection includes the good qualities and drawbacks of each program, and a description of how we modified and used each.

2.2.1 The Zimmermann Program

The first program we will discuss is presented in [1]. It was written to give the complex conductivity of BCS superconductors with arbitrary purity, and its application centers around high-temperature superconductors. However, it also is stated to yield "the exact AC conductivity of BCS superconductors at lower (non-optical) frequencies [1]," which is the frequency range needed for microwave calculations.

The complex conductivity is calculated from microscopic expressions derived by W. Zimmermann [1]. Those expressions "use the quasi-classical formalism of energy-integrated Green functions [1]." This implementation of the BCS model applies to isotropic weakly-coupled BCS-superconductors with a spherical Fermi surface, and it assumes that calculations are in the local limit [1]. The original program was in FORTRAN, but we translated it to Turbo Pascal 4.0 for our use (see program code in Appendix B). We verified that the translated program was the same as that in [1] by matching figures 1 and 2 from [1], which are simply the output of the FORTRAN program under various conditions. The results, shown in Figure 2.1 below, indicate the two programs produced the same output.

The inputs required for the program in [1] are x , y , and t_t , where $x = \hbar\omega / 2\Delta_0$, $y = \hbar / 2\tau_{tr}\Delta_0$, $t_t = T / T_c$. The output is labeled s , which is the complex conductivity in the local-electrodynamic London limit, normalized to the DC conductivity [1], i.e. $s(\omega=0) = 1$. To make our use of this program easier, we directly input Δ_0 , $\Delta_0/k_B T_c$, the coherence length ξ_0 and the mean free path l . From these inputs, the program itself could calculate the necessary x , y , and t_t . In addition, we input a value for the DC conductivity, so that the output could be in absolute units instead of normalized to the DC conductivity. (For Figure 2.1, though, we directly input x and y .)

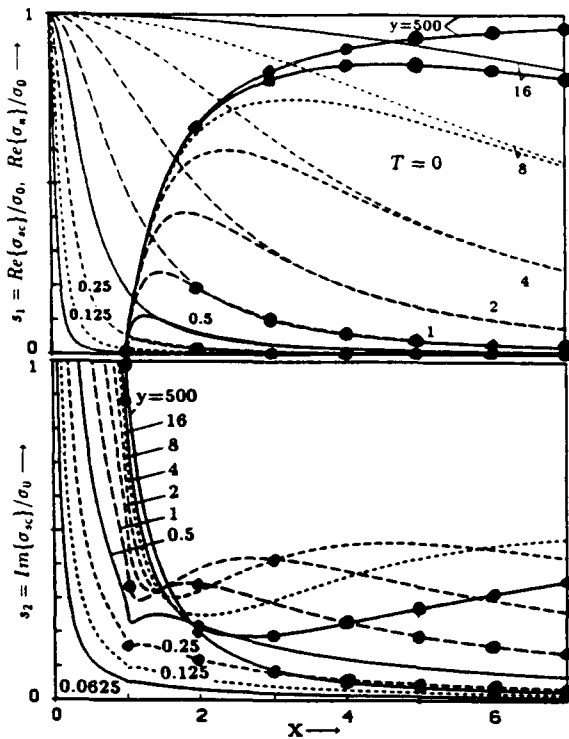


Fig. 1. Frequency dependent complex conductivity $\sigma_{sc}(\omega)$ of a BCS superconductor at temperature $T=0$ in reduced units $s = \sigma_{sc}(\omega)/\sigma_0$, $x = \hbar\omega/2\Delta$, and $y = \hbar/2\tau d$ (impurity parameter) for $y = 500$ (\approx impure limit), 16, 8, 4, 2, 1, 0.5, 0.25, 0.125 and 0.0625 (\approx pure limit). Top: real part $s_1 = \text{Re}\{\sigma_{sc}\}/\sigma_0$; also shown is the normal conductivity $\text{Re}\{\sigma_n\}/\sigma_0 = y^2/(x^2 + y^2)$ (thin dashed Lorenzians). Note that $s_1 = 0$ for $\omega \leq 2\Delta/\hbar$. Bottom: imaginary part $s_2 = \text{Im}\{\sigma_{sc}\}/\sigma_0$.

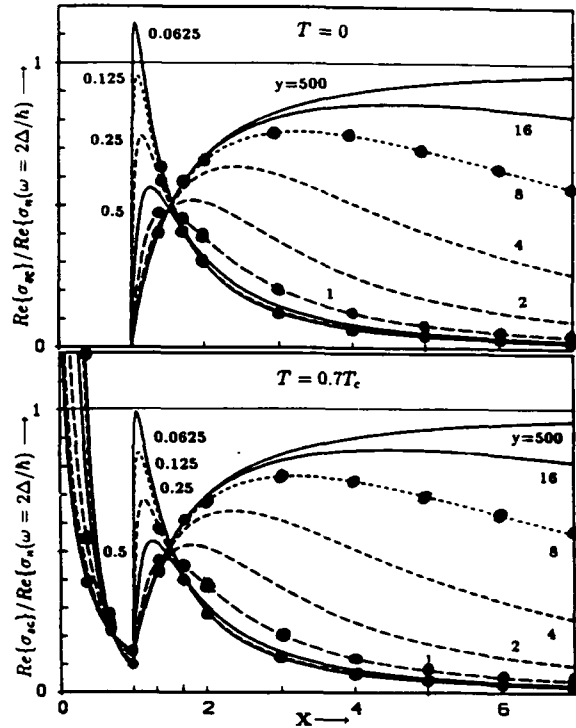


Fig. 2. Complex conductivity, real part, plotted with impurity-dependent magnification as $\text{Re}\{\sigma_{sc}\}/\text{Re}\{\sigma_n(\omega=2\Delta/\hbar)\} = (1 + y^{-2})s_1(x)$, $x = \hbar\omega/2\Delta$, for impurity parameters $y = \hbar/2\tau d = 500, 16, 8, 4, 2, 1, 0.5, 0.25, 0.125, 0.0625$ as in fig. 1. Note the sharp cusp at $x=1$ in the pure case. Top: temperature $T=0$. Bottom: $T=0.7 T_c$.

Figure 2.1 Comparison of Pascal program to FORTRAN program output from [1]. Input parameters (x and y) to both programs are identical. Pascal program output shown by dots, FORTRAN program by lines as designated in above figure captions. Figures are from [1].

We made two other modifications to the program. First, since the magnitude of the energy gap is a function of temperature, it seems that the value of x should reflect that change, that is, x should be equal to $\hbar\omega / 2\Delta(T)$, where $\Delta(T)$ is the temperature-dependent energy gap. We used the expression given in equation (2.4) to approximate the change in energy gap with temperature which approximates full BCS values [11] to within 3%.

(Incidentally, the original program uses a different expression to approximate the

temperature dependence of the energy gap for other calculations. This expression is closer than equation (2.4) to the full BCS values (good to within 0.5% [17]), but both are close enough for our purposes.) The omission of the temperature-dependence of x is fine in [1], because the output shown is always in terms of x . However, since we want to compare the conductivity in terms of the absolute frequency, we must account for this change in x versus temperature.

The other change we made was to allow $2\Delta_0/k_B T_c$ to change. In the original program, it was held at the BCS value, 3.528. Realizing that strong-coupling effects would perhaps not be properly handled, we nevertheless allowed the value to change so that we gained more flexibility in our analysis. Since we did not use this program to validate our model, for reasons detailed later, this change seems to have caused no unvalidated loss in accuracy, at least as far as our use of the BCS calculations go.

We found that there are some advantages to this program. Its output is the complex conductivity, so it offered a great deal of flexibility: we could use the conductivity directly, or use the program to get surface resistance calculations. We could look at the real and imaginary parts of the conductivity and surface resistance separately. The program is also reasonably fast (0.4 seconds/point), so simulations were easy to do for many different cases. We could modify the output any way we wished. Because of the flexibility offered by this program, we were enabled to conduct our research effectively. However, we also found some problems with this program.

We had to be careful how we specified the constant M , which was the number of steps to be taken in numerical integration, and thus the larger M was, the smaller the step size. However, we could not make M too large, because there would be division by zero at some point in the program. The maximum value we could use turned out to be 513, but we were often constrained to use values as low as about 40 in some cases. We did not investigate why this happened in detail, we simply used as high a value for M as we could.

We also found the program was limited in its range of material parameters. In general comparison to the Halbritter program, the best agreement occurs at high frequency (the higher the better, below the gap frequency), and low temperature. The two programs agree well in general in the dirty limit, but in the clean limit, the Zimmermann program did not return reasonable values, especially for high temperatures and low frequencies. The output for surface resistance would not be monotonic for frequency. This behavior was the most marked at temperatures around 0.8 to 0.9 T_C . An example of an anomalous output is shown below.

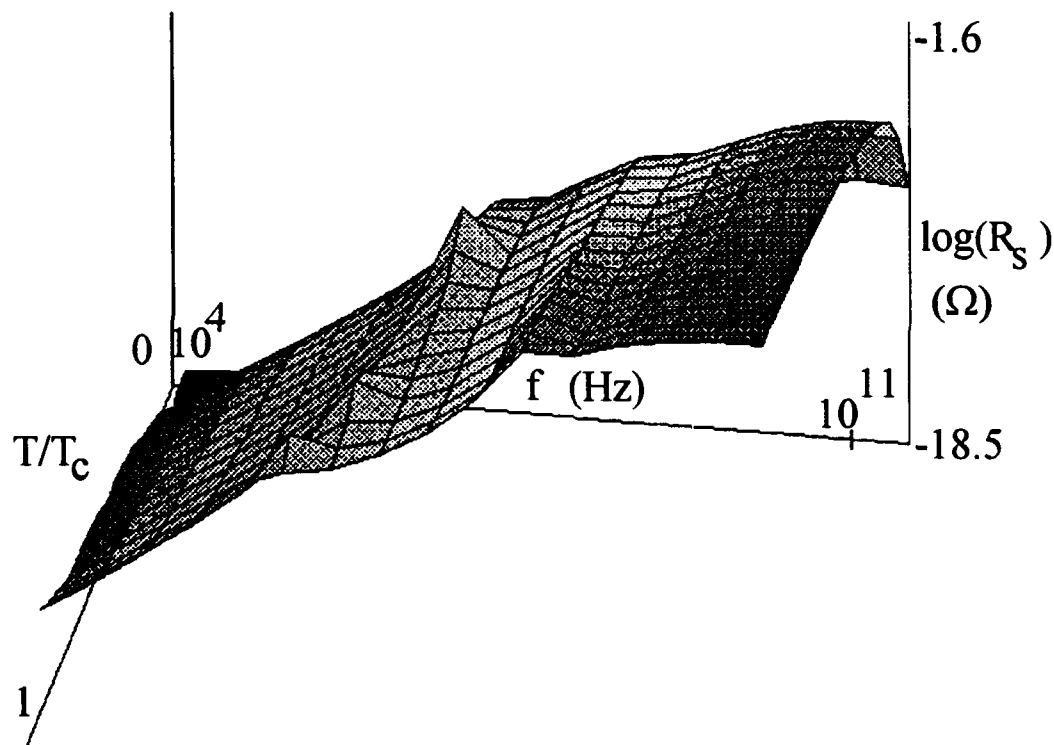


Figure 2.2 Anomalous output of Zimmermann program. Frequency dependence is on a logarithmic scale; temperature dependence is on a linear scale. Material parameters: $\Delta_0 = 7.6\text{meV}$, $\Delta_0/k_B T_C = 1.75$, $\sigma_0 = 8 \cdot 10^7 (\Omega\text{-m})^{-1}$, and $\xi_0/l = 1/35.16$.

There are maxima, minima, and inflection points in the above surface plot which should not be present. In frequency dependence the plot should be monotonic and smooth with no inflection points, and in temperature dependence it should be smooth with only one inflection point. In the above example, there are peaks at (10^6Hz , 1), ($3*10^6\text{Hz}$, 0.95), (10^7Hz , 0.85) and ($3*10^7\text{Hz}$, 0.50), and an additional ridge at $3*10^8\text{Hz}$. These extra features only appear in the clean limit, and they become more pronounced with cleaner parameters. The reason for this behavior is unknown in detail, but part of it probably lies with the limits of the accuracy of the numerical integration.

Overall, then, the Zimmermann program was a good way to gain insight into the BCS conductivity, as it afforded a great deal of flexible and fast analysis. We had to use it with care to ensure that it was indeed giving good values, but we did much of our development with the aid of this program, as we discuss in Section 3.4 of the next chapter. However, we validated our model with a more reliable, and much slower, computer program which we discuss next.

2.2.2 The Halbritter Program

The program we used to validate our model is presented by J. Halbritter in [2]. It calculates the surface impedance (assumed to be in the quasi-static limit as derived in Chapter 1) for superconductors at frequencies below the gap frequency (which quantity is discussed in Chapter 3). In contrast, the Zimmermann program has no limitation on frequency. In addition, the Halbritter program is much slower than the Zimmermann program, by a couple orders of magnitude.

The actual program we used is not the original FORTRAN program in [2], but an exact translation of it into C code by J. Steinbeck. The code for the original program and the C translation are in Appendix C. We validated our program comparing its output with the sample output in [2]. We found that the two outputs matched.

The "formulae used [by the Halbritter program] are exact within the frame work [sic] of the BCS-theory for weak-coupling superconductors. Strong-coupling effects can be introduced by using measured $[\Delta_0/k_B T_C]$ values [2]." However, this program was not as flexible as the Zimmermann program. We were able to use only the compiled C code, and, even if we were able to modify and use the source code, it is not clear that we would be able to make useful modifications to the program, since the equations implemented are not intuitive.

The inputs to this program are: the operating frequency and temperature(s), and the following material parameters: T_C , $\Delta_0/k_B T_C$, the London (clean-limit) penetration depth at zero temperature $\lambda_{L,0}$, coherence length (slightly different from the conventional value), and electronic mean free path. The difference in the coherence length follows: while the conventional formula for ξ_0 is given by equation (2.1), the formula used by the Halbritter program is $\xi = \hbar v_f / 2\Delta_0$. Therefore, the coherence length that is received as input is $(\pi/2)\xi_0$. There are four outputs of the program for each temperature: the surface resistance in ohms and the penetration depth λ in angstroms for specular reflection of charge carriers at the surface, and the surface resistance and penetration depth for diffuse reflection at the surface. From the penetration depth, one can get the surface reactance $X = \omega\mu_0\lambda$ [2] for each case. Chapter 4 shows how we used this program to validate our results against the BCS model.

There is much that is good about this program. It is a numerical implementation of the BCS model. It can handle a wide range of material parameters accurately, without the errors of the Zimmermann program. It does have some limitations too, however. First, the approximation of the energy gap temperature dependence is the same as equation (2.4), which we know is only good to within 3%, as stated above. Also, the program is not user-friendly for some applications (which is mainly a result of not being able to modify the source code). However, it is also fairly inflexible, since it calculates the surface impedance directly using rather complicated equations. While it is accurate, it is also the slowest of

the programs we used, taking between 2 and 1700 seconds per point, with the longest calculation times at lower microwave frequencies (1GHz and below). It would have been difficult to use this program alone to do our research, because of the number and variety of simulations we needed to perform. However, this program coupled with the Zimmermann program made it possible to develop and test our MTF model with reasonable speed, flexibility and accuracy. Having seen the capability of programs that implement the BCS theory, the point of this thesis is to seek a faster and simpler way to have the accuracy of the above two programs, yet increase the speed and ease of calculation.

Chapter 3

The Two-Fluid Models

3.1 Introduction

In this chapter, we will discuss the characteristics of the two-fluid model for conductivity, and how it differs from the BCS model. In the next section, we will give an overview of the two-fluid model: its origin and basic concepts and equations. Next, we will discuss the traditional two-fluid model: its assumptions, equations, strengths and limitations. Finally, we will describe in detail our modifications to the traditional two-fluid model, our reasons for making them, and begin to explore the results of the modifications. (The main analysis of the results we will save for Chapter 4.)

3.2 Two-Fluid Models—Overview

The Drude model is the basis of the two-fluid model. For the two-fluid model to work, the approximations of the Drude model have to be valid. These assumptions are [18]:

1. Electrons are independent of one another (the independent electron approximation) and of the crystal lattice (the free electron approximation) in between collisions.
2. Collisions are instantaneous events which abruptly alter electron velocity, and cause the existence of a drag term.

3. $1/\tau_{tr}$ is the probability per unit time that an electron will experience a collision.

That is, τ_{tr} is a mean free time, or transport scattering time.

4. Electrons achieve thermal equilibrium with their surroundings through collisions only.

The basic equation of carrier motion for the Drude model is based on the above assumptions and $\mathbf{F} = m\mathbf{a}$, and it is given by [7]:

$$m \frac{d\mathbf{v}}{dt} = q\mathbf{E} - \frac{m}{\tau_r} \mathbf{v} \quad (3.1)$$

where \mathbf{v} is the velocity of the carrier, τ_{tr} is the transport scattering time, m is the mass of the carrier, q is the charge of the carrier, and \mathbf{E} is the electric field. The force of the electric field on the electron is partially offset by the drag term $m\mathbf{v}/\tau_{tr}$, assumed to be directly proportional to the velocity of the carrier [7].

The two fluid model assumes that there are two distinct, noninteracting fluids of electrons that carry current. Each fluid follows a different parallel channel. The normal channel, corresponding to a conductivity $\sigma_s^{(n)}$, is governed by equation (3.1). The other channel, the superconducting channel, corresponding to $\sigma_s^{(s)}$, is governed by equation (3.1) without the drag term. The absence of the drag term is due to the lossless transport of current in a superconductor [7]. We will first derive the expression for $\sigma_s^{(n)}$ from the Drude model, and then we will derive the expression for $\sigma_s^{(s)}$.

The equation for current density $\mathbf{J} = nq\mathbf{v}$ (where n is the density of carriers) gives us a relationship between \mathbf{v} and \mathbf{J} . This relationship can be substituted into equation (3.1) to give

$$\frac{m}{nq} \frac{d\mathbf{J}}{dt} = q\mathbf{E} - \frac{m}{\tau_r} \frac{\mathbf{J}}{nq} \quad (3.2)$$

Applying Ohm's law $\mathbf{J} = \sigma \mathbf{E}$ to equation (3.2) gives

$$\frac{m}{nq} \frac{d\mathbf{J}}{dt} = \frac{q}{\sigma} \mathbf{J} - \frac{m}{\tau_r nq} \mathbf{J} \quad (3.3)$$

We also assume that the current is sinusoidally driven (since every function can be written as a superposition of sinusoids). This allows us to write \mathbf{J} in the form $\mathbf{J} = \mathbf{J}(\mathbf{r})e^{j\omega t}$, which implies that equation (3.3) can be written

$$\frac{m}{nq} j\omega \mathbf{J} = \frac{q}{\sigma} \mathbf{J} - \frac{m}{\tau_r nq} \mathbf{J} \quad (3.4)$$

which, in turn, implies

$$\frac{m}{nq^2} \left[j\omega + \frac{1}{\tau_r} \right] = \frac{1}{\sigma} \quad (3.5)$$

which gives us an expression for the conductivity. When the frequency is zero, the resulting conductivity is the DC conductivity σ_0 , and is given by $(nq^2\tau_r/m)$. Substituting this quantity in equation (3.5) gives

$$\sigma = \frac{\sigma_0}{1 + j\omega\tau_r} \quad (3.6)$$

This equation is the normal state conductivity. However, according to the two-fluid model, when a material is superconducting, only a small fraction of its electrons are in the normal state. Since the normal state DC conductivity is often known, and is proportional to the density of electrons, we can multiply equation (3.6) by a ratio $\eta(\omega, T)$ to get the normal channel conductivity. The ratio $\eta(\omega, T)$ is the density of normal state electrons over the total number of electrons. Thus we arrive at the normal channel conductivity

$$\sigma_s^{(n)} = \frac{\sigma_0}{1 + j\omega\tau_r} \eta(\omega, T) \quad (3.7)$$

For the superconducting channel, there is no drag term, so the equation for the conductivity becomes

$$\frac{j\omega m}{nq^2} = \frac{1}{\sigma} \quad (3.8)$$

that is

$$\sigma = \frac{nq^2}{m} \frac{1}{j\omega} \quad (3.9)$$

Equation (3.9) implies that nq^2/m is an inductance. This inductance was noted by Fritz and Heinz London in 1935 and is related to a characteristic length in the system--the magnetic penetration depth, denoted by λ [7]. The relationship between the inductance and penetration depth for a clean superconductor is

$$\frac{nq^2}{m} = \mu_0 \lambda^2.$$

Since the density of superconducting electrons is temperature dependent, the penetration depth is also, and the resulting superconducting complex conductivity of the channel for non-zero frequencies is

$$\sigma_s^{(s)} = \frac{1}{j\omega\mu_0\lambda^2(T)} \quad (3.10)$$

which includes the penetration depth explicitly because it is more general than the nq^2/m term. Although this derivation assumes a clean superconductor, equation (3.10) is generally true for clean or dirty superconductors when $\sigma_s^{(s)}$ is written in terms of λ [7].

Although it is a modification to the traditional model, it is worthwhile to mention here that the two-fluid model should be restricted to frequencies below a cutoff frequency. We take this frequency to be the gap frequency, given by $\omega_g = (2\Delta(T) / \hbar)$ where $\Delta(T)$ is the energy gap as a function of temperature. In this way, the two-fluid model can account for the energy gap in the superconductor. We will explain this cutoff frequency in more detail in Section 3.4. Above this frequency, we assume the conductivity is the normal state conductivity:

$$\sigma_n = \frac{\sigma_0}{1 + j\omega\tau_r} \quad (3.11)$$

The conductivity can thus be represented by the lumped-element circuit shown in Figure 3.1.

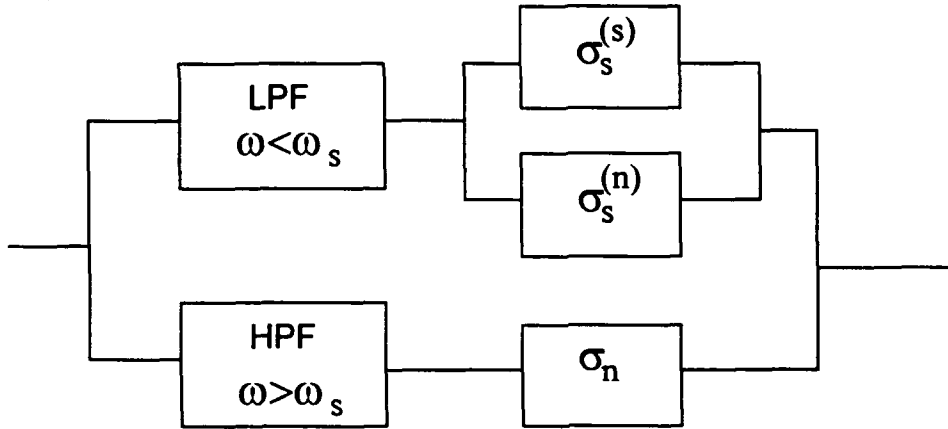


Figure 3.1. Lumped Circuit Representation of the Two-fluid Model. LPF = low pass filter (ideal), HPF = high pass filter (ideal).

Since $\sigma_s^{(s)}$ and $\sigma_s^{(n)}$ are parallel channels, the total conductivity is their sum,

$$\sigma_s = \sigma_s^{(s)} + \sigma_s^{(n)} \quad (3.12)$$

and hence the total conductivity for the circuit is

$$\sigma_T = \begin{cases} \sigma_s & 0 < \omega < \omega_s \\ \sigma_n & \omega > \omega_s \end{cases} \quad (3.13)$$

More explicitly, we write equation (3.13) as:

$$\sigma_T = \sigma_1 - j\sigma_2 = \begin{cases} \frac{1}{\mu_0 \lambda^2(T)} \left(\frac{1}{j\omega} \right) + \frac{\sigma_0}{1 + j\omega\tau_r} \eta(\omega, T) & 0 < \omega < \omega_s \\ \frac{\sigma_0}{1 + j\omega\tau_r} & \omega > \omega_s \end{cases} \quad (3.14)$$

where σ_1 and σ_2 are the real and imaginary parts of the conductivity respectively.

The two-fluid model, then, is in general an intuitive and fast model to implement and use. The equations listed in this section are straightforward and analytical, but are not complete in and of themselves. A few other relationships need defining before the model will produce a value for the conductivity. Because the quantities σ_0 , T_C , $\lambda(0)$, and Δ_0 are measurable, phenomenological parameters, we must determine reasonably accurate expressions for $\eta(\omega, T)$, $\lambda(T)$, and τ_{TF} involving the given parameters in the superconducting frequency regime in order to calculate the conductivity. The traditional two-fluid model assumes a form for these relationships, and we discuss them below.

3.3 The Traditional Two-Fluid Model

The traditional form of the two-fluid model was proposed by C. Gorter and H. B. G. Casimir [7, 14] in their 1934 publication [19]. Their idea was to describe the thermodynamic properties of the superconductor with these two distinct, *non-interacting* fluids, though they penetrate one another [7]. Fritz London coupled it with his equations [7], which gives rise to a system of equations for calculating conductivity.

The traditional form of the model has some good characteristics. It was developed prior to the BCS model, so it has the advantage of being a first-order attempt at giving a mathematical basis for the behavior of superconductors before the scientific community's paradigm changed to a quantum mechanical explanation. It therefore does not include some of the complex relationships that the BCS model illuminates, so it is able to give a basic intuitive idea of what is happening. The expressions are simple in general, so it is good for manual calculations, or for noting basic relationships between parameters (for example, the relationship between surface resistance and frequency). It is elegant and simple, yet still is accurate enough that it is still in use today as a qualitative model.

The basic equation of the Traditional Two-Fluid (TTF) model is (3.12) applied to all frequencies. Unfortunately, the TTF model thus does not account for the energy gap.

This omission is important, because leaving out the energy gap limits the TTF model to frequencies below the gap frequency (typically on the order of THz), and also makes the model nonphysical: it cannot satisfy the sum rule (discussed in Section 3.4).

The traditional two-fluid model assumes a simple relationship for $\lambda(T)$ which is [7]:

$$\lambda^2(T) = \lambda^2(0) / [1 - (T/T_c)^4] \quad (3.15)$$

which results from experimental data [7, 20], including data gathered by F. London himself [21], though not all materials have this temperature dependence (shown in Section 3.4). In addition, there is a consequence of equation (3.15) that affects $\eta(\omega, T)$. As was shown above, $\mu_0 \lambda^2(T) = m / (n_s(T) q^2)$, where n_s is the number of superconducting electrons per unit volume. This relation implies that $1/n_s(T)$ is proportional to $\lambda^2(T)$. Equation (3.15) therefore implies that $n_s(T)/n_{tot}$ is proportional to $1 - (T/T_c)^4$. Using conservation of electrons, and the fact that $(n_s + n_{normal})/n_{tot} = 1$, the TTF model mandates that

$$n_{normal} / n_{tot} = \eta_{TTF} = (T/T_c)^4 \quad (3.16)$$

There is benefit in having this simple relationship for η_{TTF} . Calculations are easy to do, even on a calculator. In addition, for low frequencies (that is, where $\omega \tau_{tr} \ll 1$) and well-developed superconduction (where $\sigma_2 \gg \sigma_1$) [10] one can get an analytic expression for surface resistance that explicitly shows its relationship to the input parameters. If one combines equations (3.16), (3.15), (3.12) and equation (1.5) for surface impedance, the surface resistance (that is, the real part of the surface impedance), can be shown to be [10]

$$R_s = 0.5 \mu_0^2 \sigma_0 \lambda^3(T) \omega^2 \eta_{TTF} = \frac{0.5 \mu_0^2 \sigma_0 \lambda^3(0) \omega^2 (T/T_c)^4}{[1 - (T/T_c)^4]^{3/2}} \quad (3.17)$$

The BCS theory, however, predicts very different behavior for $\eta(\omega, T)$ from equation (3.16), and therefore different behavior for the surface resistance. Figure 3.2

shows that $\eta(\omega, T)$ (reabeled $\eta_{\text{BCS}}(\omega, T)$ for clarity) is much larger than $\eta_{\text{TTF}}(T)$ for $T < T_c$, especially at low frequencies. Figure 3.2 also shows our modified $\eta(\omega, T)$ for comparison, which we list as equation (3.29) and label $\eta_{\text{MTF}}(\omega, T)$ (MTF standing for Modified Two-Fluid) in the figure. Note that while the BCS and MTF values show reasonable agreement, the TTF model is a very different function of temperature, and has no frequency dependence at all. Note also that $\eta(\omega, T)$ can exceed unity, reflecting coherence effects due to the BCS pairing. In the next section, we recast these coherence effects into a more intuitive form.

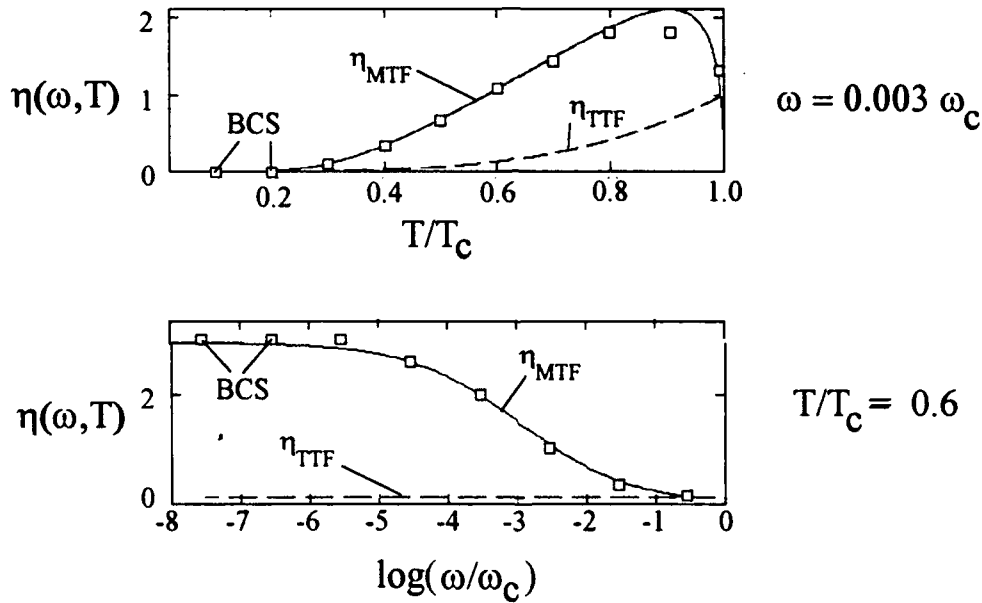


Figure 3.2. $\eta_{\text{MTF}}(\omega, T)$, $\eta_{\text{BCS}}(\omega, T)$ from [1] and $\eta_{\text{TTF}}(T)$ versus ω . $\omega_c = 6.4 \text{ THz}$, $T = 0.5 T_c$, mean free path $l = 2 \text{ nm}$, coherence length $\xi_0 = 2 \text{ nm}$, penetration depth $\lambda(0) = 140 \text{ nm}$, $\Delta_0/k_B T_c = 1.75$.

3.4 Modified Two-Fluid Model

In this section, we will show the modifications and parameter specifications we made to the TTF model in order to improve its accuracy, while keeping its speed and intuitive nature. In Subsection 3.4.1, we lay the necessary groundwork for the MTF model by

carefully defining relationships between parameters in a way consistent to the BCS model. We consider the temperature dependence of $\lambda(T)$ in Subsection 3.4.2, and the reason for a cutoff frequency in the model in Subsection 3.4.3. We discuss the new expression for $\eta(\omega, T)$ in Subsection 3.4.4. We then discuss the MTF model and its application to the sum rule and Kramers-Kronig relations in Subsection 3.4.5.

3.4.1. Parameter Relationships

We find that to fit the BCS results for conductivity with a two fluid model, we must define some parameter relationships in particular ways. The inputs to this model are: the critical temperature T_c , the superconducting gap energy Δ_0 , the penetration depth at zero temperature $\lambda(0)$, and the DC conductivity σ_0 . We chose this combination because T_c and Δ_0 are usually known for a particular material, and σ_0 and $\lambda(0)$ are measurable for a particular sample.

As mentioned in Chapter 2, throughout our numerical simulations we approximate the BCS temperature variation in the gap energy $\Delta(T)$ by [10]

$$\Delta(T) \approx \Delta_0 \left[\cos \left(\frac{\pi}{2} \left(\frac{T}{T_c} \right)^2 \right) \right]^{1/2} \quad (3.18)$$

which stays within 3% of the full BCS results [11].

The ratio of coherence length to mean free path in a superconductor affects the conductivity, thus we must determine this parameter from the inputs. For convenience, we repeat equations (2.1) and (2.2):

$$\xi_0 = \frac{\hbar v_f}{\pi \Delta_0} \quad (3.19)$$

and mean free path is:

$$l = v_f \tau_r \quad (3.20)$$

. The London penetration depth is [7]

$$\lambda_{L,0} = \frac{\tau_r}{\sigma_0 \mu_0} \quad (3.21)$$

Using the above three equations, we can solve for l/ξ_0 in terms of $\lambda_{L,0}$, Δ_0 , and σ_0 :

$$\frac{l}{\xi_0} = \frac{\pi \Delta_0 \lambda_{L,0} \sigma_0 \mu_0}{\hbar} \quad (3.22)$$

Since $\lambda(0)$ is taken as given, we must relate it to $\lambda_{L,0}$, and we restate that relation given in equation (2.3) [9]:

$$\lambda(0) = \lambda_{L,0} \left(1 + \frac{\xi_0}{l} \right)^{1/2} \quad (3.23)$$

Combining this relation with equation (3.22), we find

$$\frac{l}{\xi_0} = \frac{\sigma_0 \lambda^2(0) \mu_0 \pi \Delta_0}{\hbar} - 1 \quad (3.24)$$

from which we can find the transport scattering time τ_{tr} because it is directly proportional to l/ξ_0 (which is derived from equations (3.19) and (3.20)):

$$\tau_r = \frac{\hbar}{\pi \Delta_0} \frac{l}{\xi_0} \quad (3.25)$$

We note that equation (3.23) was developed at zero temperature and so differs from the Gor'kov relationships [22] which are valid near T_c . If the penetration depth near T_c is known, instead of $\lambda(0)$, then the usual Gor'kov and Ginzburg-Landau relations [7, 22] can be used to estimate $\lambda_{L,0}$. One can then find the ratio l/ξ_0 from equation (3.22) and τ_{tr} from equation (3.25) and one can then proceed with the same analysis that follows. (We tried another method of finding τ_{tr} using the sum rule discussed in Subsection 3.4.5, but it did not work. See Appendix D.)

3.4.2 The Temperature Dependence of $\lambda^2(T)$

We must carefully specify the temperature dependence of $\lambda(T)$ (or, equivalently, of $\lambda^2(T)$) to be consistent with the material parameters. The BCS $\lambda^2(T)$ dependence is given approximately by [23]

$$\lambda_{BCS}(T) = \lambda^2(0) / [1 - (T/T_c)^{3-(T/T_c)}] \quad (3.26)$$

However, as shown in Figure 3.3, this dependence is only valid for clean, weakly-coupling superconductors, that is, when ξ_0 is much less than l and $\Delta(T)/k_B T_c$ is about 1.76. When this ratio is larger (on the order of 2 or more) the superconductor is strongly coupled (as with Nb, Nb₃Sn, NbN, etc.). An approximate expression for the strong coupling case is the same as that of the TTF model [20], stated in equation (3.15):

$$\lambda^2(T) = \lambda^2(0) / [1 - (T/T_c)^4]$$

We implemented both of these relationships when we compared our results to BCS calculations of surface resistance in Chapter 4. We show in that comparison the MTF model is more accurate when the λ temperature dependence is properly specified.

However, even if it is not specified properly, the accuracy is not critically affected, as we will show.

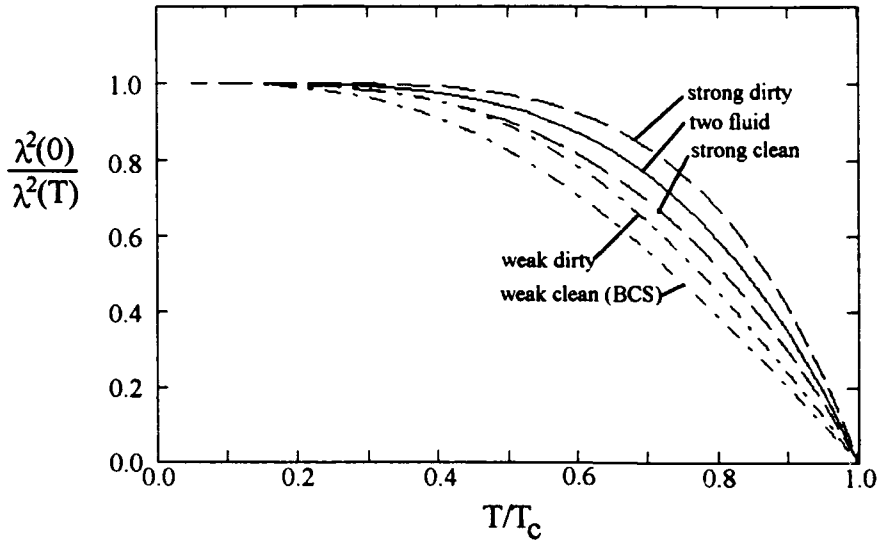


Figure 3.3. Various theoretical temperature dependencies of $\lambda^2(0)/\lambda^2(T)$ (after Figure 9 in [20]).

3.4.3 The Cutoff Frequency

Above a certain frequency, the conductivity of a superconductor behaves more like a normal metal for $T < T_c$. So that our model is accurate across a large range of frequencies, including those above this cutoff frequency, we have specifically modeled this effect. The expression for the cutoff, or gap, frequency is:

$$\omega_s = \frac{1}{\tau_s} = \frac{2\Delta(T)}{\hbar} \quad (3.27)$$

Above the gap frequency electrons have energies which exceed 2Δ . When electrons have this amount of energy, they depair and essentially behave as normal electrons regardless of temperature. This behavior does not occur sharply at the gap frequency, but over a range of frequencies near ω_s . However, because this frequency range is short, it is a reasonable approximation to treat all electrons as normal at or above the gap frequency. Above the gap frequency, then, σ_n is given by the normal state

conductivity equation (3.11), and our equation for the total conductivity at all frequencies is the same as the two-fluid model given in equation (3.14).

3.4.4 The Normal-to-Total Electron Ratio $\eta(\omega, T)$

We now proceed to the major result of our research: to recast BCS conductivity into a two-fluid form by generating the BCS equivalent of the ratio of normal to total electrons $\eta(\omega, T)$ in an analytical form. We assume the two-fluid conductivity equation (3.14) is valid. By equating $\sigma_1(\omega, T)$ from the BCS calculation with that given by the MTF model (equation (3.14)), we define what $\eta(\omega, T)$ must be. In particular, we used a program by Zimmermann [1] to give us the BCS conductivity σ_1^{BCS} , and we used,

$$\sigma_1 = \frac{\sigma_0 \eta(\omega, T)}{1 + (\omega\tau_r)^2} \quad (3.28)$$

(for $\omega > 0$) from the MTF model. One such $\eta(\omega, T)$ function as extracted from the BCS calculations is shown in Figure 3.4 as a surface versus temperature and frequency. Though different material parameters will change the exact value of $\eta(\omega, T)$, the surface plot provides a qualitative feel for how the function behaves.

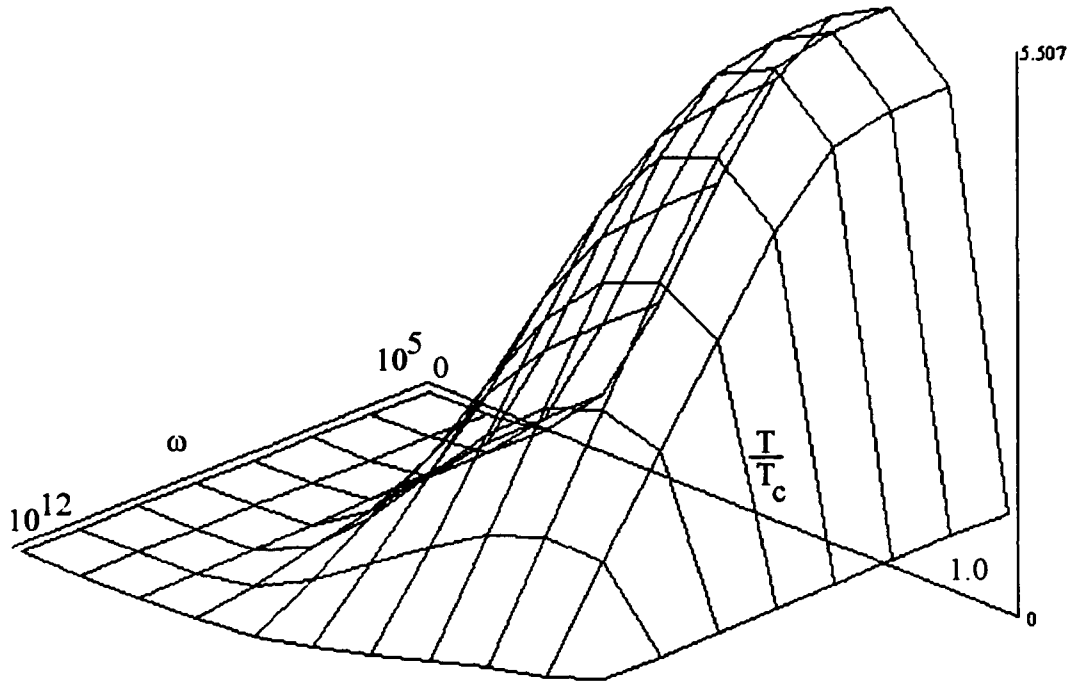


Figure 3.4. $\eta(\omega, T)$ of the MTF model vs. temperature and frequency

After extracting many $\eta(\omega, T)$ for different material parameters, we found an expression that fits the BCS $\eta(\omega, T)$. Moreover, our analytic fit not only allows the two-fluid model to fit to $\sigma_1^{\text{BCS}}(\omega, T)$ but also $\sigma_2^{\text{BCS}}(\omega, T)$. Our fit of $\eta(\omega, T)$ is

$$\eta(\omega, T) = \frac{2\Delta(T)}{k_B T} e^{\frac{-\Delta(T)}{k_B T}} \ln\left(\frac{\Delta(T)}{\hbar\omega_1}\right) \left[\frac{a}{1 + (\omega/\omega_0)^b} + c \right] \quad (3.29)$$

where $\omega_1 = 1$ rad/sec and

$$\frac{a-0.16}{0.17} = \begin{cases} 1 & l/\xi_0 < 1 \text{ and } (\omega/\omega_0)^b < e^3 \\ 1 - (1/3)\log(l/\xi_0) & 1 < l/\xi_0 < 1000 \text{ and } (\omega/\omega_0)^b < e^3 \\ 0 & \text{otherwise} \end{cases} \quad (3.30)$$

$$b \cdot \ln(10) = \begin{cases} 1 + 0.225 \log(l / \xi_0) & l / \xi_0 > 1 \\ 1 & \text{otherwise} \end{cases} \quad (3.31)$$

$$\omega_0 / 2\pi = \begin{cases} 3.98 \cdot 10^9 & l / \xi_0 < 10 \\ \left(\frac{\xi_0}{l}\right)^{0.7} (2.00 \cdot 10^{10}) & \text{otherwise} \end{cases} \quad (3.32)$$

$$c = \begin{cases} \frac{a[(\omega / \omega_0)^b < e^3]}{1 + e^3} & \left(\frac{\omega}{\omega_0}\right)^b > e^3 \\ 0 & \text{otherwise} \end{cases} \quad (3.33)$$

The temperature dependence is similar to a formula from Hinken [10]

$$\eta_H(\omega, T) \approx \frac{2\Delta(T)}{k_B T} e^{-\Delta(T)/k_B T} \ln\left(\frac{\Delta(T)}{\hbar\omega}\right) \quad (3.34)$$

which is an approximation to the Mattis-Bardeen equations under the conditions $\lambda \gg \xi_0$, $\omega \ll \omega_c$ and $k_B T \ll \Delta$ [10]. Figure 3.5 shows the temperature dependence of $\eta(\omega, T)$ (equation (3.29), and again relabeled $\eta_{MTF}(\omega, T)$ for clarity), $\eta_{TF}(T)$ (equation (3.16)), and $\eta_H(\omega, T)$ (equation (3.34)), while Figure 3.6 shows these three equations plotted versus frequency and temperature.

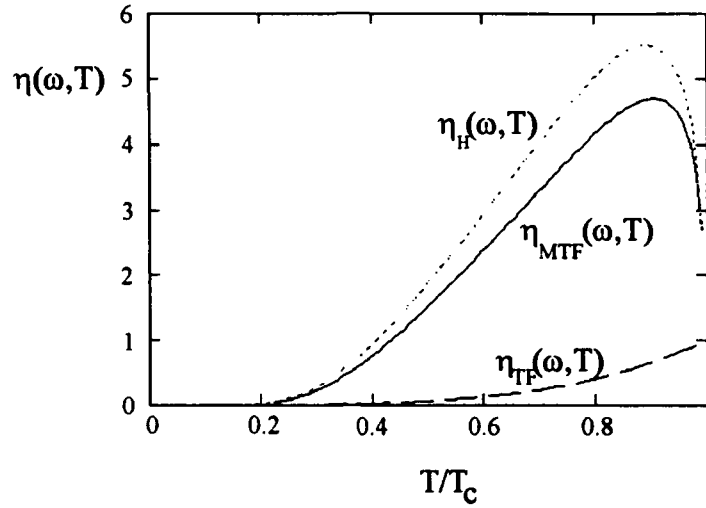


Figure 3.5. $\eta_{MTF}(\omega, T)$, $\eta_H(\omega, T)$ [10] and $\eta_{TF}(T)$ versus T . Frequency = 1GHz, mean free path $l = 2\text{nm}$, coherence length $\xi_0 = 2\text{nm}$, penetration depth $\lambda(0) = 140\text{nm}$, $\Delta_0/k_B T_c = 1.75$.

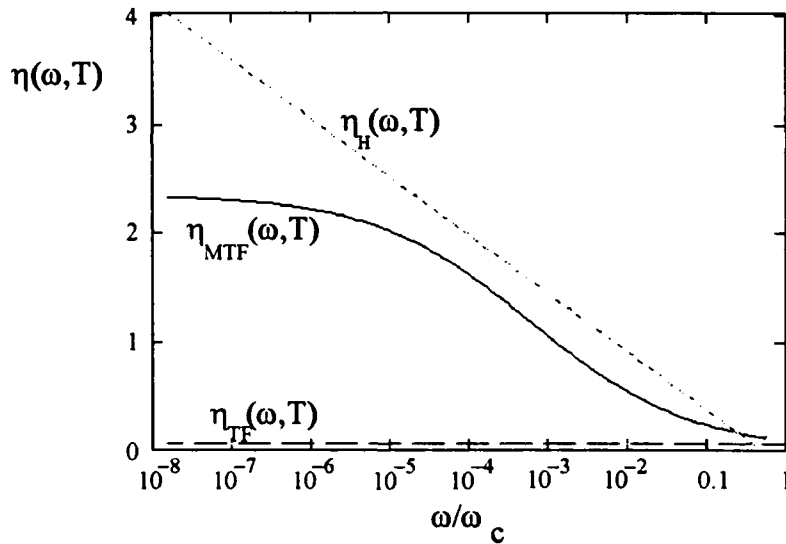


Figure 3.6. $\eta_{MTF}(\omega, T)$, $\eta_H(\omega, T)$ [10] and $\eta_{TF}(T)$ versus ω . $\omega_c = 6.4\text{THz}$, $T = 0.5T_c$, mean free path $l = 2\text{nm}$, coherence length $\xi_0 = 2\text{nm}$, penetration depth $\lambda(0) = 140\text{nm}$, $\Delta_0/k_B T_c = 1.75$.

Note that while our fit and the Hinken expression somewhat agree for a small range of frequencies, the traditional two-fluid model does not follow either. Also note the value of $\eta(\omega, T)$ is often significantly more than unity, as can be seen in Figure 3.4. However, the

above MTF $\eta(\omega, T)$ does fit well with the BCS equivalent as shown in Figure 3.2 for one set of material parameters. Other comparisons to BCS calculations yield similar results. The Hinken expression does not fit well with BCS model (or the MTF model) because it is limited by its frequency approximation. However, the cause of the discrepancy between the MTF (and the BCS) and the TTF models is more fundamental. It is due to coherence effects: neglected by the TTF model, but not negligible in reality.

Coherence effects are the result of the long-range order in the superconductor. The normal-state electrons in the superconductor behave differently than in a normal metal [24], acting in a correlated fashion. Hence their behavior differs from the independent-electron two-fluid model. We kept $\eta(\omega, T)$ and the two-fluid equation, and used BCS theory calculations to determine what $\eta(\omega, T)$ must be in order to get the same behavior from the independent electrons of the two-fluid model that BCS theory gets from its correlated electrons. We discovered that to model correlated electrons with independent electrons, we had to allow $\eta(\omega, T)$ to behave as shown above. As stated above, the Hinken expression, equation (3.34), takes these effects into account for a wide range of temperatures, but only for a limited frequency range. Our equation (3.29) fits a wide frequency range as well. Including these coherence effects in $\eta(\omega, T)$ immediately gives a great deal of accuracy in fitting the conductivity, and hence, accuracy in fitting the surface resistance. We will verify the above statements in the next chapter.

Before discussing the final part of this chapter—the application of the Kramers-Kronig relationships and the sum rule to the MTF model—it is important to note that the MTF model will still give an analytical equation for the surface resistance in a similar manner to equation (3.17). However, this expression is complicated by the form of $\eta(\omega, T)$ and by the dependence of the form of $\lambda(T)$ on material parameters. We can still state that, under the conditions $\omega\tau_{tr} \ll 1$ and $\sigma_2 \gg \sigma_1$ [10] the surface resistance is:

$$R_s = 0.5\mu_0^2 \sigma_0 \lambda^3(T) \omega^2 \eta_{MTF}(\omega, T) \quad (3.35)$$

though we need material parameters to specify the exact relationships for $\eta_{\text{MTF}}(\omega, T)$ and $\lambda(T)$.

3.4.5 The Sum Rule and Kramers-Kronig Relationships

Two important, and related, relationships in superconductors are the Kramers-Kronig relationships and the sum rule. These relationships relate the real and imaginary parts of the conductivity. We will develop both of them following a derivation in [7].

We will first develop the Kramers-Kronig relationships. We have developed a frequency-dependent form for the conductivity, but we can also use that form to find the time-dependent form by doing a Fourier transform. Let us define $\sigma(t, T)$ as the Fourier transform of $\sigma(\omega, T)$. It is intuitive that the conductivity should be causal [7], so we can write $\sigma(t, T)$ in the form $\sigma(t, T)u(t)$, where $u(t)$ is the unit step function: 0 for $t < 0$, and 1 for $t > 0$, to ensure that $\sigma(t, T)$ vanishes for $t < 0$. Since the product of two functions in the time domain is a convolution in the frequency domain [25], we can write

$$\sigma(\omega, T) = \frac{1}{2\pi} \int_{-\infty}^{\infty} \sigma(\omega', T) u(\omega - \omega') d\omega'$$

We know the Fourier transform of the step function is:

$$u(\omega) = \pi\delta(\omega) + 1/j\omega$$

which leads to the following expression:

$$\sigma(\omega, T) = \frac{1}{j\pi} \int_{-\infty}^{\infty} \frac{\sigma(\omega', T)}{\omega - \omega'} d\omega' \quad (3.36)$$

From (3.14), we know the conductivity can be written $\sigma_1(\omega, T) - j\sigma_2(\omega, T)$, and if we substitute this form into equation (3.36) and solve for the real and imaginary parts, we find these two equations result:

$$\sigma_1(\omega, T) = -\frac{1}{\pi} \int_{-\infty}^{\infty} \frac{\sigma_2(\omega', T)}{\omega - \omega'} d\omega' \quad (3.37)$$

$$\sigma_2(\omega, T) = \frac{1}{\pi} \int_{-\infty}^{\infty} \frac{\sigma_1(\omega', T)}{\omega - \omega'} d\omega' \quad (3.38)$$

These two equations are Hilbert transforms of one another [7].

An additional fact is known about $\sigma(t, T)$ —it relates a real current density to a real electric field through Ohm's law. Thus, $\sigma(t, T)$ must be a real function. As a result, we know the Fourier transform of $\sigma(t, T)$ must satisfy $\sigma_1(\omega, T) = \sigma_1(-\omega, T)$ and $\sigma_2(\omega, T) = -\sigma_2(-\omega, T)$ [7]. With these additional relationships, then we can write the Hilbert transforms as

$$\sigma_1(\omega, T) = -\frac{2}{\pi} \int_0^{\infty} \frac{\omega' \sigma_2(\omega', T)}{\omega^2 - \omega'^2} d\omega' \quad (3.39)$$

$$\sigma_2(\omega, T) = \frac{2\omega}{\pi} \int_0^{\infty} \frac{\sigma_1(\omega', T)}{\omega^2 - \omega'^2} d\omega' \quad (3.40)$$

These two equations are the Kramers-Kronig relations [7].

The sum rule follows from the Kramers-Kronig relations. First, it is noted that, as was discussed in Subsection 3.4.3, when the frequency is much greater than the gap frequency, the electrons are essentially all in the normal state. Thus, we can state

$$\lim_{\omega\tau_s \gg 1} \sigma_T(\omega, T) = \sigma_n(\omega)$$

where $\sigma_n(\omega)$ is the normal state resistance of equation (3.11). In the limit where $\omega\tau_s \gg 1$ and $\omega\tau_{tr} \gg 1$, then, we see that

$$\lim_{\substack{\omega\tau_s \gg 1 \\ \omega\tau_{tr} \gg 1}} \sigma(\omega, T) = \lim_{\omega\tau_{tr} \gg 1} \sigma_n(\omega) = -j \frac{\sigma_0}{\omega\tau_{tr}}$$

which gives the relation

$$\lim_{\omega \rightarrow \infty} \omega \sigma_T(\omega, T) = -j \frac{\sigma_0}{\tau_r}$$

but since $\sigma_T(\omega, T) = \sigma_1(\omega, T) - j\sigma_2(\omega, T)$, it is equivalent to

$$\lim_{\omega \rightarrow \infty} [\omega \sigma_1(\omega, T) - j\omega \sigma_2(\omega, T)] = -j \frac{\sigma_0}{\tau_r}$$

Solving for the real and imaginary parts,

$$\lim_{\omega \rightarrow \infty} [\omega \sigma_1(\omega, T)] = 0 \quad (3.41)$$

and

$$\lim_{\omega \rightarrow \infty} [\omega \sigma_2(\omega, T)] = \frac{\sigma_0}{\tau_r} \quad (3.42)$$

Equation (3.41) is redundant, because it is the same result as the high-frequency limit in equation (3.39). However, combining equation (3.42) with the Kramers-Kronig relation (3.40) yields

$$\lim_{\omega \rightarrow \infty} [\omega \sigma_2(\omega, T)] = \frac{2}{\pi_0} \int_0^{\infty} \sigma_1(\omega', T) d\omega' = \frac{\sigma_0}{\tau_r} \quad (3.43)$$

and hence

$$\int_0^{\infty} \sigma_1(\omega', T) d\omega' = \frac{\pi \sigma_0}{2 \tau_r} \quad (3.44)$$

This relation is known as the sum rule for conductivity [7].

We will now apply the Kramers-Kronig relations and the sum rule to the MTF model. The ideal cutoff frequency in equation (3.14) implies that the MTF model σ cannot satisfy the Kramers-Kronig relationships because the model is analogous to a system with ideal high-pass and low-pass filters. Because the time-domain representation of an ideal filter shows that input from past and future time is needed to determine the signal at the

present time, the model is non-causal [25]. Nevertheless, when the zero frequency part of σ , $\pi\delta(\omega)/\mu_0\lambda^2(T)$ [7], is included in σ_1 , we have found the MTF model numerically satisfies the sum rule. We also will show in Chapter 4 that the imaginary and real parts of the surface impedance match well with the BCS calculations (which do satisfy the Kramers-Kronig relations). Since the complex surface impedance follows directly from the complex conductivity, we see that the ideal filter approximation is still adequate here, just as it is for many applications in system analysis.

It is important to note that we initially tried to find $\eta(\omega, T)$ by constraining the TTF model, modified to include the energy gap, by the sum rule and solving for $\eta(\omega, T)$. Our result for $\eta(\omega, T)$ was:

$$\eta(\omega, T) = 1 - [1 - (T/T_c)^4] \frac{\tan^{-1}[\tau_r / \tau_s(0)]}{\tan^{-1}[\tau_r / \tau_s(T)]} \quad (3.45)$$

While this may seem to be a good idea, it still does not work, because it relies on the basic assumption of the two-fluid model that electrons are independent. However, as we have shown, electrons are not independent, and thus, in order to be accurate, the two-fluid model requires modification that goes beyond its assumptions. (See Appendix D for a more complete explanation.) In the next chapter, we show that once such modification has been made, there is very good agreement between the BCS model and the MTF model surface resistance calculations.

Chapter 4

Surface Impedance Results

4.1 Introduction

Having developed and described the MTF model, we now show how it compares to BCS calculations, and to surface resistance data. In this chapter, we first show how the MTF model compares to the BCS surface resistance and reactance calculations of [2] (Section 4.2). We compare the MTF and BCS calculations to another model for surface resistance given in [26] in Section 4.3. We then show how it compares with surface resistance data from Nb (Section 4.4), Nb₃Sn (Section 4.5), and YBa₂Cu₃O_{7- δ} (Section 4.6). We will now begin to compare the MTF model calculations to BCS calculations.

4.2 Comparison to BCS Calculations

We have compared our MTF model with BCS calculations for surface impedance across a wide range of coupling strength, cleanliness/dirtiness, frequency, and temperature. After calculating the conductivity with the MTF model, we used equation (1.5) to calculate the surface impedance. The real component of that result is the surface resistance we used to compare with the BCS calculations.

The BCS values were obtained from Halbritter's code [2] translated into C (see Appendix C) using identical inputs to the MTF model. There are four numbers the

Halbritter program calculates for a given temperature and frequency, as discussed in chapter 2: the surface resistance and penetration depth under spectral reflection at the boundary, and the surface resistance and penetration depth under diffuse reflection at the boundary. Because the parameters we used were similar to YBCO parameters, it seemed reasonable to use the diffuse boundary condition for the surface resistance calculations. The surface resistance and penetration depths were systematically lower than the numbers under spectral reflection conditions, but generally by less than 30%. To get a fit that is comparable to the one presented here for spectral reflection conditions, we found that multiplying the MTF function for $\eta(\omega, T)$ as given in equation (3.28) by a constant of 1.3 is all that is necessary.

On the other hand, because the penetration depth we used matched the output of the Halbritter program under spectral surface reflection, it seemed reasonable to use that output rather than the output for diffuse reflection. There may appear to be some inconsistency in using one set of numbers for the surface resistance and another set for the surface reactance, but they are quite separate. If we do change $\eta(\omega, T)$ by the 30% necessary to get a good comparison with the spectral results, we leave the surface reactance results almost totally unaffected, because $\eta(\omega, T)$ has a very small effect on the surface reactance, as we show in Subsection 4.2.2. Moreover, if we made no adjustment to $\eta(\omega, T)$ and did the comparison, the results would only be about 30% off either way. Hence it makes little difference which set of numbers are used in each comparison.

As stated above, we used parameters similar to YBCO for our comparisons. We assumed a T_c of 91.8K, a penetration depth of 140nm at zero temperature, and a coherence length of 2nm. In addition, each case shown here was tested at 10GHz. (However, similar results are obtained at different frequencies.) Moreover, we swept the temperature for each case from $0.022T_c$ to $0.94T_c$ with a step size of $0.022T_c$. These parameters and conditions remained unchanged throughout our tests.

We changed the ratios $\Delta_0/k_B T_C$ and $1/\xi_0$ in our tests. We tested the MTF model from the weak-coupling limit ($\Delta_0/k_B T_C = 1.75$) to the strong-coupling limit ($\Delta_0/k_B T_C = 2.75$) in increments of 0.25. For each value of $\Delta_0/k_B T_C$, we swept $1/\xi_0$ from the dirty limit ($1/\xi_0 = 0.01$) to the clean limit ($1/\xi_0 = 100$). The following figure shows the values of these ratios for our comparisons in a "parameter space," where one dimension is the ratio $1/\xi_0$ and the other is $\Delta_0/k_B T_C$. Each point corresponds to a set of parameters where the models were compared, and each point inside a circle corresponds to a figure below which graphically shows the comparison.

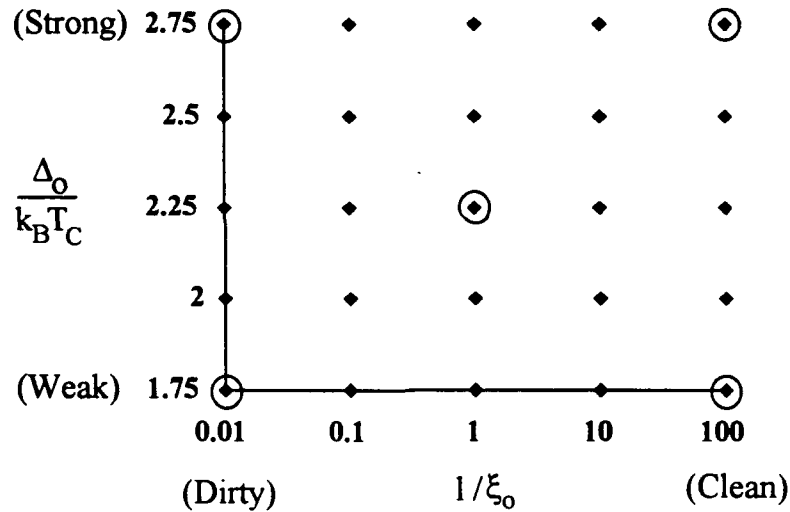


Figure 4.1 "Parameter space" representation of the comparisons of the MTF model with the BCS calculations. Each point indicates a set of parameters where a comparison was made. Each point with a circle around it corresponds to a figure graphically comparing the BCS and MTF model calculations for that set of parameters.

We present the results of our comparisons in the next two subsections, starting with the surface resistance comparison.

4.2.1 Surface Resistance Comparison of BCS and MTF Models

Below are the five figures that correspond to the five circled points in Figure 4.1, and show the weak-clean case, weak-dirty case, strong-clean case and strong-dirty case, and a case in the middle of all extremes. In all five figures, the MTF model used a penetration depth proportional to $(1-(T/T_c)^3-T/T_c)^{-1/2}$.

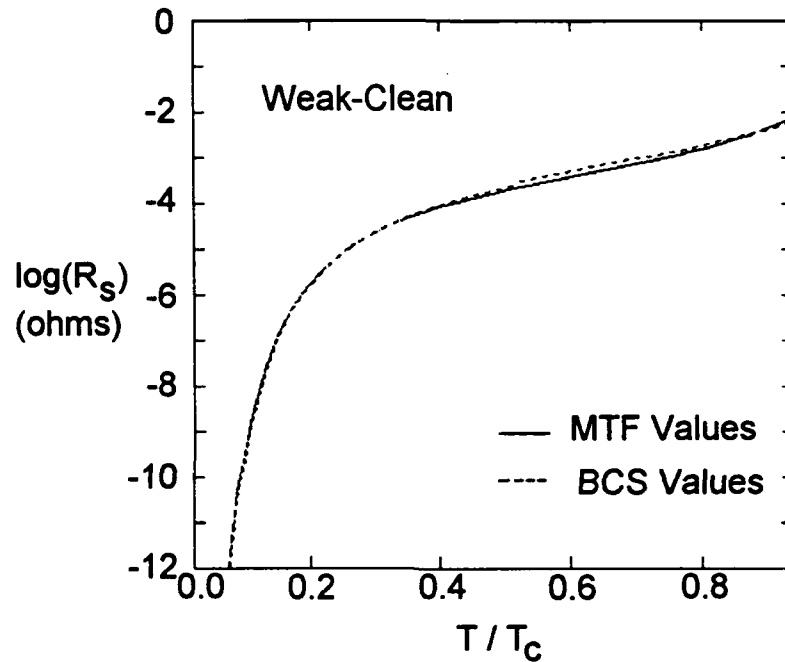


Figure 4.2. Weak-clean comparison to BCS calculations (using [2]) from $0.022T_c$ to $0.94T_c$. Penetration depth temperature dependence is proportional to $(1-(T/T_c)^3-T/T_c)^{-1/2}$. $\Delta_0/k_B T_c = 1.75$, $\lambda(0) = 140\text{nm}$, $\xi_0 = 2\text{nm}$, $l = 200\text{nm}$, Frequency = 10GHz.

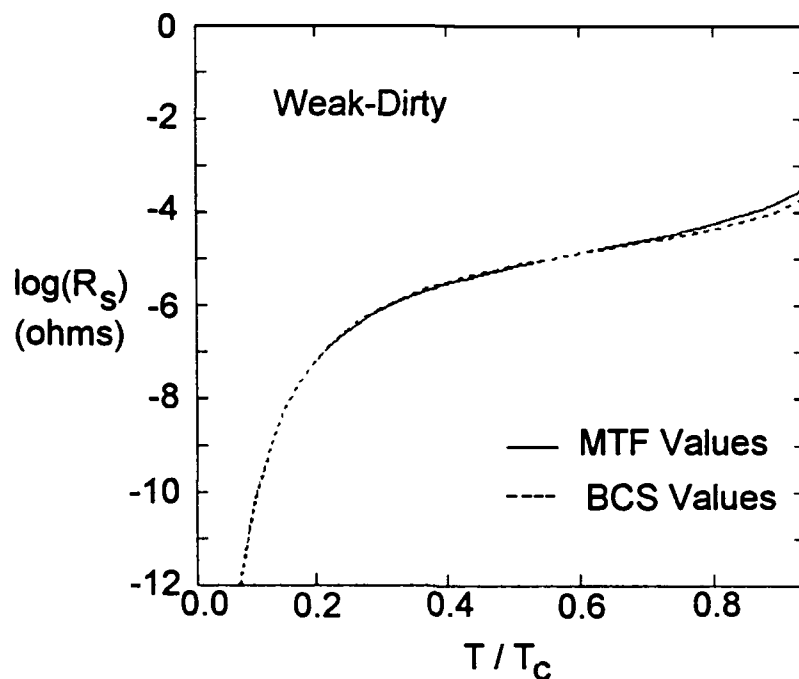


Figure 4.3. Weak-dirty comparison to BCS calculations (using [2]) from $0.022T_c$ to $0.94T_c$. Penetration depth temperature dependence is proportional to $(1-(T/T_c)^3-T/T_c)^{-1/2}$. $\Delta_0/k_B T_c = 1.75$, $\lambda(0) = 140\text{nm}$, $\xi_0 = 2\text{nm}$, $l = 0.02\text{nm}$, Frequency = 10GHz .

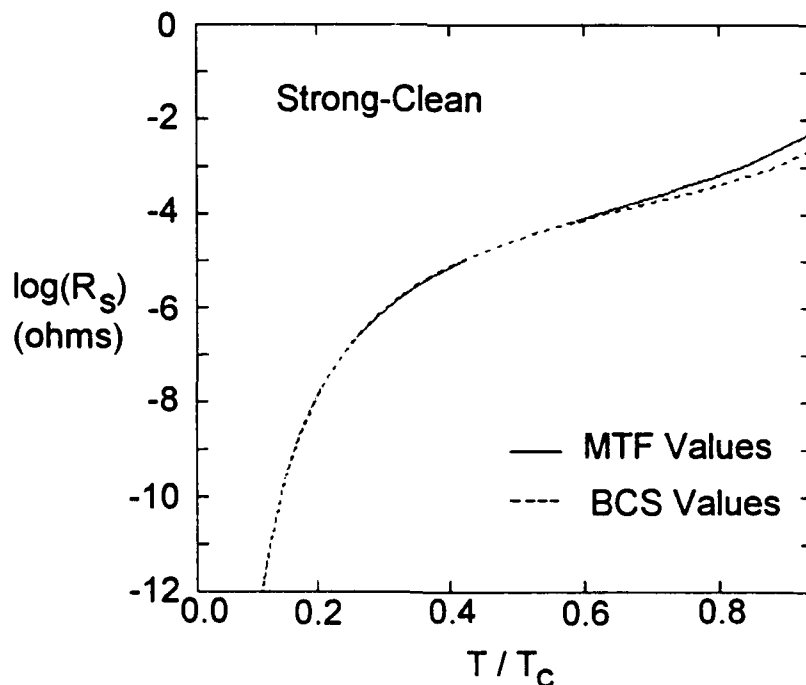


Figure 4.4. Strong-clean comparison to BCS calculations (using [2]) from $0.022T_c$ to $0.94T_c$. Penetration depth temperature dependence is proportional to $(1-(T/T_c)^3-T/T_c)^{-1/2}$. $\Delta_0/k_B T_c = 2.75$, $\lambda(0) = 140\text{nm}$, $\xi_0 = 2\text{nm}$, $l = 200\text{nm}$, Frequency = 10GHz .

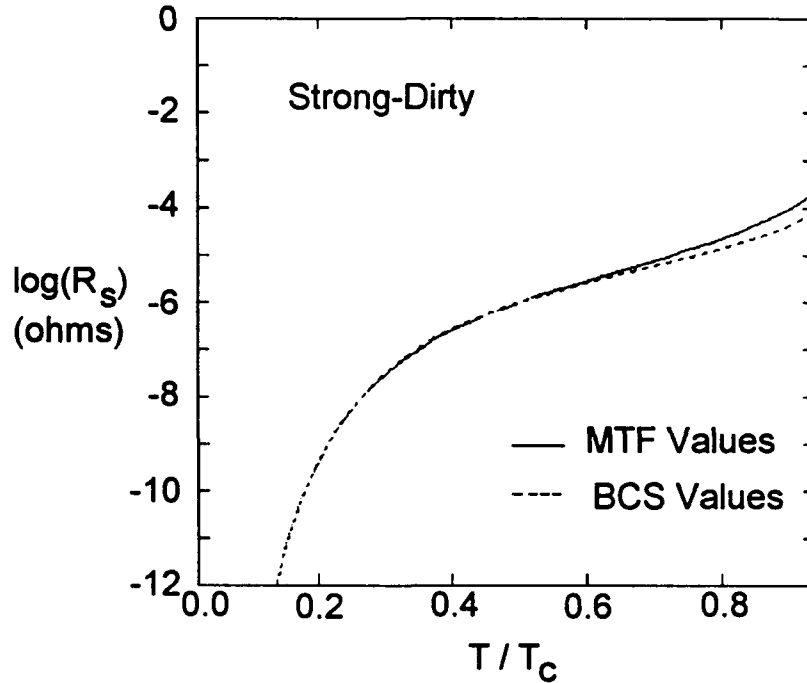


Figure 4.5. Strong-dirty comparison to BCS calculations (using [2]) from $0.022T_c$ to $0.94T_c$. Penetration depth temperature dependence is proportional to $(1-(T/T_c)^3 - T/T_c)^{-1/2}$. $\Delta_0/k_B T_c = 2.75$, $\lambda(0) = 140\text{nm}$, $\xi_0 = 2\text{nm}$, $l = 0.02\text{nm}$, Frequency = 10GHz .

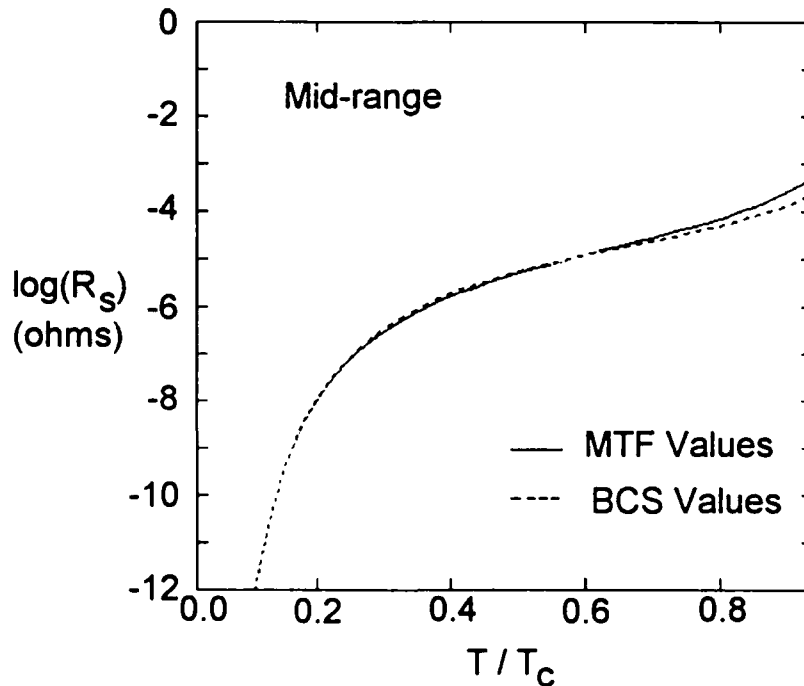


Figure 4.6. Mid-range comparison to BCS calculations (using [2]) from $0.022T_c$ to $0.94T_c$. Penetration depth temperature dependence is proportional to $(1-(T/T_c)^3 - T/T_c)^{-1/2}$. $\Delta_0/k_B T_c = 2.25$, $\lambda(0) = 140\text{nm}$, $\xi_0 = 2\text{nm}$, $l = 2\text{nm}$, Frequency = 10GHz .

While the plots above show a reasonable qualitative fit in the extreme material parameter cases, particular'y when the material is weakly coupled, we also did a more quantitative fit using all the points shown in Figure 4.1. For each set of parameters, we took the ratio of the MTF surface resistance to the BCS value at each temperature across the full range from $0.022T_c$ to $0.94T_c$. For each set of parameters, we found the mean of these ratios (the closer this mean is to one, the better the fit). We also found the standard deviation of this mean for each case (the smaller the deviation, the more consistent the fitting error). Figure 4.7 shows our results for all cases when the MTF model used the BCS penetration depth temperature dependence proportional to $(1-(T/T_c)^3-T/T_c)^{-1/2}$.

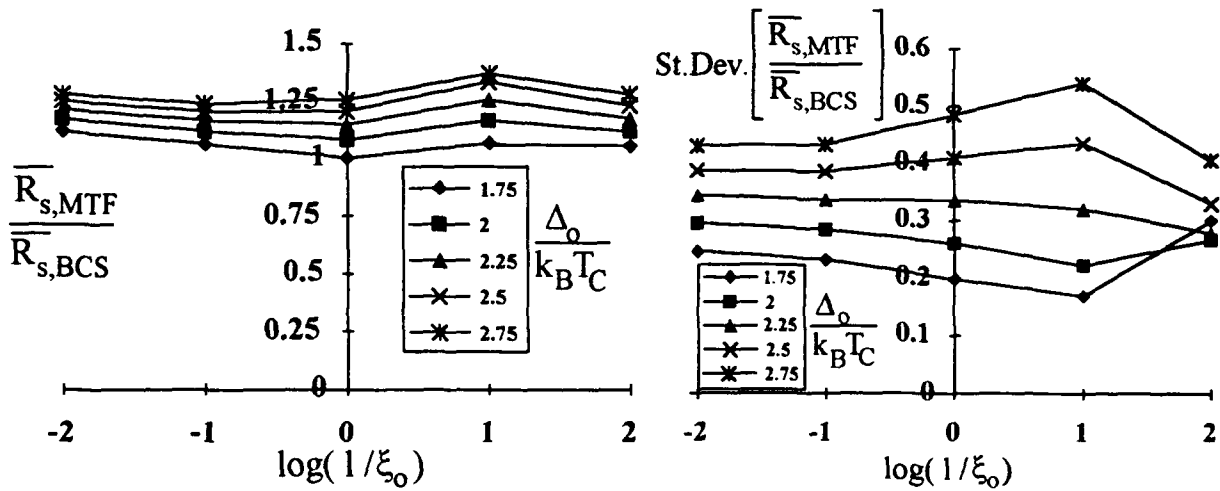


Figure 4.7. MTF model surface resistance/BCS surface resistance mean comparison for clean to dirty and strong to weak parameters. The mean is taken across a temperature range from $0.022T_c$ to $0.94T_c$. Penetration depth temperature dependence is proportional to $(1-(T/T_c)^3-T/T_c)^{-1/2}$. $\lambda(0) = 140\text{nm}$, $\xi_0 = 2\text{nm}$, Frequency = 10GHz.

Figure 4.7 allows one to see the range of parameters the MTF model can handle with accuracy. On the average, the fit to BCS values is off by only a small percentage over the entire parameter range. The MTF model is best under weak-coupling conditions, and gets systematically worse with coupling strength. The consistency of the fit to BCS is also generally worse with higher coupling strengths. However, this systematic error is

expected, because the penetration depth temperature dependence we used is only accurate in the weak-coupling case. In the strong-coupling case, the actual penetration depth is smaller than this dependence predicts, as shown in Figure 3.3, and this effect is particularly significant at high temperature. Notice that in the preceding figures showing the extreme cases, one can also see a divergence between the MTF and the BCS values at high temperature in the strong-coupling cases. While this divergence is still small, on the order of a factor of 2 at worst, it can be decreased significantly by using a proper temperature dependence of the penetration depth. The temperature dependence of the penetration depth seems to be closer to $(1-(T/T_c)^3-T/T_c)^{-1/2}$ as the material becomes more weakly-coupled, and next we will do the same analysis as above, only with a penetration depth temperature dependence in the MTF model proportional to $(1-(T/T_c)^4)^{-1/2}$ to show the difference this dependence makes.

We begin with the same five figures showing the extreme parameter cases.

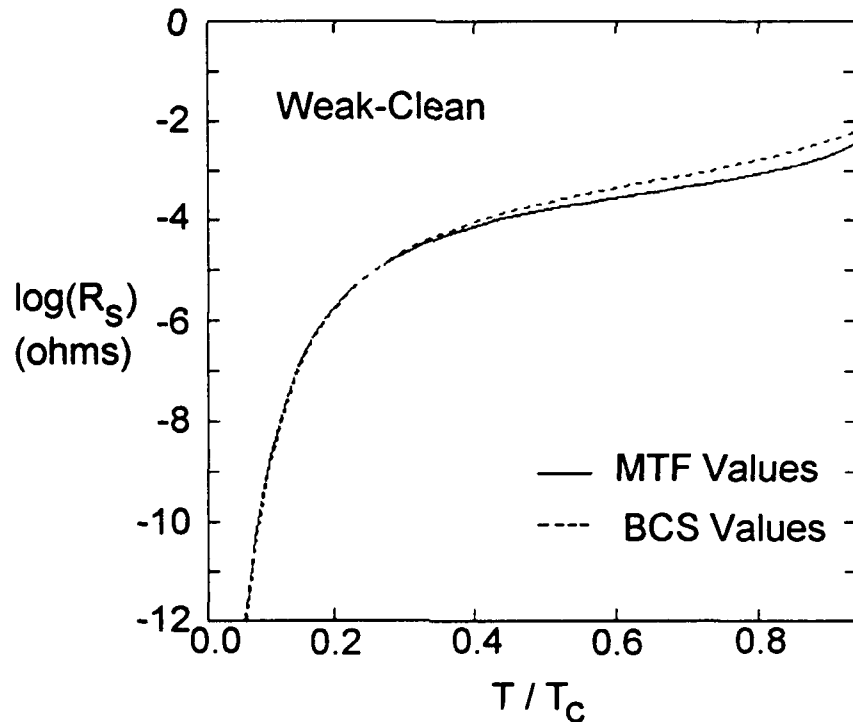


Figure 4.8. Weak-clean comparison to BCS calculations (using [2]) from $0.022T_c$ to $0.94T_c$. Penetration depth temperature dependence is proportional to $(1-(T/T_c)^4)^{-1/2}$. $\Delta_0/k_B T_c = 1.75$, $\lambda(0) = 140\text{nm}$, $\xi_0 = 2\text{nm}$, $l = 200\text{nm}$, Frequency = 10GHz.

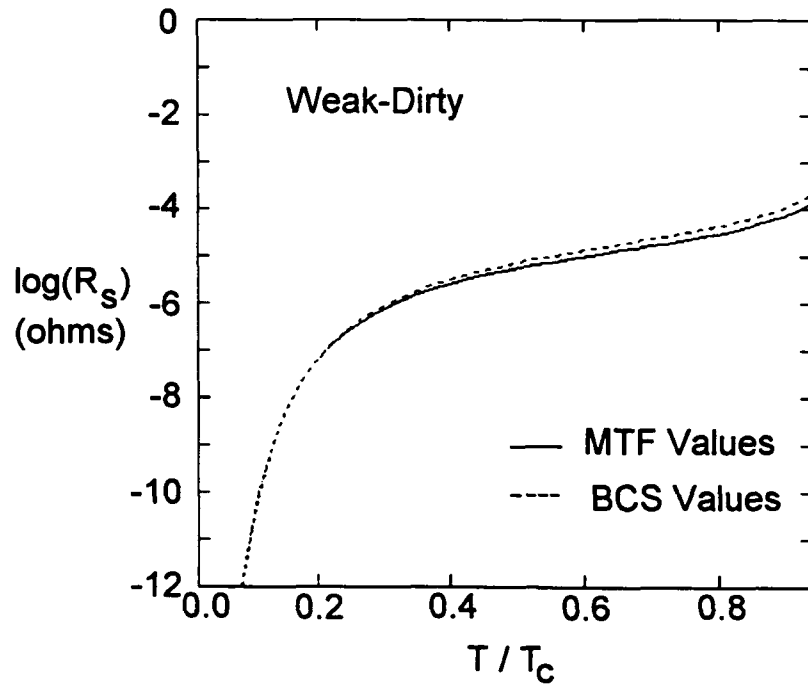


Figure 4.9. Weak-dirty comparison to BCS calculations (using [2]) from $0.022T_c$ to $0.94T_c$. Penetration depth temperature dependence is proportional to $(1-(T/T_c)^4)^{-1/2}$. $\Delta_0/k_B T_c = 1.75$, $\lambda(0) = 140\text{nm}$, $\xi_0 = 2\text{nm}$, $l = 0.02\text{nm}$, Frequency = 10GHz.

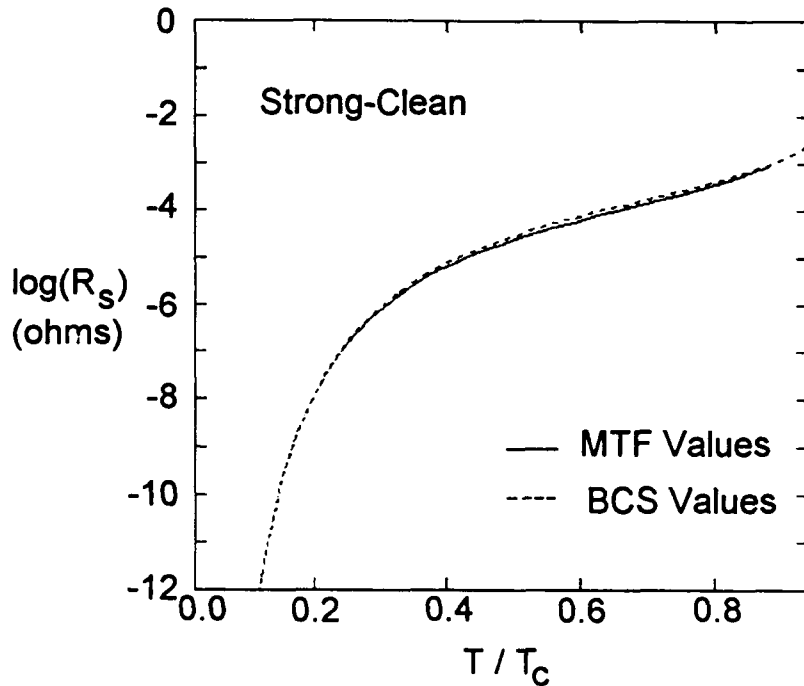


Figure 4.10. Strong-clean comparison to BCS calculations (using [2]) from $0.022T_c$ to $0.94T_c$. Penetration depth temperature dependence is proportional to $(1-(T/T_c)^4)^{-1/2}$. $\Delta_0/k_B T_c = 2.75$, $\lambda(0) = 140\text{nm}$, $\xi_0 = 2\text{nm}$, $l = 200\text{nm}$, Frequency = 10GHz.

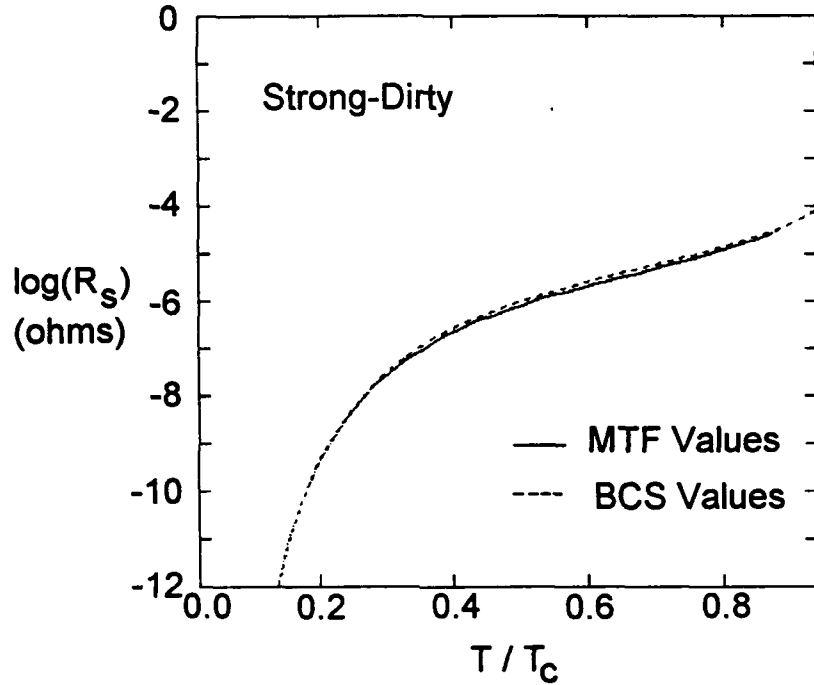


Figure 4.11. Strong-dirty comparison to BCS calculations (using [2]) from $0.022T_c$ to $0.94T_c$. Penetration depth temperature dependence is proportional to $(1-(T/T_c)^4)^{-1/2}$. $\Delta_0/k_B T_c = 2.75$, $\lambda(0) = 140\text{nm}$, $\xi_0 = 2\text{nm}$, $l = 0.02\text{nm}$, Frequency = 10GHz.

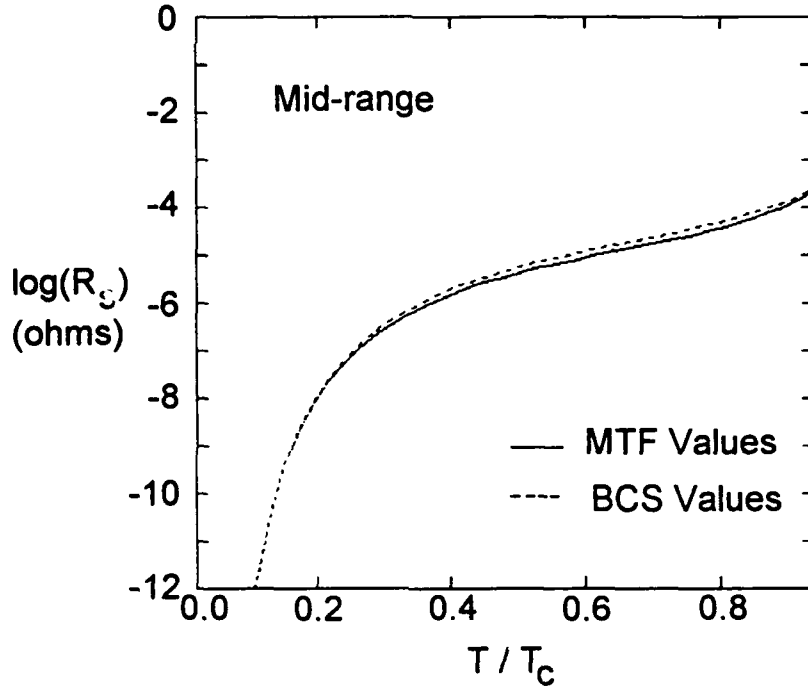


Figure 4.12. Mid-range comparison to BCS calculations (using [2]) from $0.022T_c$ to $0.94T_c$. Penetration depth temperature dependence is proportional to $(1-(T/T_c)^4)^{-1/2}$. $\Delta_0/k_B T_c = 2.25$, $\lambda(0) = 140\text{nm}$, $\xi_0 = 2\text{nm}$, $l = 2\text{nm}$, Frequency = 10GHz.

Notice that this time, the strong-coupling cases show a good fit across the whole temperature range, while the weak-coupling figures show a divergence consistent with the fact that the penetration depth predicted by the $(1-(T/T_c)^4)^{-1/2}$ temperature dependence is too small in the weak-coupling case.

Once again, we also do a more comprehensive and quantitative analysis of the comparison. Figure 4.13 presents the same data as Figure 4.7 when the MTF model uses the penetration depth temperature dependence proportional to $(1-(T/T_c)^4)^{-1/2}$.

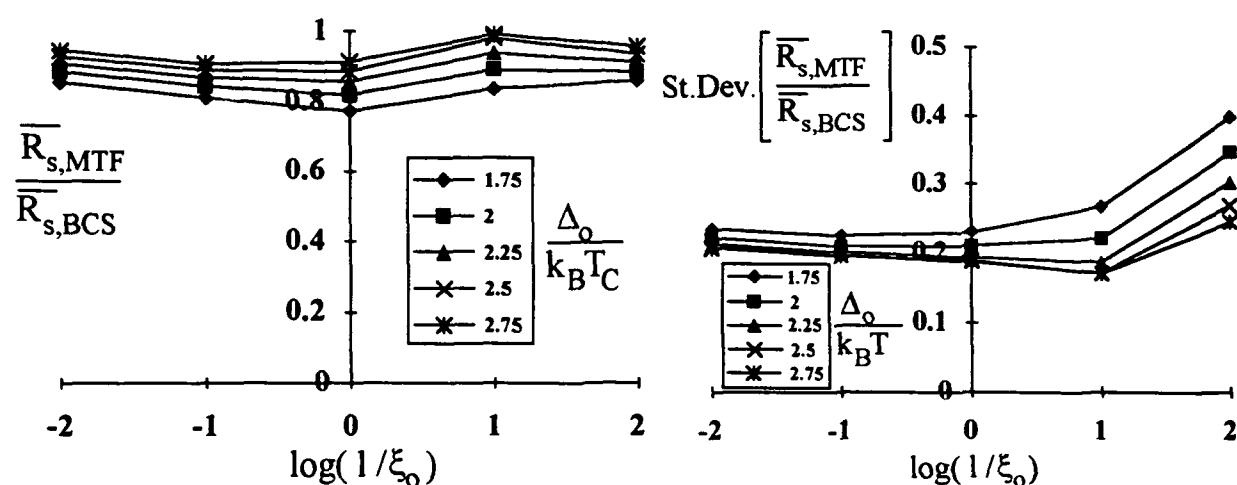


Figure 4.13. MTF model surface resistance/BCS surface resistance mean comparison for clean to dirty and strong to weak parameters. The mean is taken across a temperature range from $0.022T_c$ to $0.94T_c$. Penetration depth temperature dependence is proportional to $(1-(T/T_c)^4)^{-1/2}$. $\lambda(0) = 140\text{nm}$, $\xi_0 = 2\text{nm}$, Frequency = 10GHz.

Notice again that the fit is better when the material is stronger-coupling, and that the weaker the coupling strength, the lower the mean. However, while in Figure 4.7 the standard deviation seemed only dependent on the coupling strength, here it seems to be dependent on both the coupling strength and the cleanliness of the material. The results here indicate the cleaner the material, the less consistent the fit. Even so, the fit to BCS is still good to within a factor of order 2 at all points, and if care is taken to properly specify the penetration depth temperature dependence, the surface resistance of the MTF model

fits the BCS model well. Having compared the surface resistance calculations, we now move on to the surface reactance comparison, where we can confirm directly the form of the penetration depth temperature dependence.

4.2.2 Surface Reactance Comparison of BCS and MTF Models

Halbritter's program output includes a value for the penetration depth. Using this value, and the relation $X = \omega\mu_0\lambda$ from [2], one can get the BCS value for the surface reactance X . The MTF model will give the surface reactance as well, if we use the imaginary component of the surface impedance instead of the real component. In this subsection, we cover the same parameter space as in the previous section, and do the same kind of analysis, only the variable on the y-axis in this section is the surface reactances.

The analytical form for the surface reactance from the two-fluid model is simpler than the surface resistance, being only $X = \omega\mu_0\lambda$ under the conditions $\omega\tau_{tr} \ll 1$ and $\sigma_1 \ll \sigma_2$. Hence we expect that the surface reactance would be less complicated and easier to fit than the surface resistance, and we find this is the case.

The following five figures show the extremes of the parameter space, as was shown in the previous subsection. However, this time the axes of the graphs are scaled linearly, instead of logarithmically, because the difference between the MTF and BCS values is slight, and the values for surface reactance do not change a great deal over the temperature range. We first show plots with the penetration depth of the MTF model proportional to $(1-(T/T_c)^3-T/T_c)^{-1/2}$.

Because the MTF model and BCS model are so close in surface reactance values, we will only show the plots of the extreme cases (and the mid-range case), with a table showing the means and standard deviations of these extremes, for each both penetration depth temperature dependences: $(1-(T/T_c)^3-T/T_c)^{-1/2}$ and $(1-(T/T_c)^4)^{-1/2}$. We begin by showing the extreme cases with a temperature dependence of $(1-(T/T_c)^3-T/T_c)^{-1/2}$.

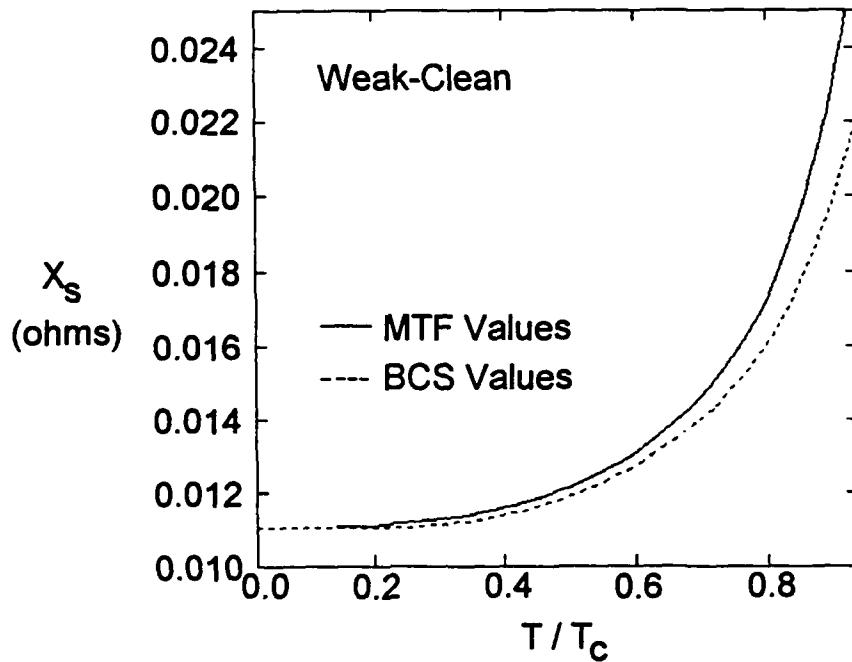


Figure 4.14. Weak-clean comparison to BCS calculations (using [2]) from $0.022T_c$ to $0.94T_c$. Penetration depth temperature dependence is proportional to $(1-(T/T_c)^3-T/T_c)^{-1/2}$. $\Delta_0/k_B T_c = 1.75$, $\lambda(0) = 140\text{nm}$, $\xi_0 = 2\text{nm}$, $l = 200\text{nm}$, Frequency = 10GHz .

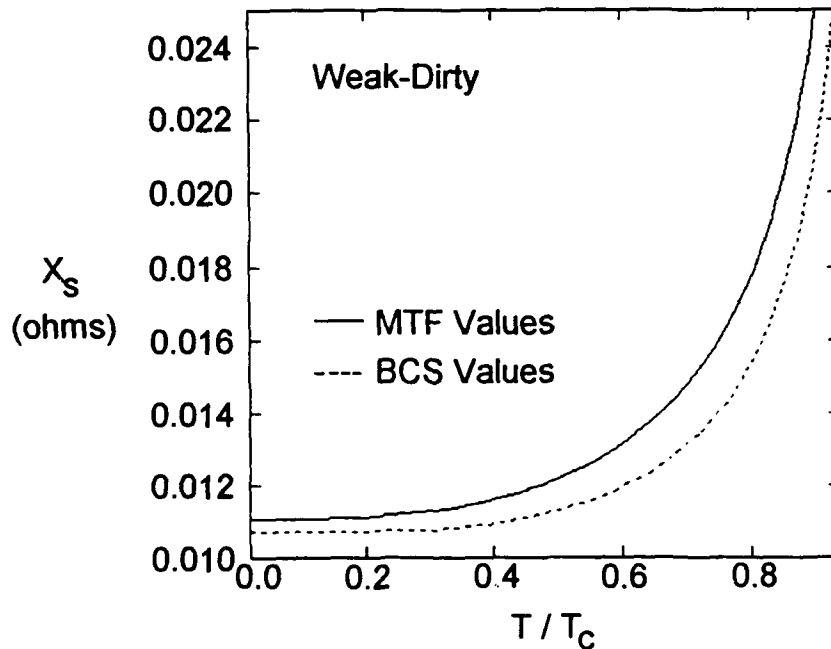


Figure 4.15. Weak-dirty comparison to BCS calculations (using [2]) from $0.022T_c$ to $0.94T_c$. Penetration depth temperature dependence is proportional to $(1-(T/T_c)^3-T/T_c)^{-1/2}$. $\Delta_0/k_B T_c = 1.75$, $\lambda(0) = 140\text{nm}$, $\xi_0 = 2\text{nm}$, $l = 0.02\text{nm}$, Frequency = 10GHz .

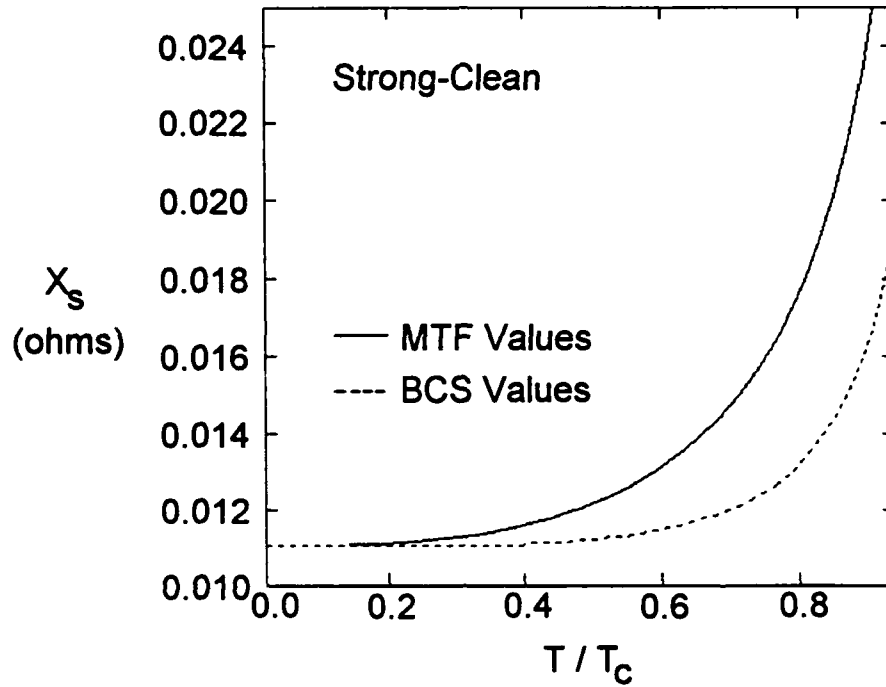


Figure 4.16. Strong-clean comparison to BCS calculations (using [2]) from $0.022T_c$ to $0.94T_c$. Penetration depth temperature dependence is proportional to $(1-(T/T_c)^3-T/T_c)^{-1/2}$. $\Delta_0/k_B T_c = 2.75$, $\lambda(0) = 140\text{nm}$, $\xi_0 = 2\text{nm}$, $l = 200\text{nm}$, Frequency = 10GHz .

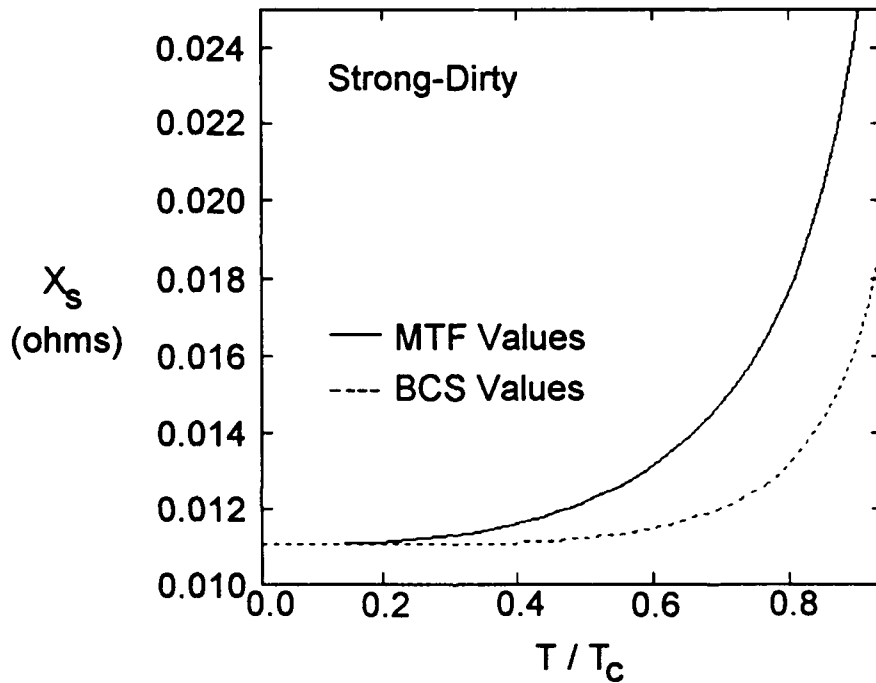


Figure 4.17. Strong-dirty comparison to BCS calculations (using [2]) from $0.022T_c$ to $0.94T_c$. Penetration depth temperature dependence is proportional to $(1-(T/T_c)^3-T/T_c)^{-1/2}$. $\Delta_0/k_B T_c = 2.75$, $\lambda(0) = 140\text{nm}$, $\xi_0 = 2\text{nm}$, $l = 0.02\text{nm}$, Frequency = 10GHz .

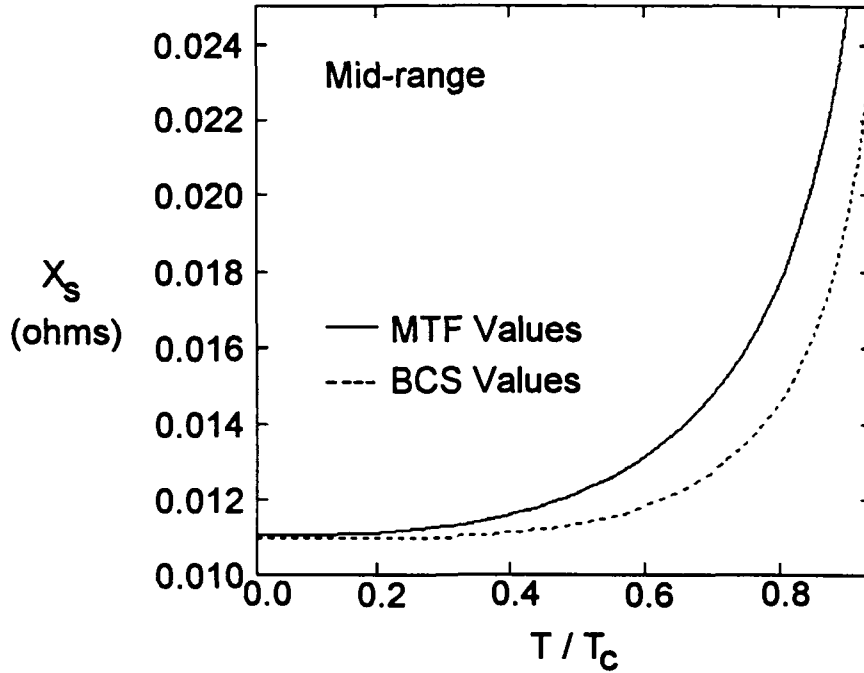


Figure 4.18. Mid-range comparison to BCS calculations (using [2]) from $0.022T_c$ to $0.94T_c$. Penetration depth temperature dependence is proportional to $(1-(T/T_c)^3-T/T_c)^{-1/2}$. $\Delta_0/k_B T_c = 2.25$, $\lambda(0) = 140\text{nm}$, $\xi_0 = 2\text{nm}$, $l = 2\text{nm}$, Frequency = 10GHz .

Notice again the trend toward more inaccuracy at high temperature as the coupling strength increases. Below we tabulate the means and standard deviations of the extreme cases shown above to give a more quantitative measure of this trend. (Although a graph was more revealing in the last subsection, since there are only a few values, a table is easier to read.)

$\Delta_0/k_B T_c$	Mean(X_s MTF/ X_s BCS)			Std. Dev.(X_s MTF/ X_s BCS)		
	(clean)	$\log(1/\xi_0)$	(dirty)	(clean)	$\log(1/\xi_0)$	(dirty)
	2	0	-2	2	0	-2
1.75	1.039		1.088	0.049		0.049
2.25		1.099			0.091	
2.75	1.142		1.149	0.156		0.170

Table 4.1. MTF model surface resistance/BCS surface resistance mean comparison for clean to dirty and strong to weak parameters. The mean is taken across a temperature range from $0.022T_c$ to $0.94T_c$. Penetration depth temperature dependence is proportional to $(1-(T/T_c)^3-T/T_c)^{-1/2}$. $\lambda(0) = 140\text{nm}$, $\xi_0 = 2\text{nm}$, Frequency = 10GHz .

The trend mentioned above is further substantiated by Table 4.1, since the fits are most accurate under weak-coupling and worst under strong-coupling. They are also slightly worse in the dirty case than in the clean case, which is expected from Figure 3.3. To complete our comparison, we will do the same plots below using a penetration depth proportional to $(1-(T/T_c)^4)^{-1/2}$.

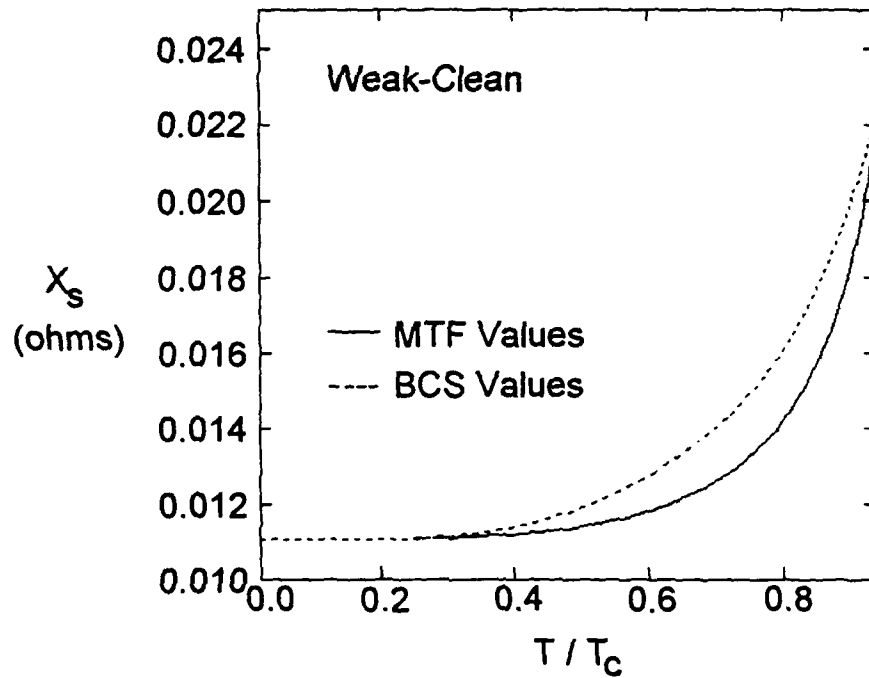


Figure 4.19. Weak-clean comparison to BCS calculations (using [2]) from $0.022T_c$ to $0.94T_c$. Penetration depth temperature dependence is proportional to $(1-(T/T_c)^4)^{-1/2}$. $\Delta_0/k_B T_c = 1.75$, $\lambda(0) = 140\text{nm}$, $\xi_0 = 2\text{nm}$, $l = 200\text{nm}$, Frequency = 10GHz.

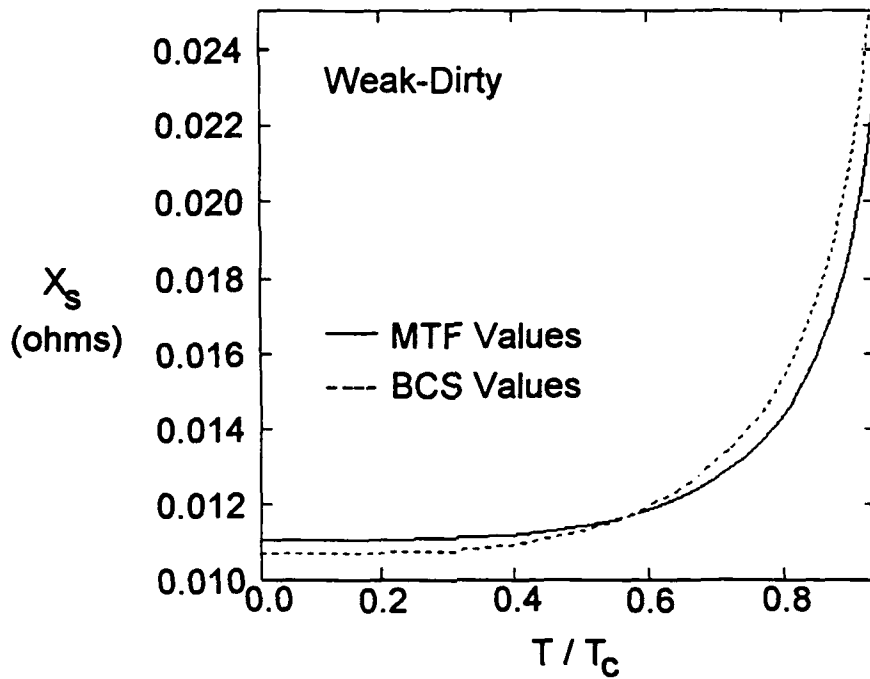


Figure 4.20. Weak-dirty comparison to BCS calculations (using [2]) from $0.022T_c$ to $0.94T_c$. Penetration depth temperature dependence is proportional to $(1-(T/T_c)^4)^{-1/2}$. $\Delta_0/k_B T_c = 1.75$, $\lambda(0) = 140\text{nm}$, $\xi_0 = 2\text{nm}$, $l = 0.02\text{nm}$, Frequency = 10GHz.

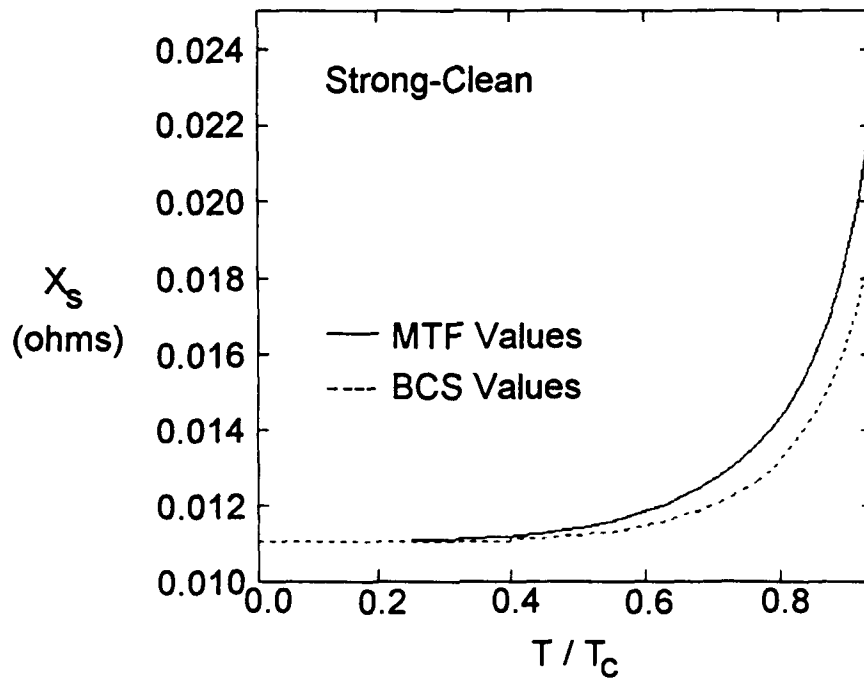


Figure 4.21. Strong-clean comparison to BCS calculations (using [2]) from $0.022T_c$ to $0.94T_c$. Penetration depth temperature dependence is proportional to $(1-(T/T_c)^4)^{-1/2}$. $\Delta_0/k_B T_c = 2.75$, $\lambda(0) = 140\text{nm}$, $\xi_0 = 2\text{nm}$, $l = 200\text{nm}$, Frequency = 10GHz.

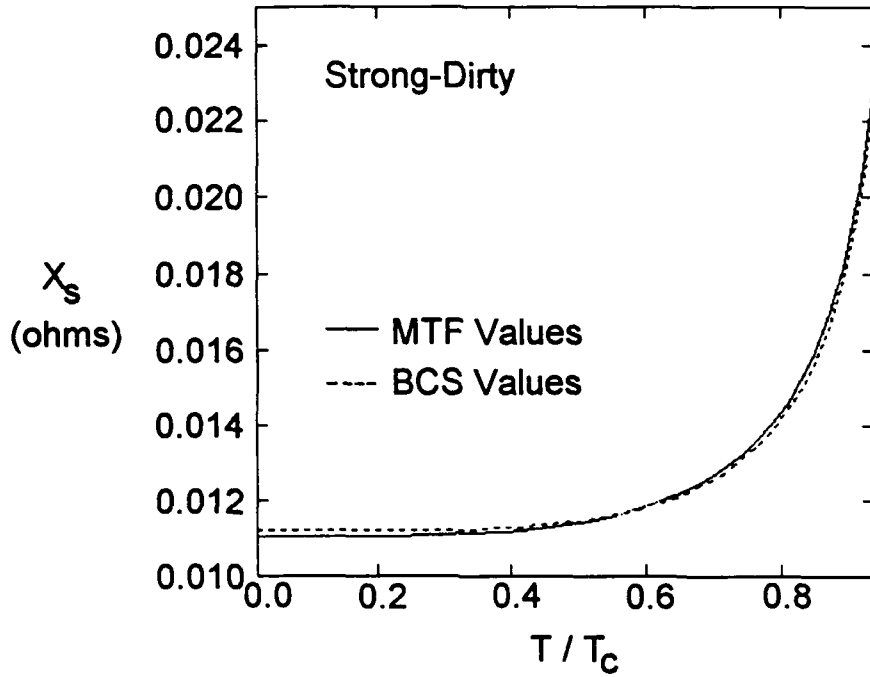


Figure 4.22. Strong-dirty comparison to BCS calculations (using [2]) from $0.022T_c$ to $0.94T_c$. Penetration depth temperature dependence is proportional to $(1-(T/T_c)^4)^{-1/2}$. $\Delta_0/k_B T_c = 2.75$, $\lambda(0) = 140\text{nm}$, $\xi_0 = 2\text{nm}$, $l = 0.02\text{nm}$, Frequency = 10GHz.

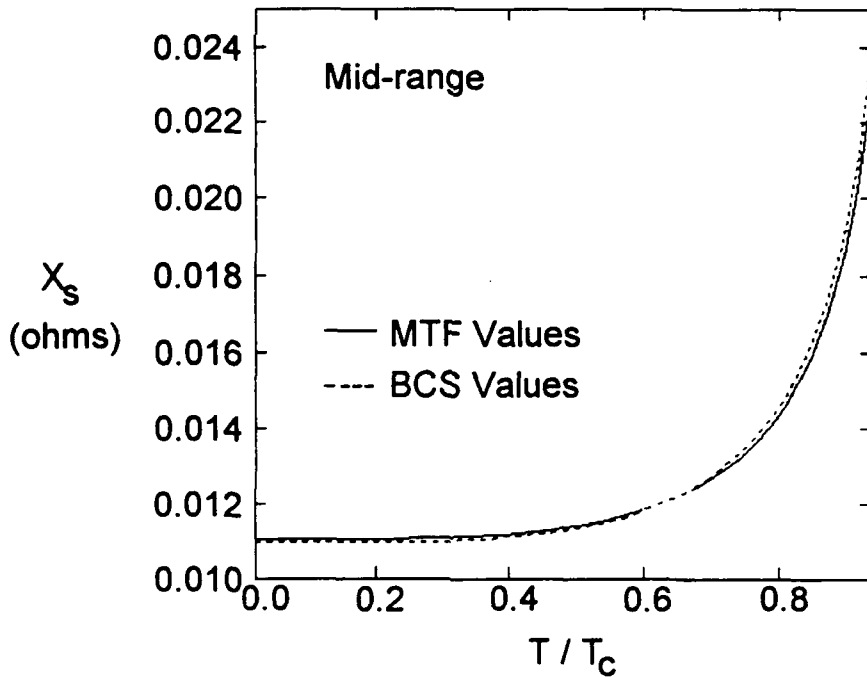


Figure 4.23. Mid-range comparison to BCS calculations (using [2]) from $0.022T_c$ to $0.94T_c$. Penetration depth temperature dependence is proportional to $(1-(T/T_c)^4)^{-1/2}$. $\Delta_0/k_B T_c = 2.25$, $\lambda(0) = 140\text{nm}$, $\xi_0 = 2\text{nm}$, $l = 2\text{nm}$, Frequency = 10GHz.

Again, the trend shown above is what we have seen before: more accuracy at high temperature in the strong-coupling cases, less in the weak-coupling cases, but even so, there is good agreement between the models overall. Table 4.2 shows the mean and standard deviation information.

$\Delta_0/k_B T_c$	Mean(X_s MTF/ X_s BCS)			Std. Dev.(X_s MTF/ X_s BCS)		
	(clean)	$\log(1/\xi_0)$	(dirty)	(clean)	$\log(1/\xi_0)$	(dirty)
	2	0	-2	2	0	-2
1.75	0.952		0.993	0.044		0.047
2.25		0.999			0.012	
2.75	1.036		0.998	0.043		0.012

Table 4.2. MTF model surface resistance/BCS surface resistance mean comparison for dirty to clean (left to right) and strong to weak parameters. The mean is taken across a temperature range from $0.022T_c$ to $0.94T_c$. Penetration depth temperature dependence is proportional to $(1-(T/T_c)^4)^{-1/2}$. $\lambda(0) = 140\text{nm}$, $\xi_0 = 2\text{nm}$, Frequency = 10GHz.

Having done the entire comparison of the surface reactance, we can conclude that it verifies Figure 3.3 except in one case. In the strong-dirty case, the BCS penetration depth was a little less than the $(1-(T/T_c)^4)^{-1/2}$ relationship predicted. The weak-clean case showed good agreement with $(1-(T/T_c)^3-T/T_c)^{-1/2}$, though the values were slightly lower than the MTF predicted (cleaner parameters might have shown better agreement), and the weak-dirty case showed slightly lower BCS values than $(1-(T/T_c)^3-T/T_c)^{-1/2}$ predicted. Unlike Figure 3.3, though, the strong-clean BCS calculations showed significantly lower values than $(1-(T/T_c)^4)^{-1/2}$, lower than even the strong-dirty case. While we do not know why this effect occurred, it appears from this comparison that when the ratio of $\Delta_0/k_B T_c$ is 2.25 or more, and/or the material is dirty, the best fit to the penetration depth is $(1-(T/T_c)^4)^{-1/2}$, while the best fit for smaller values is $(1-(T/T_c)^3-T/T_c)^{-1/2}$. To summarize this part of the comparison, then, the overall error in the surface reactance fits

is smaller than in the surface impedance, due to the small number of parameters that significantly impact the surface reactance, and excellent agreement is possible when the proper form of the equations is used depending on material parameters.

Before moving on to data for real materials, a note regarding strong-coupling effects: the BCS model is a weak-coupling theory. The strong-coupling effects were estimated by replacing the BCS value $\Delta_0/k_B T_C = 1.76$ with its non-BCS value, while keeping T_C constant. It is not clear that this estimate adequately takes into account all of the strong-coupling effects. Hence, the good agreement of the MTF model to BCS calculations in the strong-coupling case could be misleading, because the BCS estimations may be not be sufficient. However, because there is such flexibility in the two-fluid model, it is likely that further modification would allow it to correctly model strong-coupling superconductors. In this thesis, however, only the BCS calculations have been fit, so care must be taken when using this model for strong-coupling superconductors.

One other note needs to be included here. The MTF model has computation times that are one to five orders of magnitude less than its BCS equivalents. On a 386 machine running DOS at 33MHz with a math co-processor, the program from [1] requires 0.400 seconds per point, and [2] (which is more robust, as was shown in chapter 2) requires 2.73-1633 seconds per point. However, the MTF model only requires 0.0375 seconds per point. For this dramatic increase in speed, little accuracy is sacrificed, as we have shown above. Thus, to sum up this section, the MTF fits the BCS surface resistance and reactance calculations well, and works much faster. In the next section, we will compare the MTF model and BCS calculations to another model which approximates BCS surface resistance calculations. This model, presented by Andreone and Kresin in [26], is also a simple, analytical expression that has much greater accuracy than the TTF model, but, as we shall show, does not have the versatility of the MTF model.

4.3 Comparison of BCS and MTF Models to Another Model

Andreone and Kresin in [26] discuss a model of surface resistance for high-temperature superconductors, specifically La-Sr-Cu-O and YBCO in the low-temperature region. This model takes into account the effect of the mean free path on the losses, and it is claimed to be valid for "a London superconductor in the low temperature region" at low frequency [26]. The model they present is a simple analytical expression for surface resistance for $k_B T_c \ll \Delta$ (i.e. low temperature) and low frequency.

The central equation to this model is:

$$R_s = \frac{1}{4} \frac{\mu_0 \Delta \lambda_0}{\hbar} f\left(\frac{2l}{\pi \xi_0}, \omega\right) \ln\left(\frac{\Delta}{\hbar \omega}\right) \left(\frac{\hbar \omega}{\Delta}\right)^2 \left(\frac{\Delta}{k_B T}\right) e^{-k_B T}$$

where $f(x, \omega) = h(x, \omega) g(x)^{-3/2}$, and $h(x, \omega) = x / (1 + (\hbar \omega / 2\Delta) x^2)$. The function $g(x)$ is:

$$g(x) = \begin{cases} x \left(\frac{\pi}{2} - \frac{x}{(x^2 - 1)^{1/2}} \tan^{-1}(x^2 - 1)^{1/2} \right) & x > 1 \\ x \left(\frac{\pi}{2} - \frac{x}{(1 - x^2)^{1/2}} \ln \left(\frac{1 + (1 - x^2)^{1/2}}{1 - (1 - x^2)^{1/2}} \right) \right) & x < 1 \end{cases}$$

We verified that this model is a good fit to BCS calculations of [2] in the weak limit at low temperature, as stated by the authors. Although the fit in the weak-clean limit was reasonable, even at high temperature, we found it is not a good fit to BCS in the weak-dirty limit at high temperature, as shown in Figure 4.24.

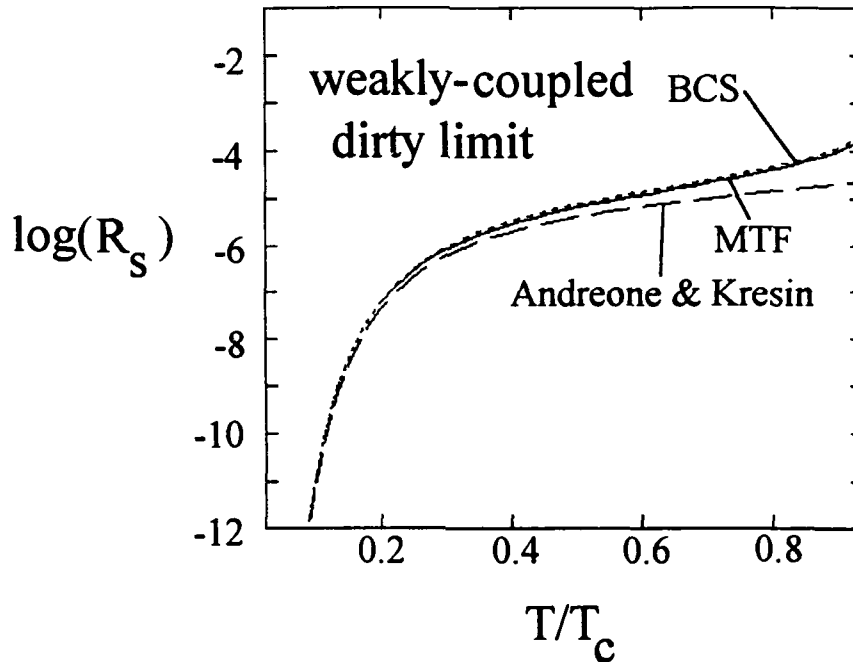


Figure 4.24. Comparison of BCS calculations of [2] to MTF and model presented by Andreone and Kresin [26]. $l \ll \xi_0$ (i.e. dirty limit), Frequency = 10GHz and gap frequency = 7THz. $\Delta_0/k_B T_c = 1.76$.

A good feature of the Andreone and Kresin model is that it is simple, giving fast calculation times and easy implementation. However, we can also see from the equations of this model that it is not as intuitive or easy to manipulate as the MTF model. In addition, we see in Figure 4.24 that the model by Andreone and Kresin becomes progressively worse as the temperature rises, and is off by an order of magnitude near T_c . Note that the authors made no claim that their model worked at high temperature, and it does work well under their restrictions. However, what Figure 4.24 shows is the model in [26] lacks the flexibility of the MTF model, which still shows good agreement with the BCS calculations throughout the temperature range. Moreover, as stated by the authors, the Andreone and Kresin model is only valid at low microwave frequencies, while the MTF model is able to cover microwave frequencies that are high or low. While the model in [26] is good in some regions with the right material parameters, it is not as comprehensive as the MTF model—nor does it claim to be.

Furthermore, also does not provide us with the conductivity, nor does it calculate the imaginary component of the surface impedance. We see, then, that the model developed by Andreone and Kresin, though good in the regions stated in [26], is more limited in scope and application than the MTF model.

Having now explored comparisons of the MTF model to the mathematical models of [2] and [26], we shall now move on to comparing the MTF model to real data, beginning with Nb, to see how well it works beyond comparison to purely theoretical calculations.

4.4 Comparison to Niobium

We compared the MTF model to niobium surface resistance data, and we will discuss our results in this section. First, we show the comparison between niobium and BCS calculations from Halbritter [2]. The dots represent data from [27], and the open squares represent BCS calculations as done by Halbritter [2]. Figure 4.25 shows that there is good agreement between the Nb data from [27] and the BCS calculations using the inputs $\Delta_0/k_B T_c = 1.97$, $T_c = 9.2\text{K}$, $\lambda(0) = 28.3\text{nm}$, $\lambda_{L,0} = 21.7\text{nm}$, $\rho_0 = 0.32\mu\Omega\text{-cm}$, $l = 56.1\text{nm}$, $\xi_0 = 39\text{nm}$. $\Delta_0/k_B T_c$, T_c , and ξ_0 were taken as given from [27]. The inputs for the mean free path, resistivity, and penetration depths were not taken as given, but were determined by fitting the BCS calculations to the data. The temperature dependence which spans a large part of temperature range for superconducting Nb, is nearly correct, as is the frequency dependence, which spans 3 decades.

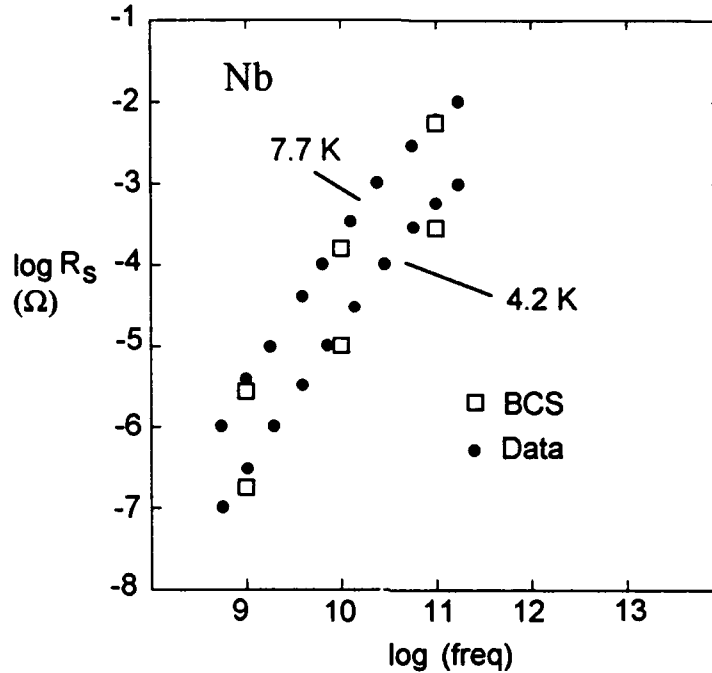


Figure 4.25. Comparison of Nb data to BCS model [2]. $\Delta_0/k_B T_c = 1.97$, $T_c = 9.2\text{K}$, $\lambda(0) = 28.3\text{nm}$, $\lambda_{L,0} = 21.7\text{nm}$, $\rho_0 = 0.32\mu\Omega\text{-cm}$, $l = 56.1\text{nm}$, $\xi_0 = 39\text{nm}$. Data from [27].

The next figure, 4.26, adds the TTF and MTF models to the comparison, using exactly the same inputs for the TTF and MTF models as was used for the BCS model. The dotted lines represent the TTF model output, and differ from the data and BCS calculations by as much as an order of magnitude at 1GHz. However, the MTF model, shown by the solid lines, show the correct temperature and frequency dependence, and matches both the Nb and BCS calculations well across the broad temperature range and three orders of magnitude of frequency. The jump which occurs just under 1THz is the transition to the normal state due to the gap frequency. (We have included the gap frequency in both the MTF and TTF models in this case.) The jump does not appear to be at a discrete frequency in the graph, however, this inaccuracy is caused by the step-size of the numerical simulation, not the equations. The jump does occur at a discrete frequency.

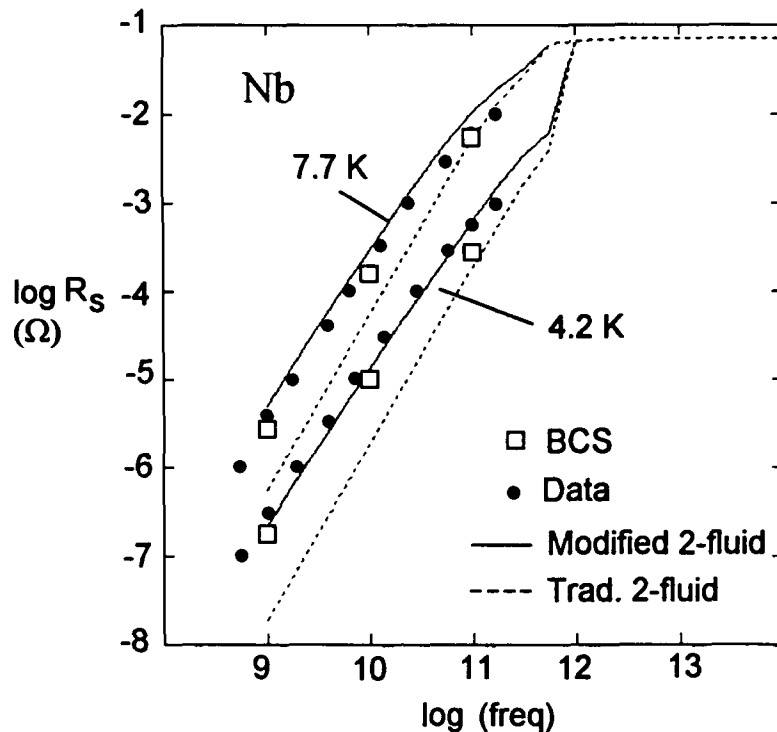


Figure 4.26. Comparison of Nb data to BCS model, TTF model and MTF model. $\Delta_0/k_B T_c = 1.97$, $T_c = 9.2\text{K}$, $\lambda(0) = 28.3\text{nm}$, $\lambda_{L,0} = 21.7\text{nm}$, $\rho_0 = 0.32\mu\Omega\text{-cm}$, $l = 56.1\text{nm}$, $\xi_0 = 39\text{nm}$. Data from [27].

One could perhaps try to salvage the TTF model by changing parameters to fit the TTF model to the data. However, this results in unreasonable penetration depths and/or conductivities, and even when such parameters are used to fit the data at one temperature and frequency, one still cannot match the temperature or frequency dependence using the traditional two-fluid model. To show this is true, Figure 4.27 shows what occurs when we try to fit the TTF to the Nb data.

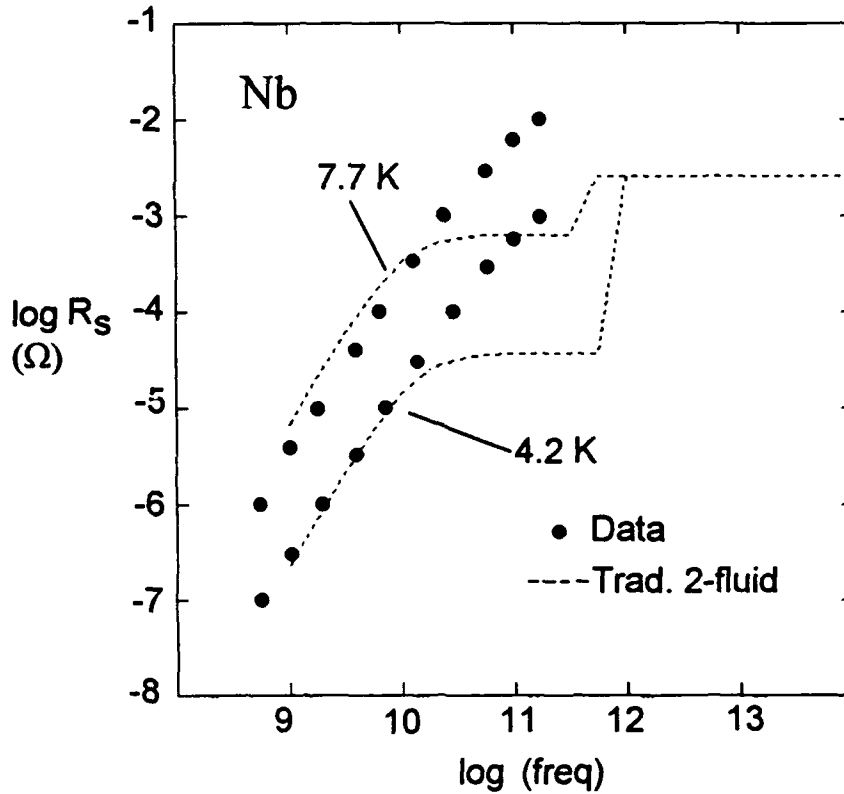


Figure 4.27. Fit of TTF model to Nb data from [27]. Given parameters into TTF model: $\Delta_0/k_B T_c = 1.97$, $T_c = 9.2\text{K}$, $\xi_0 = 39\text{nm}$. Adjusted to fit data: $\lambda(0) = 50\text{nm}$, $\sigma_0 = 40 \cdot 10^8 (\Omega\text{-m})^{-1}$ (or $\rho_0 = 0.025 \mu\Omega\text{-cm}$), $l = 3611\text{nm}$.

The penetration depth and DC conductivity were adjusted to fit the data, and the value of the conductivity implies a mean free path that is too long to be reasonable. The penetration depth is reported to be 39nm in [27], and the value in Figure 4.27 is only 28% larger. This variation is reasonable. However, in [27] the mean free path is reported to be >100nm, and in Figure 4.27 the TTF mean free path is 3.6 μm . This mean free path implies that the Nb is very clean, which causes the sharp knee in the TTF surface resistance above. This knee is not matched by the data, and the fit is accurate for less than 1 decade of frequency. Moreover, even if we assume that such a mean free path is consistent with [27], we have only been able to fit one temperature (4.2K). We cannot fit temperature dependence with the TTF model. Hence, just because the traditional two-fluid model gives an R_s which increases as ω^2 (at least for small ω) and is a reasonable fit at one

temperature, it does not follow that the traditional two-fluid model is an acceptable approximation at other temperatures or higher frequencies, or is acceptable for inferring material parameters.

On the other hand, our MTF model overcomes the limitations of the TTF model and is nearly as accurate for R_s as the full BCS results. The MTF model fits Nb data successfully, because the BCS model can also fit Nb data. We therefore expect the MTF model to be very useful for Nb circuit design.

4.5 Comparison to Nb₃Sn

Another advantage of the MTF model is that it can lead to more intuitive approximations for materials which are not fit well by the BCS theory. We consider two examples, Nb₃Sn and YBa₂Cu₃O_{7- δ} (the latter discussed in the next section). We emphasize, however, that the MTF model results are nearly the same as the full BCS results, and that the following adjustments for $\eta(\omega, T)$ are only anzats for each given material.

We first consider Nb₃Sn data as reported in [27] and shown in Figure 4.28. The dots represent the data, and the open squares are the BCS calculations with the inputs listed. With the same inputs, the MTF model (shown by the solid lines) follows the BCS calculations for Nb₃Sn with the same inputs. However, to get this good fit to the BCS values, we used a penetration depth proportional to $(1-(T/T_c)^4)^{-1/2}$, because Nb₃Sn is a strong-coupling, dirty material. As shown in Subsection 4.2.1, for such materials a better fit to BCS calculations is obtained with a TTF temperature dependence for the penetration depth. While both models fit the data well at low frequency and their temperature dependence is correct, they do not fit the data at high frequency. The traditional two-fluid model (shown by the dotted lines), while correct in frequency dependence, has an incorrect temperature dependence. The discontinuity of the lines at about 1THz is due to the gap frequency.

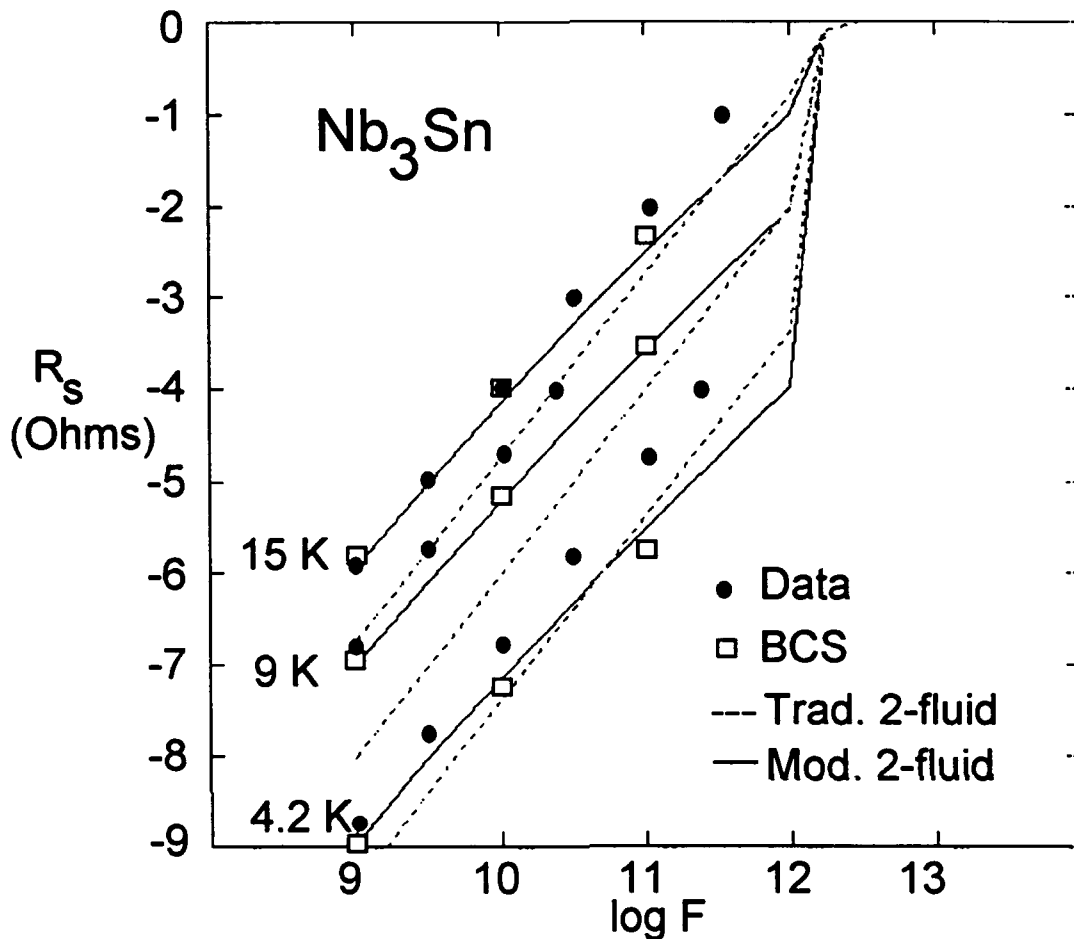


Figure 4.28. Nb₃Sn compared with BCS theory, the TTF model, and MTF model. $\Delta_0/k_B T_c = 2.2$, $T_c = 18\text{K}$, $\lambda(0) = 75.9\text{nm}$, $\lambda_{L,0} = 29.3\text{nm}$, $\rho_0 = 10\mu\Omega\text{-cm}$, $l = 1\text{nm}$, $\xi_0 = 5.7\text{nm}$. Data and parameters from [27], except for $\lambda(0)$, which was derived from [1] and the other parameters.

We attempted to fit the data using modified inputs. Figure 4.29 shows this attempt. We were able to fit the 4.2K line to some degree, but the frequency dependence is still incorrect. The data at other temperatures are not fit well either. The inputs listed are not physically reasonable—the resulting mean free path is too short. Moreover, no physically reasonable set of parameters for the MTF nor BCS model was found to fit the data.

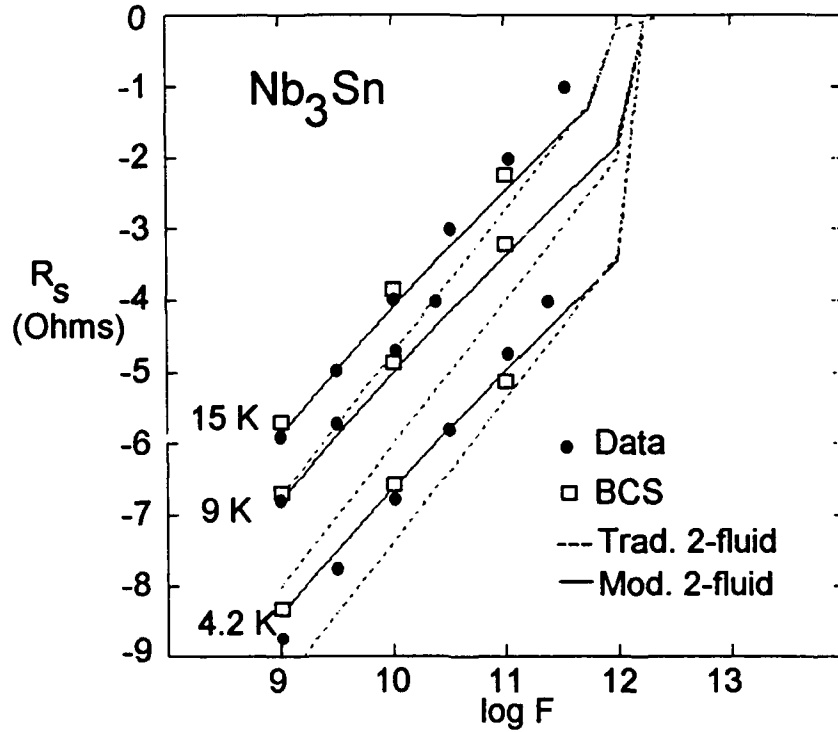


Figure 4.29. Attempt to fit Nb₃Sn data from [27] with BCS theory, the TTF model, and MTF model. Inputs are: $\Delta_0/k_B T_c = 1.88$, $T_c = 18\text{K}$, $\lambda(0) = 75.9\text{nm}$, $\lambda_{L,0} = 2.48\text{nm}$, $\rho_0 = 10\mu\Omega\text{-cm}$, $l = 0.0061\text{nm}$, $\xi_0 = 5.7\text{nm}$.

Since fitting with parameters failed, we tried to modify $\eta(\omega, T)$ to allow us to fit the temperature and frequency dependence of the Nb₃Sn data. We found that by keeping the temperature dependence of $\eta(\omega, T)$ from equation (3.28) but eliminating its frequency dependence, that is, making $\eta(\omega, T)$

$$\eta_{\text{Nb}_3\text{Sn}}(T) = \frac{2\Delta(T)}{k_B T} e^{-\Delta(T)/k_B T} \ln\left(\frac{\Delta(T)}{\hbar\omega_1}\right) \quad (4.1) \quad (0.2)$$

fits the data well using the parameters in Figure 4.28. Figure 4.30 shows that this approximation fits both the temperature and frequency dependence of the data. The dots represent the data. The dotted lines show the TTF model still has an incorrect temperature dependence. The BCS model/MTF model are represented by the open squares. The adjusted MTF model, with equation (4.1) for $\eta(\omega, T)$, shown by the solid lines, is a good

fit to the data, and it uses the physically reasonable inputs listed. Thus, it appears that Nb_3Sn is behaving like a two-fluid material in its frequency dependence and a BCS material in its temperature dependence.

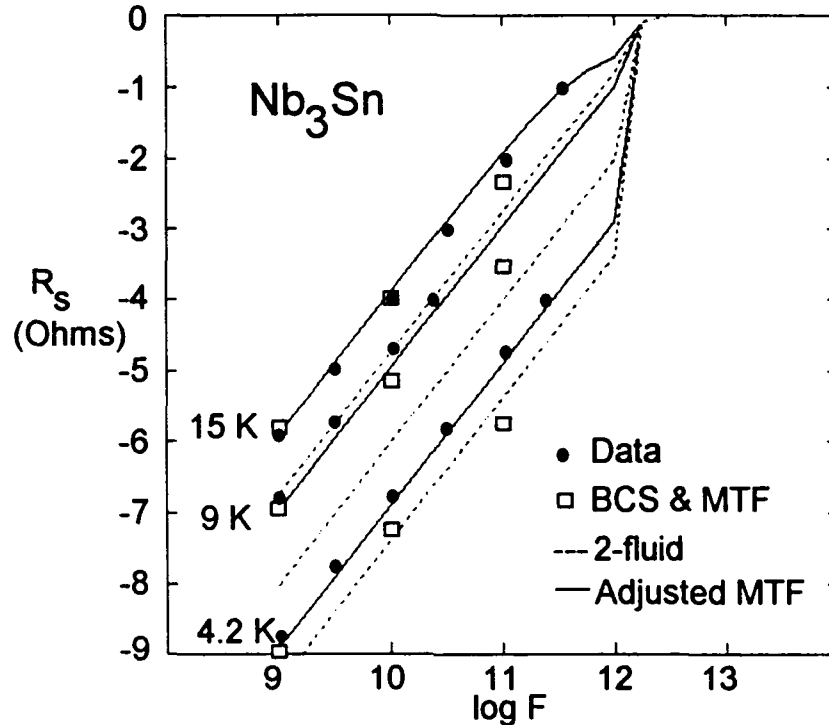


Figure 4.30. Nb_3Sn compared with BCS theory, the TTF model, MTF model and Adjusted MTF model using (4.1) for $\eta(\omega, T)$. $\Delta_0/k_B T_c = 2.2$, $T_c = 18\text{K}$, $\lambda(0) = 75.9\text{nm}$, $\lambda_{L,0} = 29.3\text{nm}$, $\rho_0 = 10\mu\Omega\text{-cm}$, $l = 1\text{nm}$, $\xi_0 = 5.7\text{nm}$. Data and parameters from [27], except for $\lambda(0)$, which was derived from [1] and the other parameters.

A possible reason that the frequency dependence of the TTF model for η works here is that the TTF model for η has been noted to be reasonable for strong-coupling superconductors [26], and Nb_3Sn is indeed strong-coupling. Although we do not clearly know the reasons for this behavior, this example illustrates the intuitive power of the MTF model. In addition, insight can be gained into $\text{YBa}_2\text{Cu}_3\text{O}_{7-\delta}$ through the MTF model.

4.6 Comparison to $\text{YBa}_2\text{Cu}_3\text{O}_{7-\delta}$

To compare the MTF model to YBCO, we first show a comparison of data from several sources (Lincoln Laboratory, et al. [28]) to the TTF, MTF and BCS models. The figure below shows good agreement among the BCS and MTF models and the data. The TTF model is off by an order of magnitude at lower frequency. The parameters used are physically reasonable. However, while this result shows good agreement with the frequency dependence of YBCO, the temperature dependence is more difficult.

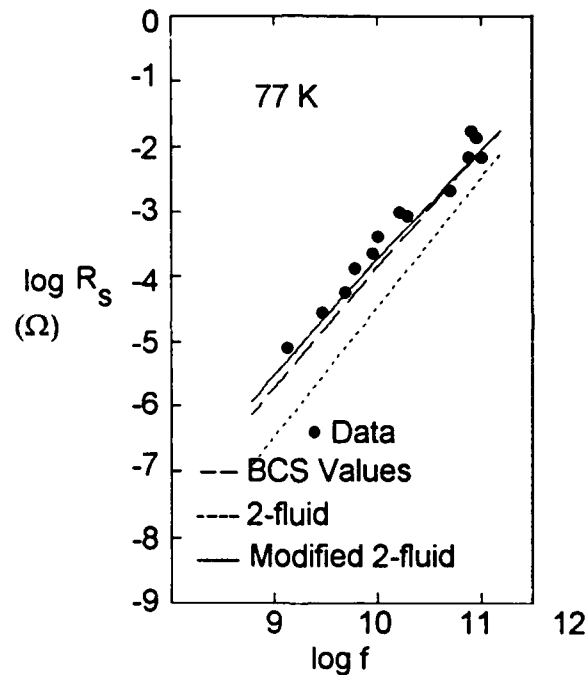


Figure 4.31. Comparison of MTF model to BCS model, TTF model, and data from Lincoln Laboratory, et al. [28] Numbers used for calculations: $T_c = 91.8\text{K}$, $\Delta_0/k_B T_c = 1.75$, $\lambda(0) = 140\text{nm}$, $\rho = 71.4 \mu\Omega\text{-cm}$, $\xi_0 = 2.00\text{nm}$, $l = 2.55\text{nm}$. After Piel and Mueller [27].

The temperature dependence of YBCO has been examined by Bonn, et al. in [23]. They have fabricated some excellent single crystals of YBCO, and the following two figures show their results. They stated that they are able to explain the increase in surface resistance from 75K to 35K by an increase in the scattering time with lower temperature,

although their analysis in [23], shown in Figure 4.32, is only qualitative. They used a form of the TTF to get an idea of this temperature dependence.

Berlinski, et al. [24] also attempted to analyze in detail the data in [23] along the line of a changing scattering time. They used a two-fluid interpretation of the BCS model which was mathematically intricate. Their method was to derive from the BCS equations the modifications to the TTF model. They found that the problem was complicated, and did not reduce to a simple series of equations. They were also unable to fit the data using this approach. Using the MTF model, on the other hand, we were able to fit the Bonn, et al. results using their method of a changing scattering time, with reasonable accuracy over a wider range of temperatures. The difference in success of the two approaches, that of ours and of Berlinski, et al., is attributable to the difference in approaches. While Berlinski, et al. tackled the formidable challenge of analytically deriving a modified two-fluid model, we used the outputs of BCS programs and fit our MTF model to them. Since our goal was to develop a numerical tool for CAD, we approached the problem from a numerical rather than analytical standpoint. Hence, we avoided the intense analytical calculations that Berlinski, et al. encountered, and arrived at a more usable model.

To fit the data of Bonn, et al., after subtracting out the $15 \mu\Omega$ residual resistance, we included a temperature dependent DC conductivity, which is equivalent to changing the scattering time with temperature. We found this temperature dependence by fitting the Bonn data at each temperature while changing only the DC conductivity. Our fit was not physically reasonable at high temperature—the value of the scattering time seemed to decrease rapidly and then saturate, causing a "kink" in the temperature dependence. We made this fit physically reasonable by smoothing out this kink. The resulting "smoothed" scattering time temperature dependence is fit well by

$$\tau_r(T) = AT^{-8} + B(\exp[(0.568 - T/T_c)112.6]) \quad (4.2)$$

where $A = 2.12 \cdot 10^{14} \text{ sec} \cdot (\text{K}^8)$ and $B = 4.22 \cdot 10^{-8} \text{ sec}$. We show equation (4.2) plotted in Figure 4.32. Using this equation in the MTF model, we can fit the data from [23] down to

35K, where Bonn says the scattering time saturates due to impurities, and another effect becomes dominant and causes the further linear decrease in surface resistance with temperature.

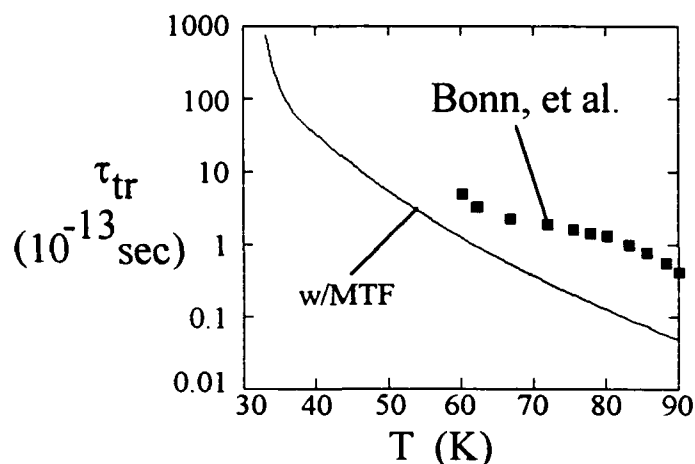


Figure 4.32. Transport scattering time vs. temperature from Bonn, et al. and MTF model to give fit in Figure 4.33.

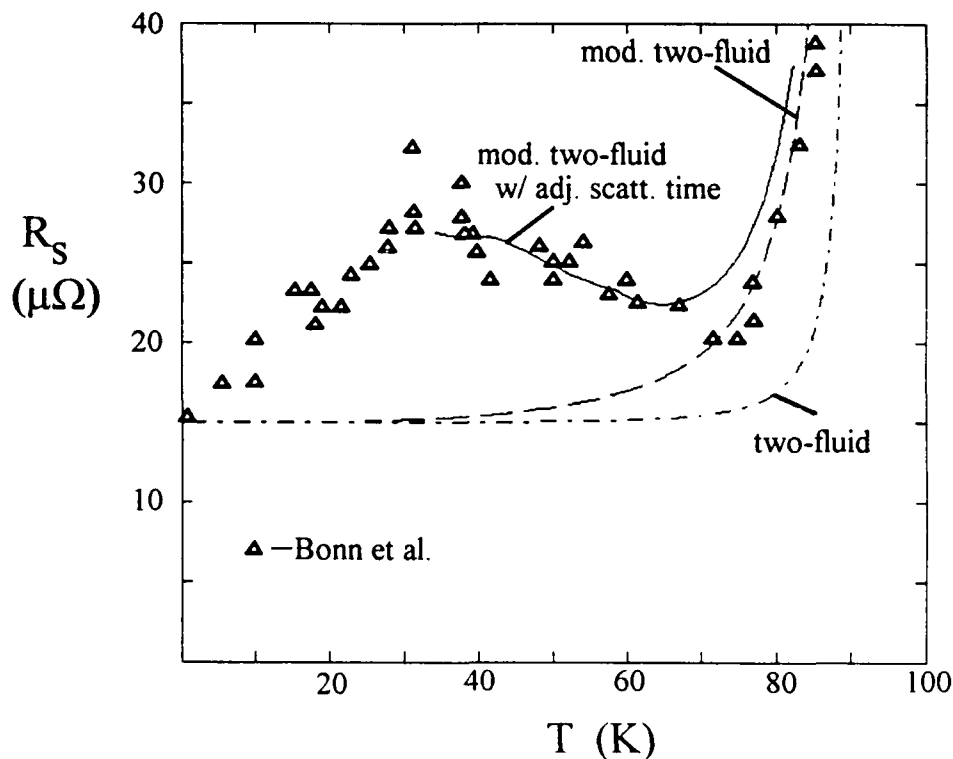


Figure 4.33. Surface resistance data from Bonn, et al. compared with TTF, MTF and MTF with scattering time in previous figure. Parameters used for curves: $T_c = 91.5\text{K}$, $\Delta_0/k_B T_c = 1.76$, $\lambda_{L,0}(0) = 58\text{nm}$, $\rho(91.5\text{K}) = 49.5 \mu\Omega\text{-cm}$, penetration depth temp. dependence proportional to $(1-(T/T_c)^3 - T/T_c)^{-1/2}$

In Figure 4.33 we see the result of changing the scattering time with temperature. The MTF model without the changing scattering time (which is essentially the same as the BCS model) is unable to fit the data, as is the TTF model. However, the peak in the surface resistance is matched by the MTF model with adjusted scattering time. The adjusted MTF does not fit the data as well in the high-temperature regime as the MTF without adjustment, but it fits the data reasonably well over a much larger temperature range. While a better fit could perhaps be obtained, Figure 4.33 as presented shows the power of the MTF model in its flexibility. It is simple to do "what if" calculations with this model, while keeping the accuracy of the BCS model. If one is going to use the TTF model anyway, as Bonn, et al. did, one may as well use the MTF model, which has the same speed, but much more accuracy.

We see, then, from this and the previous sections that the MTF model is useful for doing rapid, intuitive calculations to test ideas. We see, too, from the rest of this chapter that the MTF model gives a good fit to the BCS surface impedance calculations, while remaining fast and intuitive. Having made this point, we now summarize the thesis in the next chapter.

Chapter 5

Summary

As was stated in Chapter 1, there is a need for an accurate and fast model for surface resistance calculations. The BCS model is accurate and microscopically sound for conventional superconductors with a wide range of material parameters, at a wide range of frequencies and temperatures. Unfortunately, calculations with this model are time-consuming, and programs which implement it are difficult to modify. In addition, approximations to the BCS model, as shown in Chapter 4, are useful only in certain regimes and/or material parameters.

In contrast, the traditional two-fluid (TTF) model is good for fast calculations. It is a simple analytic series of expressions, and as such, programs which implement it will run quickly. In addition, programs which use this model will be easy and straightforward to write and modify. Moreover, the TTF model is intuitive and conceptual—it is easy to visualize what is happening in the superconductor when one uses this model. The equations make logical and intuitive sense. Unfortunately, the TTF model lacks microscopic soundness, and while it accepts a wide range of parameters, frequencies and temperatures as inputs, it is inaccurate for most of these inputs.

In this thesis, we have shown that the Modified Two-Fluid (MTF) model combines the best of the BCS model—its accuracy for many inputs—and the best of the TTF model—its speed and intuitive nature. We have shown that it is more physically sound than the TTF model, including as it does the coherence effects and the energy gap, but it

keeps its intuitive nature and speed. We have also shown how well the MTF compares to the BCS model calculations over a wide range of parameters.

Because of the speed and accuracy of the MTF model, we can not only find surface resistance data from parameter inputs at speeds necessary for CAD applications, but we can also quickly find material parameters from surface resistance data. Because of the intuitive nature of the model, we also gain insight into the physics of the material, as shown in the case of Nb_3Sn and $\text{YBa}_2\text{Cu}_3\text{O}_{7-\delta}$.

There are a few items that constitute future work. We wish to modify the two-fluid model further to include anisotropy and residual resistance, and we would like to investigate strong coupling effects. We also would like to conduct some surface resistance experiments in order to help verify this model.

Bibliography

- [1] Zimmermann, W., E.H. Brandt, M. Bauer, E. Seider and L. Genzel. "Optical conductivity of BCS superconductors with arbitrary purity." *Physica C*. Vol 183, pp. 99-104, 1991.
- [2] Halbritter, J. Kernforschungszentrum Karlsruhe Externer Bericht 3/70-6 Karlsruhe: Institute fuer Experimentelle Kernphysik, Juni 1970.
- [3] J.G. Bednorz and K.A. Mueller. *Z. Phys. B*. Vol 64, p. 189, 1986.
- [4] Hammond, Robert B., Gregory L. Hey-Shipton and George L. Matthaei. "Designing with Superconductors." *IEEE Spectrum*. Vol 30, no 4, pp. 34-39, April, 1993. .
- [5] Withers, Richard S. "Wideband Analog Signal Processing" *Superconducting Devices*. Steven T. Ruggiero and David A. Rudman, ed. Boston: Acad. Press, Inc., 1990. pp. 228-272.
- [6] Griffiths, David J. *Introduction to Electrodynamics*. 2nd ed. New Jersey: Prentice Hall, 1989.
- [7] Orlando, Terry P. and Kevin A. Delin. *Foundations of Applied Superconductivity*. Reading, Mass.: Addison-Wesley Publishing Co., 1991.
- [8] Kittel, Charles. *Introduction to Solid State Physics*. 6th ed. New York: John Wiley and Sons, Inc., 1986.
- [9] Tinkham, Michael. *Introduction to Superconductivity*. Malibar, Florida: Robert E. Krieger Publishing Co., 1980.
- [10] Hinken, Johann H. *Superconductor Electronics: Fundamentals and Microwave Applications*. Berlin: Springer-Verlag, 1988.
- [11] Muehlschlegel, Bernhard. "The Thermodynamic Functions of the Superconductor." *Zeitschrift fuer Physik*. Vol 155, pp. 313-327, 1959.

- [12] Mattis, D.C. and J. Bardeen. *Phys. Rev.* Vol 111, p. 412, 1958.
- [13] Abrikosov, A.A., L.P. Gor'kov and I.M. Khalatnikov. *Eksp. Teor. Fiz.* Vol 35, p. 265, 1958. [*Sov. Phys.—JETP* Vol 8, 1959. 182.]
- [14] Turneaure, J.P., J. Halbritter and H.A. Schwettman. "The Surface Impedance of Superconductors and Normal Conductors: The Mattis-Bardeen Theory." *Journal of Superconductivity*. Vol 4, no 5, pp. 341-355, 1991.
- [15] Turneaure, J. PhD Dissertation. Stanford University, 1967.
- [16] Abrikosov, A.A., L.P. Gor'kov, and I. Yu. Dzyaloshinskii. *Quantum Theoretical Methods in Statistical Physics*. New York: Pergamon Press, 1965.
- [17] D.C. Carless, H.E. Hall and J.R. Hook. "Vibrating Wire Measurements in Liquid ^3He : II. The Superfluid B Phase." *Journal of Low Temperature Physics*. Vol 50, Nos 5/6, pp. 605-633, 1983.
- [18] Ashcroft, Neil W. and David N. Mermin. *Solid State Physics*. Philadelphia: W. B. Saunders Co., 1976.
- [19] Gorter, C.J. and H.G.B. Casimir. *Phys. Z.*, Vol 35, 1934. 963. [21] London, F. *Superfluids: Macroscopic Theory of Superconductivity*. Vol 1. Dover Publications, Inc., 1961.
- [20] Puempin, B., H. Keller, W. Kuendig, W. Odermatt, I.M. Savic, J.W. Schneider, H. Simmler, P. Zimmermann, E. Kaldis, S. Rusiecki, Y. Maeno and C. Rossel. "Muon-spin-rotation measurements of the London penetration depths in $\text{YBa}_2\text{Cu}_3\text{O}_{6.97}$." *Physical Review B*. Vol 42, no 13, pp. 8019-8029, 1 November 1990.
- [21] London, F. *Superfluids: Macroscopic Theory of Superconductivity*. Vol 1. Dover Publications, Inc., 1961.
- [22] Orlando, T.P., E.J. McNiff, S. Foner and M.R. Beasley. "Critical fields, Pauli paramagnetic limiting, and material parameters of Nb_3Sn and V_3Si ." *Phys. Rev. B*. Vol 19, no 9, pp. 4545-4561, 1 May 1979.
- [23] Bonn, D. A., P. Dosanjh, R. Liang and W.N. Hardy. "Evidence for Rapid Suppression of Quasiparticle Scattering below T_c in $\text{YBa}_2\text{Cu}_3\text{O}_{7-\delta}$." *Physical Review Letters*. Vol 68, no 15, pp. 2390-2393, 13 April 1992.
- [24] Berlinski, A. John, C. Kallin, G. Rose and A.-C. Shi, at the Institute for Materials Research and Department of Physics and Astronomy, McMaster University, Hamilton,

Ontario. "Two-Fluid Interpretation of the Conductivity of Clean BCS Superconductors."
Submitted to *Phys. Rev. B.* on 5 March, 1993.

[25] Siebert, William McC. *Circuits, Signals and Systems*. Cambridge, MA: The MIT Press, 1986.

[26] Andreone, Antonello and Vladimir Z. Kresin. "On Microwave Properties of High- T_c Oxides." Presented at the Applied Superconductivity Conference, Chicago, August 1992.

[27] Piel, H. and G. Mueller. "The Microwave Surface Impedance of High- T_c Superconductors." *IEEE Trans. on Mag.* Vol 27, no 2, pp. 854-862, March 1991.

[28] Lyons, W. G. "Surface Resistance (After Piel, U. Wuppertal)" Internal Slide for MIT Lincoln Laboratory #2325B TCLGS/aml.

[29] Werthamer, N. R., in *Superconductivity*. R. E. Parks, ed. New York: Marcel Dekker, 1969. Vol 2, p. 321.

Appendix A: Comprehensive list of equations for the MTF model

This list of equations will aid the programmer in including all the pertinent relationships for the Modified Two-Fluid (MTF) model into his or her program. Following the list of equations is a sample MathCAD 3.1 spreadsheet that we used to calculate the surface impedance using the MTF model.

Required inputs: T_c , Δ_0 or $\Delta_0/k_B T_c$, the penetration depth at zero temperature $\lambda(0)$ (NOT the penetration depth in the clean limit), and the DC conductivity σ_0 . The operating temperature T and operating circular frequency ω are also taken as given.

Each equation that follows will be completely specified by the inputs and/or the equations above it. Hence, a computer program that implements each equation in sequence should have no trouble with unspecified arguments. Following is the list of equations:

$$\Delta(T) = \Delta_0 \left[\cos \left(\frac{\pi}{2} \left(\frac{T}{T_c} \right)^2 \right) \right]^{1/2}$$

$$\frac{l}{\xi_0} = \frac{\sigma_0 \lambda^2(0) \mu_0 \pi \Delta_0}{\hbar} - 1$$

$$\tau_r = \frac{\hbar}{\pi \Delta_0} \frac{l}{\xi_0}$$

$$\lambda_{BCS}(T) = \lambda^2(0) / [1 - (T/T_c)^{3-(T/T_c)}] \text{ or } \lambda^2(T) = \lambda^2(0) / [1 - (T/T_c)^4]$$

$$\omega_s = \frac{1}{\tau_s} = \frac{2\Delta(T)}{\hbar}$$

$$\omega_1 = 1 \text{ rad/sec}$$

$$\frac{a-0.16}{0.17} = \begin{cases} 1 & l/\xi_0 < 1 \text{ and } (\omega/\omega_0)^b < e^3 \\ 1 - (1/3)\log(l/\xi_0) & 1 < l/\xi_0 < 1000 \text{ and } (\omega/\omega_0)^b < e^3 \\ 0 & \text{otherwise} \end{cases}$$

$$b \cdot \ln(10) = \begin{cases} 1 + 0.225\log(l/\xi_0) & l/\xi_0 > 1 \\ 1 & \text{otherwise} \end{cases}$$

$$\omega_0/2\pi = \begin{cases} 3.98 \cdot 10^9 & l/\xi_0 < 10 \\ \left(\frac{\xi_0}{l}\right)^{0.7} (2.00 \cdot 10^{10}) & \text{otherwise} \end{cases}$$

$$c = \begin{cases} \frac{a[(\omega/\omega_0)^b < e^3]}{1+e^3} & \left(\frac{\omega}{\omega_0}\right)^b > e^3 \\ 0 & \text{otherwise} \end{cases}$$

$$\eta(\omega, T) = \frac{2\Delta(T)}{k_B T} e^{\frac{-\Delta(T)}{k_B T}} \ln\left(\frac{\Delta(T)}{\hbar\omega_1}\right) \left[\frac{a}{1+(\omega/\omega_0)^b} + c \right]$$

$$\sigma_r = \sigma_1 - j\sigma_2 = \begin{cases} \frac{1}{\mu_0 \lambda^2(T)} \left(\frac{1}{j\omega}\right) + \frac{\sigma_0}{1+j\omega\tau_r} \eta(\omega, T) & 0 < \omega < \omega_s \\ \frac{\sigma_0}{1+j\omega\tau_r} & \omega > \omega_s \end{cases}$$

$$Z_s = \sqrt{j\omega\mu_0 / \sigma_r}$$

Following is the MathCAD 3.1 Spreadsheet. Keep in mind that equations are read left to right and top to bottom.

$$k_B := 1.38 \cdot 10^{-23}$$

$$h_{\text{bar}} := 1.055 \cdot 10^{-34}$$

$$\mu_0 := 4 \cdot \pi \cdot 10^{-7}$$

$$\sigma_0 := 5 \cdot 10^6 \quad \lambda := 140 \cdot 10^{-9}$$

$$T := 4.2 \quad T_c := 91.8 \quad \Delta_0 := k_B \cdot T_c \cdot 1.75$$

$$\omega := 10 \cdot 10^9 \cdot 2 \cdot \pi$$

$$\Delta(T) := \Delta_0 \cdot \cos \left[\frac{\pi}{2} \cdot \left(\frac{T}{T_c} \right)^2 \right]^5 \quad \Lambda_0 := \mu_0 \cdot \lambda^2 \quad \Lambda_0 = 2.463 \cdot 10^{-20}$$

$$\tau_s(T) := \frac{h_{\text{bar}}}{2 \cdot \Delta(T)} \quad \tau_s(0) = 2.379 \cdot 10^{-14} \quad \text{TOL} := 10^{-14}$$

$$A := \frac{\sigma_0 \cdot \lambda^2 \cdot \mu_0 \cdot \pi \cdot \Delta_0}{h_{\text{bar}}} \quad B := A - 1 \quad B = 7.13005$$

$$\tau_{\text{tr}} := \frac{h_{\text{bar}}}{\pi \cdot \Delta_0} \cdot B \quad \tau_{\text{tr}} = 1.08 \cdot 10^{-13}$$

$$f_0 := 10^{9.6} \cdot \Phi(10 - B) + B^{-\frac{2}{3}} \cdot 10^{10.3} \cdot \Phi(B - 10) \quad b := 1 + .225 \cdot \log(B) \cdot \Phi(B - 1)$$

$$a := \left[.17 \cdot \Phi(1 - B) + \left[\left[.17 - \left[.17 \cdot \left(\frac{\log(B)}{3} \right) \right] \right] \cdot \Phi(B - 1) \cdot \Phi(1000 - B) \right] + .16 \right]$$

$$a1(f) := a \cdot \Phi \left[e^3 - \left(\frac{f}{f_0} \right)^{\frac{b}{\ln(10)}} \right]$$

$$c(f) := \Phi \left[\left(\frac{f}{f_0} \right)^{\frac{b}{\ln(10)}} - e^3 \right] \cdot \frac{a}{1 + e^3}$$

$$\eta(f, T) := \frac{2 \cdot \Delta(T)}{k_B \cdot T} \cdot e^{-\frac{\Delta(T)}{k_B \cdot T}} \cdot \ln \left(\frac{\Delta(T)}{h_{\text{bar}}} \right) \cdot \left[\frac{a1(f)}{1 + \left(\frac{f}{f_0} \right)^{\frac{b}{\ln(10)}}} + c(f) \right]$$

$$\sigma_s(\omega, T) := \frac{1}{\Lambda(T)} \cdot \left(\frac{1}{i \cdot \omega} \right) + \frac{\sigma_0}{1 + i \cdot \omega \cdot \tau_{\text{tr}}} \cdot \eta \left(\frac{\omega}{2 \cdot \pi}, T \right)$$

$$\Lambda(T) := \left[\frac{\Lambda_0}{1 - \left(\frac{T}{T_c} \right)^{3 - \frac{T}{T_c}}} \right]$$

$$\sigma_n(\omega) := \frac{\sigma_0}{1 + i \cdot \omega \cdot \tau_{\text{tr}}}$$

$$\sigma(\omega, T) := \sigma_s(\omega, T) \cdot \Phi(1 - \omega \cdot \tau_s(T)) + \sigma_n(\omega) \cdot \Phi(\omega \cdot \tau_s(T) - 1)$$

$$Z(\omega, T) := \sqrt{i \cdot \omega \cdot \frac{\mu_0}{\sigma(\omega, T)}} \quad R(\omega, T) := \operatorname{Re}(Z(\omega, T))$$

$$R(\omega, T) = 2.647 \cdot 10^{-19}$$

Appendix B: Pascal code translation of Zimmermann program [1]

Our translation of the Zimmermann program listed in [1] into Turbo Pascal 4.0 follows. The program is identical in mathematical function, but the required inputs are slightly different. The output of the code listed here is the complex surface impedance. One can easily modify the code to output only the complex conductivity.

```
{ $N+ }
program Zimmermann;

var
  delta0, doverk, sigma0, xi0, l:real;
  fil : text;
  redkey : string[1];
  s, s1, s2, s3,GK,sig : array[1..2] of real;
  M,incr,loops : integer;
  abc:string[1];
  dx,stemp, A, B, C, D, R, delta, w : real;
  u, d1, maxf, x, y, tt, t,max : real;
  num, numb, total: integer;

function tanh(p:real):real; {hyperbolic tan function}
begin
  if p<10000 then
    tanh := (exp(p) - exp(-p))/(exp(p)+exp(-p))
  else tanh := 1.0;
end;

function expo(base, power:real):real;
begin
  expo:=exp(power*ln(base));
end;

procedure ggkk(e, x, y, t:real; k : integer; var re,im:real); {real part}

var
  p1, p2, p3, p4re, p4im, cyre, cyim, c42re, c42im, c12, c32, th:real;
  a,b,a1,b1,b2,a2,a3:real;

begin
  if k = 2 then p1:=sqrt((e+x)*(e+x) - 0.25);
  p2 := sqrt(e*e -0.25);
  if k = 3 then p3 := sqrt((e-x)*(e-x) - 0.25);
```

```

if k = 1 then
  begin
    p4re := 0;
    p4im := sqrt(0.25 -(e-x)*(e-x));
  end;

cyim := y;
cyre := 0;

if k=1 then
  begin
    a := p4re*p2 + 1E-20;
    b := p4im*p2;
    c42re := (0.25+e*(e-x))*a/(a*a+b*b);
    c42im := (0.25+e*(e-x))*(-b)/(a*a+b*b);
  end;
if k=2 then c12 := (0.25 + e*(e+x))/(p1*p2 + 1E-20);
if k=3 then c32 := (0.25 + e*(e-x))/(p3*p2 + 1E-20);
th := tanh(e/(t+t+0.001));
if k=1 then
  begin
    a := p4re + cyre + p2;
    b := p4im + cyim;
    a1 := 1+ c42re;
    a3 := 1-c42re;
    b1 := c42im;
    b2 := -c42im;
    a2:=p4re+cyre-p2;
    re:=th*((a3*a+b2*b)/(a*a+b*b)-(a1*a2+b1*b)/(a2*a2+b*b));
    im:=th*((b2*a-b*a3)/(a*a+b*b)-(b1*a2-b*a1)/(a2*a2+b*b));
  end;
if k=2 then
  begin
    a:=cyre+p1-p2;
    a1:=cyre-p1-p2;
    a2:=cyre+p1+p2;
    re:=tanh((e+x)/(t+t+0.001))*
    ((1+c12)*a/(a*a+cyim*cyim)-(1-c12)*a1/(a1*a1+cyim*cyim))
    + th*((1-c12)*a2/(a2*a2+cyim*cyim)-(1+c12)*a/(a*a+cyim*cyim));
    im:=tanh((e+x)/(t+t+0.001))*
    ((1+c12)*(-cyim)/(a*a+cyim*cyim)-(1-c12)*(-cyim)/(a1*a1+cyim*cyim))
    + th*((1-c12)*(-cyim)/(a2*a2+cyim*cyim)-(1+c12)*(-cyim)/(a*a+cyim*cyim));
  end;
if k=3 then
  begin

```

```

a:= p3+p2+cyre;
b:=cyim;
a1:=p3-p2+cyre;
re:=th*((1-c32)*a/(a*a+b*b)-(1+c32)*a1/(a1*a1+b*b));
im:=th*((1-c32)*(-b)/(a*a+b*b)-(1+c32)*(-b)/(a1*a1+b*b));
end;
end;

begin {main}
write('inputs:Delta0 (mks) Delta0/kTc sigma0 (mks)=> ');
readln(delta0, doverk, sigma0);{energy gap, energy gap over kTc, DC cond.}
write('inputs: xi0(A) l(A) => ');
readln(xi0, l); {coherence length, mean free path}
write('out to printer? y or n => ');
readln(redkey);
if (redkey = 'y') then
begin
assign(fil, 'PRN');
rewrite(fil);
end
else begin
assign(fil, "");
rewrite(fil);
end;

writeln(fil,"");
writeln(fil,'inputs:Delta0 (mks) = ',delta0:5);
writeln(fil,' sigma0 (mks) = ',sigma0:5);
writeln(fil,' Delta0/kTc = ',doverk:5);
writeln(fil,' xi0(A) = ',xi0:10:0);
writeln(fil,' l(A) = ',l:10:0);
y := (pi/2)*(xi0/l); {impurity factor}
writeln(fil,' y = ',y:8:4);
for loops := 0 to 4 do {determines number of different temps.}
begin
{readln(tt); can be used to input temperature manually}
tt:= (loops*0.2+0.1); {tt = T/Tc}
if tt < 0 then tt := 0;
writeln(fil,"");
writeln(fil,'T/Tc #',loops, ' = ',tt:3:4);
delta := delta0 * sqrt(cos((pi/2)*tt*tt));
for incr:=6 to 11 do {determines no. of freqs.}

begin

```

```

w:=pi*2*(expo(10,incr)); {circ. freq.}
x:=(1.055E-34/(2*delta))*w; {another factor from Zimm.}
s[1]:= 0.0; {sigma1/sigma0 (real part) }
s[2]:= 0.0; {sigma2/sigma0 (imag. part) }

M := 40; {no. of integration steps--adjust down if
          getting div. by zero }

d1 :=1.0/M;
if 1.0 >= sqrt(x) then max:=1.0 else max := sqrt(x);
dx := (1.0/int(M*max));

t := tt/(doverk*2*sqrt(1-tt)*(0.9963 + 0.7733*tt)); {incl. temp. dep of
          gap}
{following are math routines from Zimm., but since Pascal has no
  complex math capability, complex variables are treated
  as arrays}

s1[1]:= 0.0;
s1[2]:= 0.0;
s2[1]:= 0.0;
s2[2]:= 0.0;
s3[1]:= 0.0;
s3[2]:= 0.0;

u := dx*0.5;
while u <= 1.0 do
  begin

    ggkk(0.5 + (u/(1.0-u))*(u/(1.0-u)), x, y, t, 2, GK[1], GK[2]);
    s2[1] := s2[1] + GK[1]*u/((1.0-u)*(1.0-u)*(1.0-u));
    s2[2] := s2[2] + GK[2]*u/((1.0-u)*(1.0-u)*(1.0-u));
    u := u + dx;
  end;

s[1] := s2[1]*dx*2.0;
s[2] := s2[2]*dx*2.0;

if x < 1.0 then
  begin
    u := dx*0.5;
    while u <= 1.0 do
      begin

```

```

    ggkk(0.5+x*u*u*(3.0-u-u),x,y,t,1,GK[1],GK[2]);
    s1[1] := s1[1] + GK[1]*u*(1.0-u);
    s1[2] := s1[2] + GK[2]*u*(1.0-u);
    u := u + dx;
end;
s[1] := s[1] + s1[1]*dx*6.0*x;
s[2] := s[2] + s1[2]*dx*6.0*x;
end
else
begin
u := dx*0.5;
while u <= 1.0 do
begin
ggkk(0.5+(x-1)*u*u*(3.0-u-u),x,y,t,3,GK[1],GK[2]);
s3[1] := s3[1] + GK[1]*u*(1.0-u);
s3[2] := s3[2] + GK[2]*u*(1.0-u);
u := u + dx;
end;

u := d1 * 0.5;

while u <= 1.0 do
begin
ggkk(x-0.5+u*u*(3.0-u-u),x,y,t,1,GK[1],GK[2]);
s1[1]:=s1[1]+GK[1]*u*(1.0-u);
s1[2]:=s1[2]+GK[2]*u*(1.0-u);
u := u + d1;
end;

s[1] := s[1] + (s3[1]*dx*(x-1)+s1[1]*d1)*6;
s[2] := s[2] + (s3[2]*dx*(x-1)+s1[2]*d1)*6;
end;
stemp:=s[1];
s[1] := s[2]*(-y)* 0.5/x;
s[2] := stemp * y * 0.5/x;
sig[1] := s[1]*sigma0; {real part of conduct.}
sig[2] := s[2]*sigma0; {imag. part of conduct.}
A := (w*4*pi*1E-7);
B := sqrt( A / ( sig[1]*sig[1] + sig[2]*sig[2] ) );
C := sqrt( sqrt( sig[1]*sig[1] + sig[2]*sig[2] ) );
D := 0.5*(arctan(sig[1]/sig[2]));
R := B*C*sin(D);
write(fil,'f = ',w/(2*pi):2);
writeln(fil,' and Z = ',R:3,' + i*',B*C*cos(D):3);

```

```
end;  
end;
```

```
close(fil);  
end.
```

Appendix C: FORTRAN and C code for Halbritter's BCS Surface Impedence Program [2]

The FORTRAN listing comes straight from Halbritter's code, but, as noted in Chapter 2, the C translation was performed by J. Steinbeck.

Halbritter's FORTRAN code:

(Note: due to printing restrictions, margins have been altered, and some comment lines exceed the margins. Therefore, lines that begin with comment text that do not begin with an initial "C" are meant to be part of the previous line. The first line of the program is an example.)

```
C    SURFACE IMPEDENCE OF SUPERCONDUCTORS FOR FREQUENCIES
SMALLER THAN
C    THE ENERGY GAP.
    DIMENSION G(6),ID(6),TE(20)
    REAL*8 DELT,DET,DQ(6),DA,DE,DZ,DX(1000),PI,DQ1,DS(1000)
    COMPLEX*8 CHS,CHD,CI
    COMPLEX*16 CDS(1000),CT(1000),CS,CD
    COMMON/HL1/ID,IQ,MS,IS,IP
    COMMON/HL2/AK,A2,FL,O,GP
    COMMON/HL3/PI,DQ,DX,DQ1,DS
    COMMON/HL4/CHS,CHD,CI
    COMMON/HL5/CDS,CT,CS,CD

csma
csma Add statements to open the input and output files
csma
    open(unit=5,file='halb.inp',status='old')
    open(unit=6,file='halb.out',status='new')
csma
C    IT=NUMBER OF TEMPERATURE VALUES.
    READ(5,1) IT
C    FO=FREQUENCY (HERTZ), TE(I)=TEMPERATURES (KELVIN).
    READ(5,2) FO,(TE(I),I=1,IT)
C    MATERIAL PARAMETERS (UNITS: DEGREE KELVIN, ANGSTROM)
    READ(5,2) TC,FAK,DLON,XKOH,FREI
C    REST GIVES THE ACCURACY OF THE COMPUTATION.
    READ(5,2) REST
1  FORMAT(I5)
2  FORMAT(8E10.4)
    WRITE(6,2) FO,(TE(I),I=1,IT),REST
```

```

C    THE MOMENTUM INTEGRAL IS SPLIT IN 6 PARTS OVER THE
INTERVALS
C    (G(I), G(I+1)).
      G(1)=1.E-6
      G(2)=1.E-2
      G(3)=0.2
      G(4)=2.
      G(5)=5.
      G(6)=50.
C    THESE SIX INTERVALS ARE EVALUATED BY SIMPSON'S RULE. 1/ID(I)
GIVES
C    THE SPACING OF THE ABCISSAS.
      ID(1)=5
      ID(2)=7
      ID(3)=15
      ID(4)=20
      ID(5)=20
      ID(6)=9
      IS=(6.E-4/REST)**0.25+1.
      DO 38 N=1,6
38  ID(N)=ID(N)*IS
      PI=3.1415926535
      PH=0.479*10.**(-10)
      CI=(0.,1.)
      FLO=XKOH/FREI
      AL=DLON/XKOH
      OG=PH*FO/TC/FAK
      DX(1)=0.
      DX(2)=G(1)
      IQ=2
      DO 40 N=1,5
        LL=ID(N)-1
        D=ID(N)*2
        ID(N)=LL
        DA=G(N)
        DZ=G(N+1)
        DELT=(DZ-DA)/D
        DET=DELT*2.
        DQ(N)=DELT/3.
        DO 39 K=1,LL
          DA=DA+DET
          DE=DA-DELT
          IQ=IQ+1
          DX(IQ)=DE
          IQ=IQ+1

```

```

39  DX(IQ)=DA
    DE=DZ-DELT
    IQ=IQ+1
    DX(IQ)=DE
    IQ=IQ+1
40  DX(IQ)=DZ
    LL=ID(6)-1
    D=ID(6)*2
    ID(6)=LL
    DA=G(1)
    DZ=1./G(6)
    DELT=(DZ-DA)/D
    DET=DELT*2.
    DQ(6)=DELT/3.
    IQ=IQ+1
    DX(IQ)=1./DA
    DO 41 K=1,LL
      DA=DA+DET
      DE=DA-DELT
      IQ=IQ+1
      DX(IQ)=1./DE
      IQ=IQ+1
41  DX(IQ)=1./DA
    DE=DZ-DELT
    IQ=IQ+1
    DX(IQ)=1./DE
    IQ=IQ+1
    DX(IQ)=1./DZ
    WRITE(6,100)
    WRITE(6,101)
    WRITE(6,102)
    WRITE(6,103) TC,FAK,DLON,XKOH,FREI
    WRITE(6,107) FO
    WRITE(6,108)
    DO 22 K=1,IT
      T=TE(K)/TC
      B=PI/2.*(1.-T*T)
      AG=SQRT(SIN(B))
      FL=FLO/AG
      O=OG/AG
      IF(O-0.5)69,22,22
69  GP=AG/T*FAK
    IS=1./SQRT(O*REST)/5.
    IP=1./SQRT((2.-O)*REST)/5.
    DO 19 I=1,IQ

```

```

      DS(I)=0.
19   CDS(I)=0.
      CALL NONAN
      MS=GP/(SQRT(REST)*2.*PI)
      CALL ISUM
      DQ1=CDABS(CDS(1))
      ENP=1./DSQRT(DQ1)
      AK=AL*ENP*AG
      A2=AK*AK
      CALL HAUPT
      CHS=CHS*ENP
      CHD=CHD*ENP
      XS=REAL(CHS)*DLON
      XD=REAL(CHD)*DLON
      B=(FO/10.**17)*8.*PI*PI*DLON
      RS=AIMAG(CHS)*B
      RD=AIMAG(CHD)*B
      WRITE(6,109) TE(K),XS,RS,XD,RD,CHS,CHD
22   CONTINUE
100  FORMAT(1H1,48H SURFACE IMPEDANCE IN THE SUPERCONDUCTING
STATE )
101
FORMAT(1H0,48H=====)
102  FORMAT(1H0/2X,21H MATERIAL PARAMETERS:)
103  FORMAT(1H0,6H TC = ,F4.2,24H K   GAP(T=0)/KTC = ,F4.2/32H LOND
1DON PEN. DEPTH(T=0,1/L=0) = ,F7.1,9H ANGSTROM/32H COHERENCE
LENGTH
2(T=0,1/L=0)F = ,F7.1,9H ANGSTROM/32H MEAN FREE PATH
3= ,F7.1,9H ANGSTROM)
107  FORMAT(1H0,9H FOR F = ,E10.4,29H HERTZ THE BCS-THEORY
RESULTS/3H
1 /14X,9HSPECULAR-,10X,17HDIFFUSE REFLEXION)
108  FORMAT(1H0,3X,4HTEM-
,6X,4HPEN.,4X,7HSURFACE,5X,4HPEN.,4X,7HSURFACE

1/2X,8HPERATURE,3X,5HDEPTH,3X,10HRESISTANCE,2X,5HDEPTH,3X,10HRES
IST
2ANCE/4X,3H(K),7X,3H(A),6X,5H(OHM),6X,3H(A),6X,5H(OHM))
109  FORMAT(1H0,3X,F4.2,3X,F8.1,1X,E10.3,1X,F8.1,1X,E10.3,8X,4E11.4)
      STOP
      END
C
C*****
*****
C

```

```

SUBROUTINE HAUPT
DIMENSION ID(6)
REAL*8 DQ(6),DX(1000),PI,DQ1,DS(1000)
COMPLEX*8 CHS,CHD,CI
COMPLEX*16 CDS(1000),CS,CT(1000),CIS,CID,CES,CED,CAS,
1CAD,CD
COMMON/HL1/ID,IQ,MS,IS,IP
COMMON/HL2/AK,A2,FL,O,GP
COMMON/HL3/PI,DQ,DX,DQ1,DS
COMMON/HL4/CHS,CHD,CI
COMMON/HL5/CDS,CT,CS,CD
M=1
I=2
CALL INTQ(I,M)
CIS=DX(2)*CS
CID=DX(2)*CD+2.*DX(2)
DO 40 J=1,6
  IF(J-6)11,10,10
10  M=2
    CALL INTQ(I,M)
    CIS=CIS+CS*DX(2)
    CID=CID+CD*DX(2)
11  CES=0.
    CED=0.
    CAS=0.5*CS
    CAD=0.5*CD
    LL=ID(J)
    DO 39 K=1,LL
      CALL INTQ(I,M)
      CES=CES+CS
      CED=CED+CD
      CALL INTQ(I,M)
      CAS=CAS+CS
      CAD=CAD+CD
39  CONTINUE
    CALL INTQ(I,M)
    CES=CES+CS
    CED=CED+CD
    CALL INTQ(I,M)
    CIS=CIS+DQ(J)*(4.*CES+(2.*CAS+CS))
40  CID=CID+DQ(J)*(4.*CED+(2.*CAD+CD))
    A=2./PI*AK
    CHS=A*CIS
    CHD=2./A/CID
RETURN

```

END

C

C*****

C

```
SUBROUTINE INTQ(L,M)
DIMENSION ID(6)
REAL*8 DQ(6),DX(1000),PI,DX2,DA,DQ1,DS(1000)
COMPLEX*8 CHS,CHD,CI
COMPLEX*16 CDS(1000),CT(1000),CS,CD,CDG
COMMON/HL1/ID,IQ,MS,IS,IP
COMMON/HL2/AK,A2,FL,O,GP
COMMON/HL3/PI,DQ,DX,DQ1,DS
COMMON/HL4/CHS,CHD,CI
COMMON/HL5/CDS,CT,CS,CD
CDG=CDS(L)/DQ1
DX2=DX(L)*DX(L)
DA=DX2*A2
GO TO (10,11),M
10 CS=1./(DA+CDG)
CD=CDLOG(1.+CDG/DA)
GO TO 9
11 CS=1./(A2+CDG/DX2)
CD=CDLOG(1.+CDG/DA)*DX2
9 L=L+1
RETURN
END
```

C

C*****

C

```
SUBROUTINE NONAN
DIMENSION ID(6)
REAL*8 D,DX(1000),PI,DQ1,DS(1000),DV,DZ,DU,DG,DA,DC,DP,DM,
1DW,DWO,DQ(6),OT,O2
COMPLEX*8 CHS,CHD,CI
COMPLEX*16 CDS(1000),CT(1000),CS,CD,CY
COMMON/HL1/ID,IQ,MS,IS,IP
COMMON/HL2/AK,A2,FL,O,GP
COMMON/HL3/PI,DQ,DX,DQ1,DS
COMMON/HL4/CHS,CHD,CI
COMMON/HL5/CDS,CT,CS,CD
OT=O/2.*GP
IF(OT-0.2)10,10,9
10 O2=OT*OT
```

```

DV=OT*(1.+O2/6.*(1.+O2/20.*(1.+O2/42.*(1.+O2/72.*(1.+O2/110.)))))))*
1DEXP(-OT)
OT=-OT*2.
GO TO 8
9 OT=-OT*2.
DV=(1.-DEXP(OT))/2.
8 B=4*IS
BS=PI/B
DO 48 K=1,IS
  B=4*(IS-K)+2
  D=B*BS
  DZ=0.5*(1.+DCOS(D))
  DU=GP/DZ
  DA=DEXP(-DU)
  DG=DEXP(-DU+OT)
  DC=DA/((1.+DG)*(1.+DA))*DV
  DP=DZ+1.
  DM=1.-DZ
  DU=DP*DM
  DW=DSQRT(DU)
  DA=DZ*O
  DWO=DSQRT(DU+DA*(2.+DA))
  DP=DZ*DSQRT(DZ*DP)
  DU=DA/DU
  IF(DU-0.1)7,7,6
7 DU=DU*(2.+DA)/2.
  DM=DU*(1.-0.5*DU*(1.-DU*(1.-1.25*DU*(1.-1.4*DU*(1.-1.5*DU*(1.-11.*
  1DU/7.*(1.-1.5*DU*(1.-13.*DU/9*(1.-1.4*DU)))))))))))*DW
  GO TO 5
6 DM=DWO-DW
5 CY=-CI*DM/2./DZ+FL
  CALL WINK(CY)
  DU=DC/DP/DWO
  DWU=DWO*DW
  DM=1.+DZ*(DZ+O)
  DPS=(DM+DWU)*DU
  DMS=(DM-DWU)*DU
  DO 20 I=1,IQ
20 CDS(I)=CDS(I)+DPS*CT(I)
  DM=DWO+DW
  CY=CI*DM/2./DZ+FL
  CALL WINK(CY)
  DO 21 I=1,IQ
21 DS(I)=DS(I)+DMS*CT(I)
48 CONTINUE

```

```

CY=-CI*BS*4.
DO 22 I=1,IQ
  CDS(I)=(CDS(I)+DS(I))*CY
22 DS(I)=0.
  B=4*IP
  BS=PI/B
  DO 47 K=1,IP
    B=4*(IP-K)+2
    D=B*BS
    DZ=1.+0.5*O*(1.+DCOS(D))
    DU=GP*DZ
    DA=DEXP(-DU)
    DG=DEXP(-DU-OT)
    DC=DG/((1.+DG)*(1.+DA))*DV
    DP=DZ+1.
    DM=DZ-1.
    DW=DSQRT(DP*DM)
    DA=O-DM
    DU=DP-O
    DWO=DSQRT(DA*DU)
    CY=DWO+CI*DW+FL
    CALL WINK(CY)
    CY=(1.+DZ*(DZ-O)+CI*DW*DWO)/DSQRT(DP*DU)*DC
    DO 23 I=1,IQ
23 DS(I)=DS(I)+CY*CT(I)
47 CONTINUE
  B=+BS*4.
  DO 24 I=1,IQ
24 CDS(I)=CDS(I)+DS(I)*B
  RETURN
  END

```

C

C*****

C

```

SUBROUTINE ISUM
DIMENSION ID(6)
REAL*8 DQ(6),DX(1000),PI,G,DU,DW,DS(1000),DQ1
COMPLEX*8 CHS,CHD,CI
COMPLEX*16 CDS(1000),CS,CB,CU,CW,CL,CP,CA,CT(1000),CD
COMMON/HL1/ID,IQ,MS,IS,IP
COMMON/HL2/AK,A2,FL,O,GP
COMMON/HL3/PI,DQ,DX,DQ1,DS
COMMON/HL4/CHS,CHD,CI
COMMON/HL5/CDS,CT,CS,CD

```

```

G=PI/GP
DO 20 I=1,IQ
20 DS(I)=0.
DO 30 M=1,MS
  B=2*(MS-M)+1
  B=B*G
  DU=B*B+1.
  CB=B+O*CI
  CU=CB*CB+1.
  DW=DSQRT(DU)
  CW=CDSQRT(CU)
  CL=(DW+CW)/2.+FL
  CP=DW*CW
  CA=(1.-B*CB+CP)/CP
  CALL WINK(CL)
  DO 21 I=1,IQ
21 DS(I)=DS(I)+CA*CT(I)
30 CONTINUE
DO 22 I=1,IQ
22 CDS(I)=DS(I)*G+CDS(I)
RETURN
END

```

C
C*****

```

C
SUBROUTINE WINK(CL)
DIMENSION ID(6)
REAL*8 DQ(6),DX(1000),PI,D,DQ1,DS(1000)
COMPLEX*8 CHS,CHD,CI
COMPLEX*16 CDS(1000),CS,CT(1000),CD,CC,C2,CL
COMMON/HL1/ID,IQ,MS,IS,IP
COMMON/HL2/AK,A2,FL,O,GP
COMMON/HL3/PI,DQ,DX,DQ1,DS
COMMON/HL4/CHS,CHD,CI
COMMON/HL5/CDS,CT,CS,CC
DO 20 I=1,IQ
  D=DX(I)
  CD=D/CL
  C2=CD*CD
  U=CDABS(CD)
  IF(U-0.2)10,10,11
10 CT(I)=3./CL*(1./3.-C2*(1./15.-C2*(1./35.-C2*(1./63.-C2*(1./99.-
1C2*(1./143.-C2*(1./195.-C2/255.))))))
  GO TO 20

```

```

11  CD=1./CD
    CT(I)=0.75/D*(-2.*CD+(1.+CD*CD)/CI*(CDLOG(CD+CI)-CDLOG(CD-CI)))
20  CONTINUE
    RETURN
    END

```

J. Steinbeck's translation of the above program into C follows:

```

/* Surface of superconductors for frequencies less than the energy
gap. As rewritten by J. Steinbeck */

```

```

/* I have tried to give all of the variables meaningful names, unlike the
original FORTRAN version of the program. The naming convention is as follows:

```

(varA varB ...)_ (vara varb ...) Generally means

```

varA varB .....

```

```

vara varb .....

```

For some functions (like the Kernel evaluated by the program) the variables are named

name_(varA varB) which means name(varA, varB,)

Other Notes:

1) The temperature dependence of the energy gap is presently given as
 $\Delta(T)/\Delta(0) = \cos(\pi/2 * t^2)$

```

*/

```

```

#include<stdio.h>

```

```

#include<math.h>

```

```

#include"e:\math\cmath.h"

```

```

#define PI    3.1415926535

```

```

#define PI2   (PI * PI)

```

```

Complex chs, cs, Zs;      /* Variables for specular reflection */

```

```

Complex chd, cd, Zd;     /* Variables for diffuse reflection */

```

```

Complex cds[1000], ct[1000];

```

```

double ds[1000];

```

```

double T[20];                /* temperature values */
double q[1000];             /* wave vectors for integration */
int id[6];
double dq[6];
int iq,is,ip,ms;           /* numbers of things */
double kappa_Tlw, k_Tlw2; /* kappa(T,l,w) and squared */
double hw_deltaT;         /* hw/delta(T) */
double deltaT_kT;         /* delta(T)/kT */
double fl;
double Q_0w;               /* Kernel Q(0,w) */

void haupt();              /* Main integration routine */
void nonan();
int intq(int , int);      /* calculates integrands */
void wink(Complex);
void isum();

main()
{
    double h_k = 0.479951e-10; /* h/k */

    int n, k, i;

    int it;                /* number of temperature values */
    double f0;             /* frequency in Hz */
    double Tc;             /* critical temperature */
    double delta0_kTc;     /* delta0_kTc */
    double lambda0;        /* lambda0 with mfp infinte, T = 0 */
    double chi0;           /* chi0 , coherence length at T = 0 */
    double l0;             /* mean free path of carriers */
    double rest;           /* accuracy factor (?) */

    double hw_delta0;     /* hw/delta(0) */
    double delT_del0;     /* delta(T)/delta(0) */
    double t;             /* reduced temperature */
    double chi_l;         /* chi(0)/l(0) */
    double kappa;         /* lambda0/chi0 */
    double lamb_Tlw;     /* lambda(T,l,w) */

    double g[6];         /* interval data */

    double d,da,dz,delt,det;

    /* get the input data to run the desired case */

```

```

printf("Frequency (Hz) --");
scanf("%lf", &f0);
printf("Number of temperatures ( <= 20) --");
scanf("%d", &it);
for (n=0; n<it; n++) {
    printf("\nTemperature %d --",n);
    scanf("%lf", T+n);
}
printf("\nMaterial parameters\n");
printf("\tCritical temperature (K) --");
scanf("%lf", &Tc);
printf("\tDelta(0)/kTc ratio --");
scanf("%lf", &delta0_kTc);
printf("\tLondon penetration depth (T = 0) (A) -- ");
scanf("%lf", &lambda0);
printf("\tCoherence length (T = 0) (A) --");
scanf("%lf", &chi0);
printf("\tElectronic mean free path (A) --");
scanf("%lf", &l0);
printf("\n\nAccuracy factor (??????) --");
scanf("%lf", &rest);

```

/* basically do the momentum integral in six parts to weight the regions properly. Integration is done by Simpson's rule and the regions are assigned as follows: */

```

g[0] = 1.e-06;
g[1] = 1.e-02;
g[2] = 0.2;
g[3] = 2.;
g[4] = 5.;
g[5] = 50.;

```

/* 1./id[] gives the spacing of the abscissas (?) */

```

id[0] = 5;
id[1] = 7;
id[2] = 15;
id[3] = 20;
id[4] = 20;
id[5] = 9;

```

```

is = 1 + (int)pow((6.e-04/rest), 0.25);

```

```

for (n=0; n<6; n++) id[n] *= is;

chi_1 = chi0/10;          /* dirty limit ratio */

kappa = lambda0/chi0;    /* type I or II */

hw_delta0 = h_k * f0/(Tc * delta0_kTc); /* hw/delta(0) */

/* set limits for first interval */

q[0] = 0.;
q[1] = g[0];

iq = 1;
for (n=0; n<5; n++) {
    /* set up for Simpson's rule integration */

    d = (double)(2 * id[n]);
    id[n]--;
    da = g[n];          /* lower limit */
    dz = g[n+1];       /* upper limit */

    delt = (dz - da)/d; /* interval size */
    det = 2. * delt;
    dq[n] = delt/3.;
    for (k=0; k<id[n]; k++) {
        da += det;
        q[+iq] = da - delt;
        q[+iq] = da;
    }
    q[+iq] = dz - delt;
    q[+iq] = dz;
}
d = (double)(2 * id[5]);
id[5]--;
da = g[0];
dz = 1./g[5];
delt = (dz - da)/d;
det = 2. * delt;
dq[5] = delt/3.;
q[+iq] = 1./da;
for(k=0; k<id[5]; k++){
    da +=det;
    q[+iq] = 1./(da - delt);
    q[+iq] = 1./da;
}

```

```

    }
    q[++iq] = 1./(dz-delt);
    q[++iq] = 1./dz;

/* fortran version chooses to write a bunch of stuff */

/* do for each temperature */
    printf("Temp.\t Rs_s\tlambda_s\t Rs_d\tlambda_d\n");

    for (k=0; k<it; k++) {
        t = T[k]/Tc; /* reduced temp */
        delT_del0 = sqrt(cos(0.5 * PI * t * t)); /* gap at T */
        fl = chi_1/delT_del0;
        hw_deltaT = hw_delta0/delT_del0;

/* do only if hw < half gap */

        if ((hw_deltaT - 0.5) < 0.) {
            deltaT_kT = delT_del0/t*delta0_kTc;
            is = (int)(0.2/sqrt(hw_deltaT * rest));
            ip = (int)(0.2/sqrt((2. - hw_deltaT)*rest));
            for (i=0; i<iq; i++) {
                ds[i] = 0;
                cds[i] = Comp(0);
            }
            nonan();
            ms = (int)(deltaT_kT/(sqrt(rest)*2. * PI));
            isum();
            Q_0w = cmag(cds[0]);
            lamb_Tlw = 1./sqrt(Q_0w);
            kappa_Tlw = kappa * lamb_Tlw * delT_del0;
            k_Tlw2 = kappa_Tlw * kappa_Tlw;
            haupt();
            chs = cmul(chs,Comp(lamb_Tlw));
            chd = cmul(chd,Comp(lamb_Tlw));

/* Specular Impedance */

            Im(Zs) = Re(chs) * lambda0;
            Re(Zs) = fabs(Im(chs)) *
                (f0 * 1.e-17) * 8. * PI2 * lambda0;

/* Diffuse Impedance */

            Im(Zd) = Re(chd) * lambda0;

```

```

        Re(Zd) = fabs(Im(chd)) *
                (f0 * 1.e-17) * 8. * PI2 * lambda0;
    }
    printf("%4.2f\t%e\t%e\t%e\t%e\n",
           T[k], Re(Zs), Im(Zs), Re(Zd), Im(Zd));
    }
}

```

/ Main integration routine. Basically, accumulate results in ciX for final summation at the end .*/*

```

void haupt()
{
    int i, j, k, m;

    Complex cis,cid,cas,cad,ces,ced;
    double a;

    m = 1;
    i = 1;

    i += intq(i, m);
    cis = cmul(Comp(q[1]), cs);
    cid = cadd(cmul(Comp(q[1]), cd), Comp(2. * q[1]));
    for (j=0; j<6; j++) {
        if (j == 5) {
            m = 0;
            i += intq(i, m);
            cis = cadd(cis, cmul(cs, Comp(q[1])));
            cid = cadd(cid, cmul(cd, Comp(q[1])));
        }
        ces = Comp(0.);
        ced = Comp(0.);
        cas = cmul(Comp(0.5), cs);
        cad = cmul(Comp(0.5), cd);
        for (k=0; k<id[j]; k++) {
            i += intq(i, m);
            ces = cadd(ces, cs);
            ced = cadd(ced, cd);
            i += intq(i, m);
            cas = cadd(cas, cs);
            cad = cadd(cad, cd);
        }
    }
}

```

```

        i += intq(i, m);
        ces = cadd(ces, cs);
        ced = cadd(ced, cd);
        i += intq(i, m);
        cis = cadd(cis, cmul(Comp(dq[j]), cadd(cmul(Comp(4.), ces),
            cadd(cmul(Comp(2.), cas), cs))));
        cid = cadd(cid, cmul(Comp(dq[j]), cadd(cmul(Comp(4.), ced),
            cadd(cmul(Comp(2.), cad), cd))));
    }
    a = 2./PI * kappa_Tlw;
    chs = cmul(Comp(a), cis);
    chd = cdiv(Comp(2./a), cid);
}

```

/* Calculate integrands for specular and diffuse scattering cases. */

```

int intq(int l, int m)
{
    double q2;
    double temp;
    Complex Q_qw;

    Q_qw = cdiv(cds[l], Comp(Q_0w));
    q2 = q[l] * q[l];
    temp = q2 * k_Tlw2;
    if ( m ) {
        cs = cdiv(unity, cadd(Comp(temp), Q_qw));
        cd = clog(cadd(unity, cdiv(Q_qw, Comp(temp))));
    }
    else {
        cs = cdiv(unity, cadd(Comp(k_Tlw2), cdiv(Q_qw, Comp(q2))));
        cd = cmul(clog(cadd(unity, cdiv(Q_qw, Comp(temp)))), Comp(q2));
    }
    return(1);
}

```

/* nonan, isum and wink evaluate the kernel Q(k,w) which is then integrated in the other routines. */

```

void nonan()
{
    int i,k;
    double hw_2kT;          /* hw/2kT */
    double hw_kT;          /* hw/kT */
}

```

```

double dv, bs, d, dz, du, da, dg, dc, dzpl, dzml, dw,dwo,dp,dm;
double dps,dms,dwu;
double expdu, exphwkT, expduhwkT;
Complex temp;

hw_kT = hw_deltaT * deltaT_kT;
hw_2kT = 0.5 * hw_kT;

if ( hw_2kT <= 0.2 ) {
    double h2;

    h2 = hw_2kT * hw_2kT;
    dv = hw_2kT * (1. + h2/6. *(1.+h2/20. *(1.+h2/42. *(1.+h2/72. *
        (1.+h2/110.)))))) * exp(-hw_2kT);
}
else {
    dv = (1. - exp(-hw_kT))/2.;
}
bs = 0.25 * PI/(double)is;

/* This loop eats up the most time */

exphwkT = exp(-hw_kT);
for (k=0; k<is; k++) {
    d = bs * (double)(4 * (is - k) - 2);
    dz = 0.5 * (1. + cos(d));
    du = deltaT_kT/dz;
    expdu = exp(-du);
    expduhwkT = expdu * exphwkT;
    dc = expdu/((1.+expduhwkT) * (1.+expdu)) * dv;
    dzpl = dz + 1.;
    dzml = dz - 1.;
    du = -dzpl * dzml;
    dw = sqrt(du);
    da = dz * hw_deltaT;
    dwo = sqrt(du+da*(2.+da));
    dp = dz * sqrt(dz*dzpl);
    du = da/du;
    if (du <= 0.1) {
        du *= 0.5 * (2. + da);
        dm = du *(1. - 0.5*du*(1. - du*(1. -1.25*du*(1.-1.4*du*
            (1.-1.5*du*(1. - 11.*du/7.*(1.-1.5*du*(1.-13.*
                du/9.*(1.-1.4*du)))))))))) * dw;
    }
    else dm = dwo - dw;
}

```

```

temp = dcomplex(fl, -dm * 0.5/dz);
wink(temp);
du = dc/(dp * dwo);
dwu = dwo * dw;
dm = 1. + dz * (dz + hw_deltaT);
dps = (dm + dwu) * du;
dms = (dm - dwu) * du;
for(i=0; i<iq; i++)
    cds[i] = cadd(cds[i],cmul(Comp(dps), ct[i]));
dm = dwo + dw;
temp = dcomplex(fl, dm * 0.5 /dz);
wink(temp);
for(i=0; i<iq; i++)
    ds[i] += dms * Re(ct[i]);
}
temp = dcomplex(0,-bs * 4.);
for (i=0; i<iq; i++) {
    cds[i] = cmul(cadd(cds[i],Comp(ds[i])), temp);
    ds[i] = 0.;
}
bs = 0.25 * PI/(double)ip;

expawkT = exp(hw_kT);
for(k=0; k<ip; k++) {
    d = bs * (double)(4 * (ip - k) - 2);
    dz = 1. + 0.5 * hw_deltaT * (1. + cos(d));
    du = deltaT_kT * dz;
    expdu = exp(-du);
    expduawkT = expdu * expawkT;
    dc = expduawkT/((1. + expduawkT) * (1. + expdu)) * dv;
    dzp1 = dz + 1.;
    dzm1 = dz - 1.;
    dw = sqrt(dzp1 * dzm1);
    da = hw_deltaT - dzm1;
    du = dzp1 - hw_deltaT;
    dwo = sqrt(da * du);
    temp = dcomplex(dwo + fl, dw);
    wink(temp);
    temp = cdiv(dcomplex(dc * (1. + dz * (dz - hw_deltaT)),
        dc * dw * dwo), Comp(sqrt(dzp1 * du)));
    for (i=0; i<iq; i++) ds[i] += Re(cmul(temp,ct[i]));
}
bs *= 4.;
for(i=0; i<iq; i++) Re(cds[i]) += ds[i] * bs;
}

```

```

void isum()
{
    int i,m;
    double g,b;
    double du,dw;
    Complex cb,cu,cw,cl,cp,ca;

    g = PI/deltaT_kT;
    for(i=0; i<iq; i++) ds[i] = 0.;

    for(m=0; m<ms; m++) {
        b = g * (double)(2 * (ms - m) - 1);
        du = b * b + 1.;
        cb = dcomplex(b, hw_deltaT);
        cu = cadd(cmul(cb, cb), unity);
        dw = sqrt(du);
        cw = csqrt(cu);
        cl = cadd(cmul(cadd(Comp(dw),cw), Comp(0.5)), Comp(fl));
        cp = cmul(Comp(dw), cw);
        ca = cdiv(cadd(cmul(Comp(-b), cb), cadd(unity,cp)),cp);
        wink(cl);
        for (i=0;i<iq;i++) ds[i] += Re(cmul(ca, ct[i]));
    }
    for(i=0; i<iq; i++) Re(cds[i]) += ds[i] * g;
}

```

```

Complex coef[8] = {1./255., 0., 1./195., 0., 1./143., 0., 1./99., 0.,
                  1./63., 0., 1./35., 0., 1./15., 0., 1./3., 0. };

```

```

void wink(Complex cl)
{
    int i;
    double d,u;
    Complex cd, cd2;

    for(i=0;i<iq;i++) {
        d = q[i];

        cd = cdiv(Comp(d),cl);

        cd2 = cmul(cd, cd);
        u = cmag(cd);
        if (u <= 0.2) {
            /*
            ct[i] = 3./cl*(1./3.-cd2*(1./15.-cd2*(1./35.-cd2*(1./63.-

```

```

cd2*(1./99. - cd2*(1./143.-cd2.*(1./195.-cd2/255.
)))))); */
int j;
Complex temp;

temp = coef[0];
for(j=1; j<8; j++) {
    temp = csub(coef[j], cmul(cd2,temp));
}
temp = cdiv(temp,cl);

ct[i] = cmul(Comp(3.),temp);
}
else {
    Complex temp,temp1;
    double t1;

    cd = cdiv(unity,cd);

/*
ct[i] = 0.75/d*(-2.*cd+(1.+cd *cd)/ci*(log(cd+ci)-
log(cd-ci))) */

temp = cadd(unity, cmul(cd,cd));
temp = cdiv(temp,I);
temp = cmul(temp,
(csub(clog(cadd(cd,I)),clog(csub(cd,I)))));

temp1 = cmul(Comp(-2.),cd);
temp = cadd(temp,temp1);
t1 = 0.75/d;
temp = cmul(Comp(t1), temp);

ct[i] = temp;
}
}
}

```

Appendix D: The Transport Scattering Time and Normal-Total Electron Ratio from The Sum Rule

During the course of developing the MTF model, we attempted to use the sum rule to find two quantities: the transport scattering time τ_{tr} and the normal-total electron ratio $\eta(\omega, T)$. We present in this appendix the method by which we tried to find these quantities, and why this method failed.

We started by making the following assumptions:

1. The sum rule argument works at all temperatures, including zero. The sum rule, equation (3.44) from Subsection 3.4.5, is

$$\int_0^{\infty} \sigma_1(\omega', T) d\omega' = \frac{\pi\sigma_0}{2\tau_r}$$

To find a solution to the sum rule, recall equation (3.14):

$$\sigma_T = \sigma_1 - j\sigma_2 = \begin{cases} \frac{1}{\mu_0\lambda^2(T)} \left(\frac{1}{j\omega} \right) + \frac{\sigma_0}{1+j\omega\tau_r} \eta(\omega, T) & 0 < \omega < \omega_s \\ \frac{\sigma_0}{1+j\omega\tau_r} & \omega > \omega_s \end{cases}$$

Applying (3.14) to (3.44) and integrating gives the expression:

$$\frac{\pi}{2\mu_0\lambda^2(T)} = \frac{\sigma_0}{\tau_r} (1 - \eta(\omega, T)) \tan^{-1} \left(\frac{\tau_r}{\tau_s(T)} \right) \quad (D.1)$$

where $\tau_s(T) = 1/\omega_s(T)$. Equation (D.1) is the two-fluid solution of the sum rule.

2. The value of the penetration depth, whether the material is clean or dirty, must have a Ginzburg-Landau temperature dependence near T_C , that is, it must be proportional to $(1-T/T_C)^{-1/2}$ near T_C .

3. The penetration depth has the TTF temperature dependence and hence is proportional to $(1-(T/T_C)^4)^{-1/2}$. This assumption ensures assumption 2.
4. The function $\eta(\omega, T)$ is the fraction of electrons in the normal channel, and that it is only temperature dependent, i.e. $\eta(\omega, T) = \eta(T)$, and goes to zero at zero temperature.

Assumptions 1 and 2 are well-founded, and assumptions 3 and 4 are used to preserve the two-fluid model picture. In addition, τ_{tr} is assumed to remain constant.

We will use these assumptions to find the scattering time. At zero temperature, assumptions 1 and 4 imply

$$\frac{\pi}{2\mu_0\lambda^2(0)} = \frac{\sigma_0}{\tau_{tr}} \tan^{-1}\left(\frac{\tau_{tr}}{\tau_s(0)}\right) \quad (D.2)$$

and, because all the quantities except τ_{tr} are taken as given, we can solve for τ_{tr} . The problem with this method is that equation (D.2) is a transcendental equation, and must be solved numerically. Not only does such an iterative solution increase the time and difficulty of calculation, we found that solving this equation numerically was not straightforward, as it is sensitive to the tolerance of the numerical processor and converges to a solution for some parameters and does not for others that are only different by a small percentage. However, it is possible to use this expression if one is careful.

We also discovered another effect of using equation (D.2): it gives a particular dependence for the ratio of the penetration depth to the London (or clean-limit) penetration depth at zero temperature. Using equation (3.22)

$$\frac{l}{\xi_0} = \frac{\pi\Delta_0\lambda_{L,0}\sigma_0\mu_0}{\hbar}$$

and equation (3.25)

$$\tau_v = \frac{\hbar}{\pi \Delta_0} \frac{l}{\xi_0}$$

we can relate $\lambda(0)$ to $\lambda_{L,0}$.

Following is a graph of $\lambda(0) / \lambda_{L,0}$ using four methods of finding this ratio. They are: the Tinkham method (equation (3.25)), the Gor'kov method [29], the above method and the Zimmermann program from [1] which will give the BCS calculation. The independent variable is the ratio ξ_0 / l .

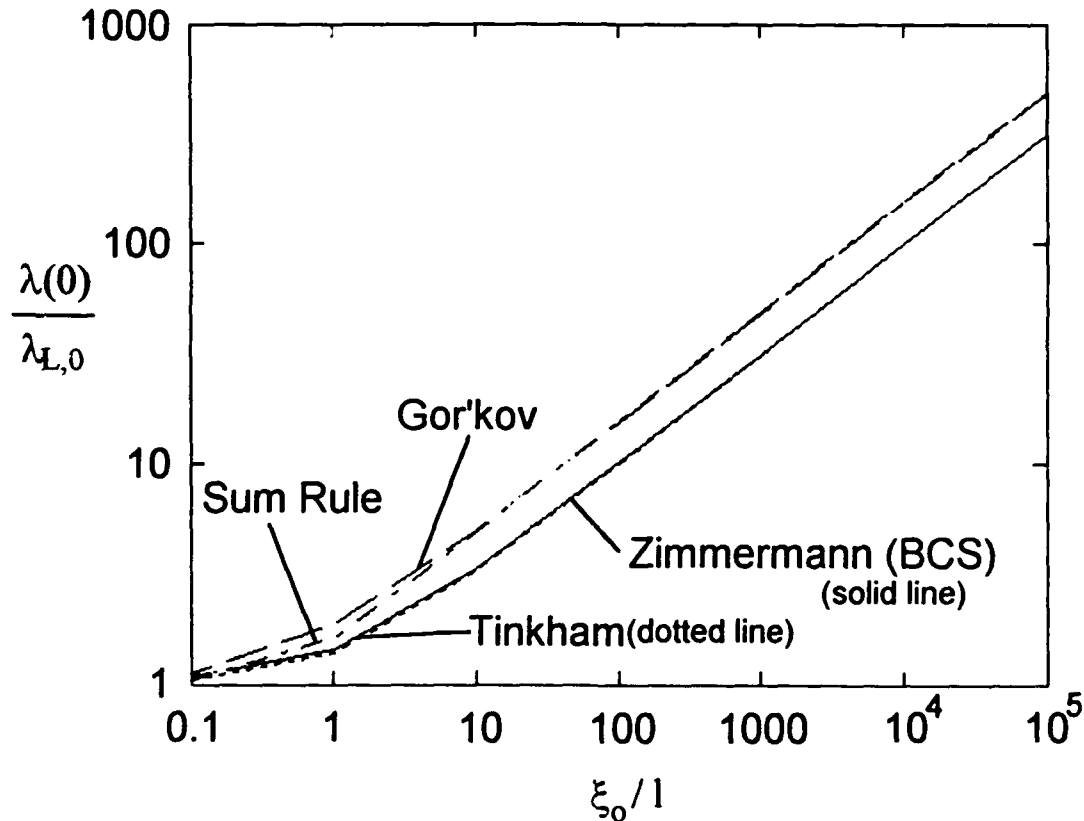


Figure D.1 $\lambda(0) / \lambda_{L,0}$ versus ξ_0 / l , using four methods of finding this relationship: Tinkham's equation (equation (3.25)), the Gor'kov relations [29], the sum rule method, and Zimmermann's BCS program (from [1]). The ratio of ξ_0 / l goes from clean to dirty going left to right. At larger ξ_0 / l , the Zimmermann and Tinkham methods are nearly identical, as are the sum rule and Gor'kov methods.

It is interesting that the sum rule and Gor'kov relationships match, except for clean materials where the sum rule method seems to approach 1 faster than Gor'kov. Of course, all methods converge to 1 in the clean limit. It is also interesting that BCS and Tinkham's equation match well across the whole parameter range from clean to dirty.

As stated in Subsection 3.4.5, we can also find $\eta(\omega, T)$ from the sum rule. We know the two-fluid form of the sum rule at any temperature is equation (D.1), and at zero temperature it is equation (D.2). Using these two equations and assumption 3, we can solve for $\eta(\omega, T)$, which results in equation (3.45):

$$\eta(\omega, T) = 1 - [1 - (T/T_c)^4] \frac{\tan^{-1}[\tau_r / \tau_s(0)]}{\tan^{-1}[\tau_r / \tau_s(T)]}$$

which we have stated does not work for the same reason the TTF model $\eta(\omega, T) = (T/T_c)^4$ does not work: they both ignore coherence effects. However, just to give an idea of how equation (3.45) and the TTF expression behave compared to one another, we include graphs of both functions in the dirty limit and in the clean limit. The two functions are almost indistinguishable in the clean limit, but are different in the dirty limit, particularly as the temperature approaches T_c . Even so, they are similar in that they are monotonically increasing functions, and have similar curvatures.

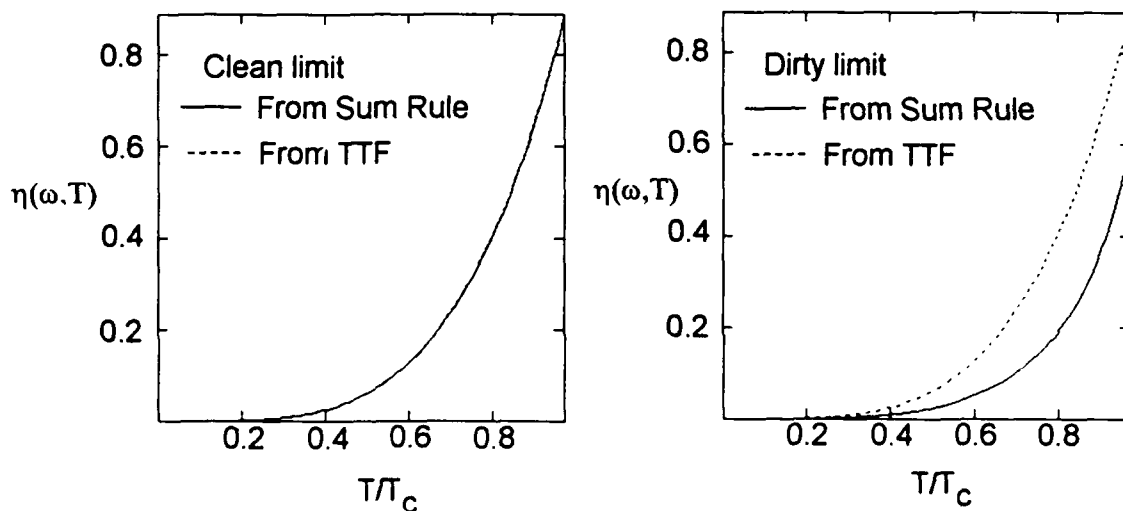


Figure D.2 Comparison of $\eta(\omega, T)$ from sum rule method and from TTF model. ξ_0/l for the clean limit is 0.0124, while for the dirty limit it is 12.4.